# Development of a Physically-based Sediment Transport Model for Green Bay, Lake Michigan

Bahram Khazaei[1], Hector Bravo[1], Eric J Anderson[2], and J. Val Klump[1]

[1]University of Wisconsin-Milwaukee
[2]National Oceanic and Atmospheric Administration (NOAA)

November 24, 2022

## Abstract

Green Bay is a large freshwater estuarine system that drains one-third of the Lake Michigan basin. The International Joint Commission designated southern Green Bay as an area of concern (AOC) in the 1980s due to ecosystem degradation including eutrophication, harmful algal blooms (HABs), hypoxia, lost or altered habitat, and reduced water quality. Restoration studies have found excessive nutrient loading and release of toxic materials, primarily produced in farmlands and industrial units, to be major drivers of Green Bay environmental/ecological issues. The Green Bay geomorphology and restricted mixing is a barrier to the efficient transport of sediments (as well as the accompanying nutrients and contaminants), acting as a retention basin for Lake Michigan. The purposes of this research were to: a) use the existing database of hydrodynamic, wave, and sediment field data to develop a three-dimensional (3D) predictive model of sediment transport in Lake Michigan, with an emphasis in Green Bay; b) use the sediment transport model to contribute to understanding ecological and environmental problems in the bay, and to recommend long-term solutions to those problems; and c) analyze summer patterns of circulation, wave action, current and wave-induced bottom shear stress, thermal structure, and sediment transport in Lake Michigan, with special attention to Green Bay.

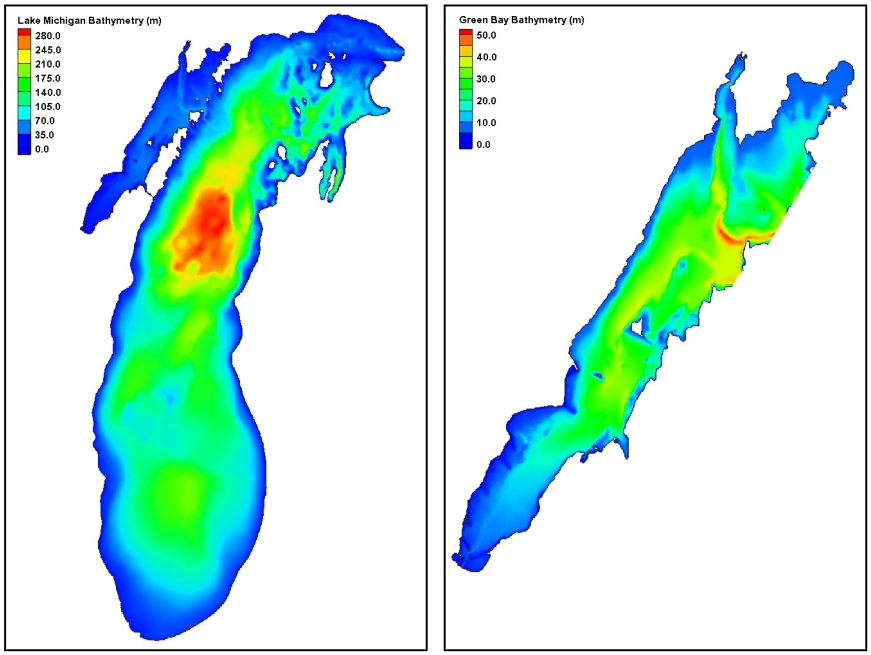

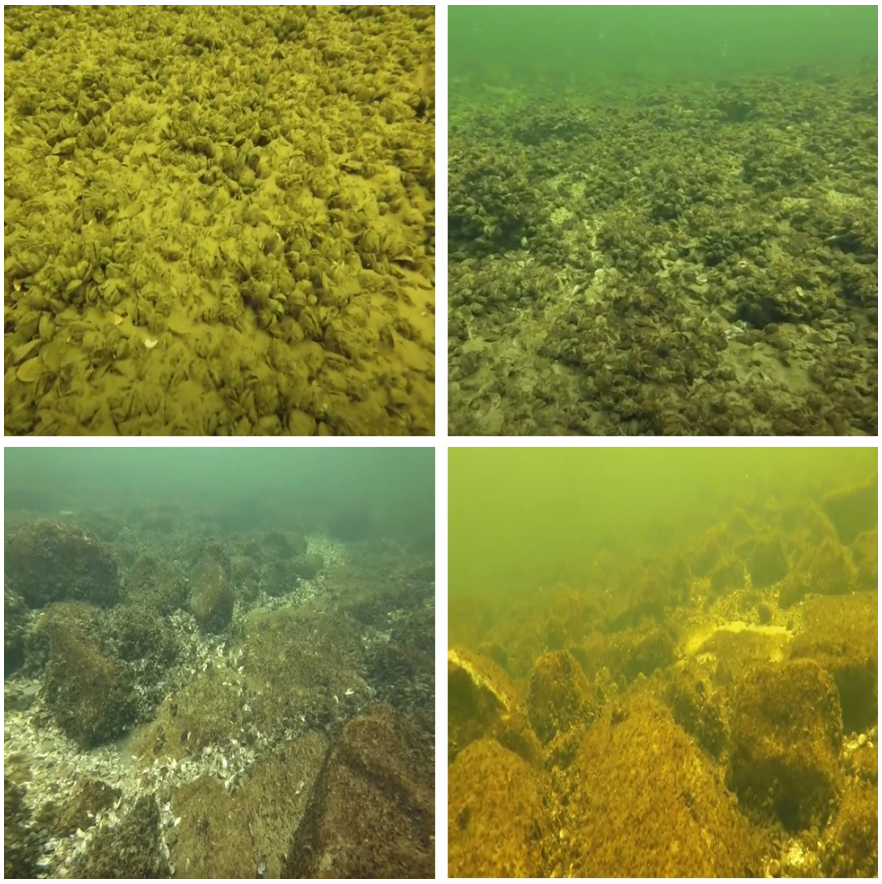

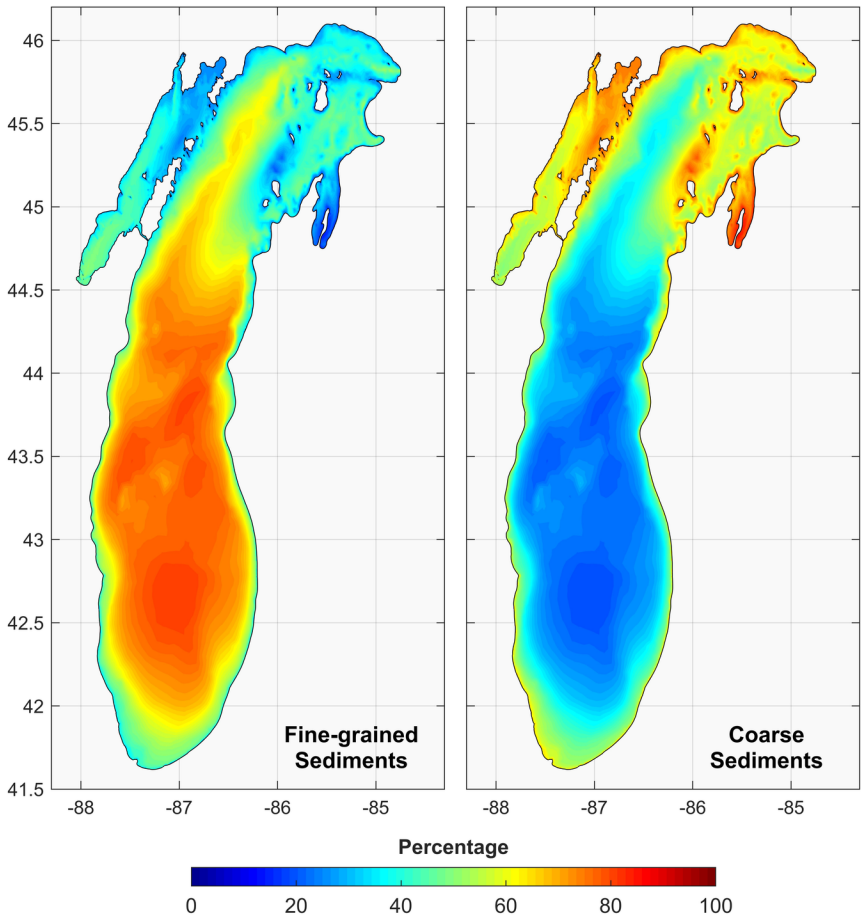

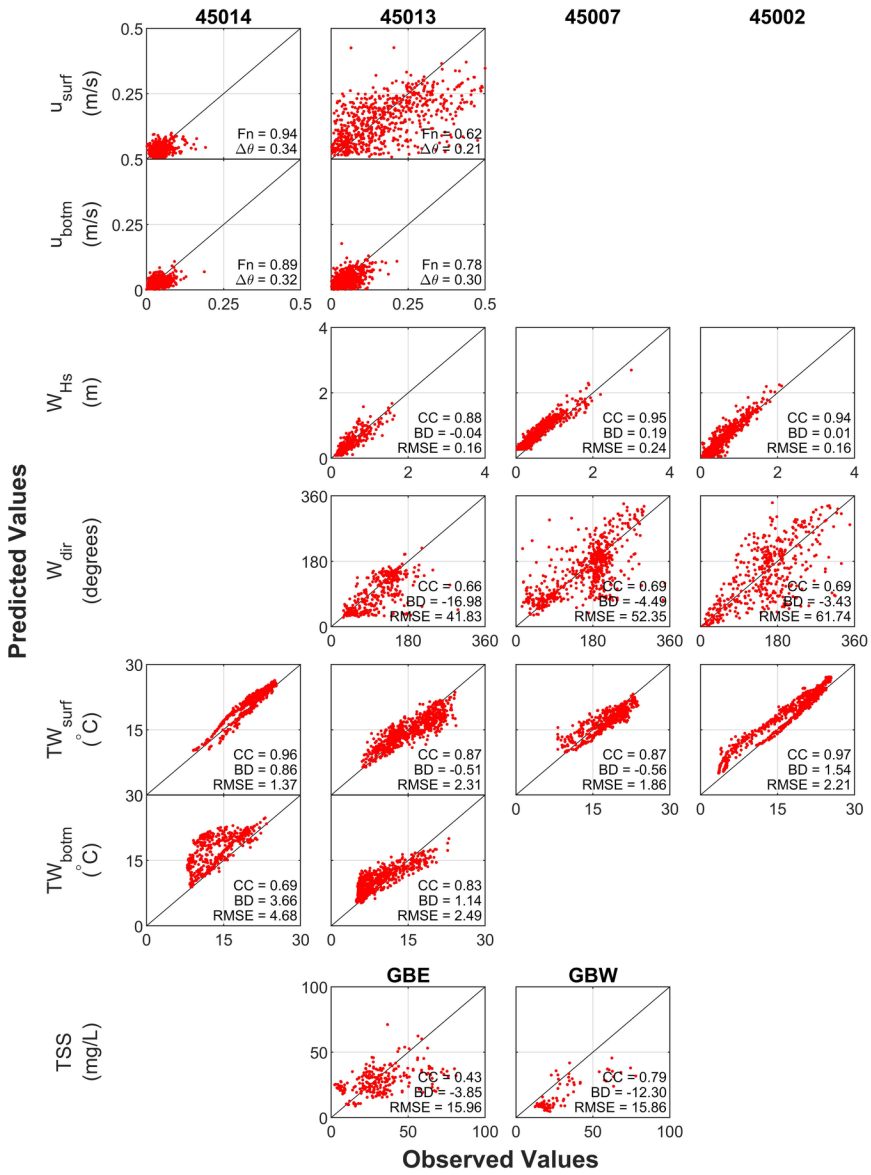

# Development of a Physically-based Sediment Transport Model for Green Bay, Lake Michigan

**Bahram Khazaei[1,4], Hector R. Bravo[1], Eric J. Anderson[2], and Jeffrey V. Klump[3]**

[1] Department of Civil and Environmental Engineering, University of Wisconsin-Milwaukee.

[2] Great Lakes Environmental Research Laboratory, National Oceanic and Atmospheric Administration.

[3] School of Freshwater Sciences, University of Wisconsin-Milwaukee.

[4] Current position: Research Application Laboratory, National Center for Atmospheric Research.

Corresponding author: Hector R. Bravo (hrbravo@uwm.edu)

Key Points:

- Sediment transport in Green Bay is primarily due to the wind-induced combined effects of currents and wave actions
- Sediment movement from Green Bay (especially southern bay areas) to Lake Michigan is physically restricted by the morphology of the system
- The Fox River contributes significantly to the turbid plume and high sediment concentrations in lower Green Bay

## Abstract

Green Bay is a large freshwater estuarine system that drains one-third of the Lake Michigan basin. The International Joint Commission designated southern Green Bay as an area of concern (AOC) in the 1980s due to ecosystem degradation including eutrophication, harmful algal blooms (HABs), hypoxia, lost or altered habitat, and reduced water quality. Restoration studies have found excessive nutrient loading and release of toxic materials, primarily produced in farmlands and industrial units, to be major drivers of Green Bay environmental/ecological issues. The Green Bay geomorphology and restricted mixing is a barrier to the efficient transport of sediments (as well as the accompanying nutrients and contaminants), acting as a retention basin for Lake Michigan. The purposes of this research were to: a) use the existing database of hydrodynamic, wave, and sediment field data to develop a three-dimensional (3D) predictive model of sediment transport in Lake Michigan, with an emphasis in Green Bay; b) use the sediment transport model to contribute to understanding ecological and environmental problems in the bay, and to recommend long-term solutions to those problems; and c) analyze summer patterns of circulation, wave action, current and wave-induced bottom shear stress, thermal structure, and sediment transport in Lake Michigan, with special attention to Green Bay.

**Keywords:** Green Bay, sediment transport, restoration, FVCOM, physical models.

## Plain Language Summary

Green Bay is a unique ecosystem located in the largest freshwater system on earth, the Laurentian Great Lakes. Almost one-third of tributary waters to Lake Michigan flow through Green Bay. Human activities in the watershed produce excessive amounts of contaminated and/or nutrient-rich sediments that are discharged to the bay. Sediments are not efficiently transported to Lake Michigan due to physical conditions in Green Bay, led to ecosystem degradation and caused environmental and public health risks. We studied the movement, transport, and fate of sediments in Green Bay by developing a physically-based, 3D sediment transport model. This model development effort helps to predict circulation of contaminants and nutrients that are attached to the sediments, their settlement and burial, and the detachment from the bottom during storm events. The knowledge gained in this study will enhance our understanding of water quality conditions and nutrient recycling in the bay, and will improve future restoration efforts and management plans.

## 1 Introduction

For decades, natural resources have experienced increasing pressures as population growth and development have stressed ecosystem services and impaired beneficial uses. In particular, lakes as major supplies of freshwater, have faced major water quality problems, desiccation, and ecosystem degradation worldwide (Allinger & Reavie, 2013; Clites et al., 2014; Destouni et al., 2010; Hecky et al., 2003; Khazaei et al., 2019; Marx et al., 2016; Shibuo et al., 2007). Located in the Great Lakes basin in North America, Green Bay of Lake Michigan is a prominent example of an environment under stress (Harris et al., 2018; Klump et al., 2018b).

Green Bay is the largest freshwater estuarine system on earth and drains one-third of Lake Michigan basin (Klump et al., 2018a). The International Joint Commission designated southern Green Bay as an area of concern (AOC) in the 1980s due to several instances of ecosystem degradation including (but not limited to) eutrophication, harmful algal blooms (HABs), hypoxia, lost or altered habitat, and reduced water quality. Thereafter, a comprehensive restoration program was initiated to diagnose the main causes of environmental degradation in Green Bay and to prescribe effective solutions to those problems.

Almost four decades of restoration studies have found excessive nutrient loading and release of toxic materials, primarily produced in farmlands and industrial units, to be a major driver of Green Bay environmental/ecological issues. Approximately 70% of the total sediment load to the bay originates from the Fox River and are transported throughout the bay until eventually they reach the main body of Lake Michigan. However, Green Bay's geomorphology and restricted mixing is a barrier to the transport of sediments (as well as the accompanying nutrients and contaminants), and the bay acts as an efficient retention basin for Lake Michigan (Klump et al., 2009), sequestering up to 75% of the phosphorus load via sediment accumulation and burial (Klump et al., 1997).

Previous research has focused on studying sediment transport in Green Bay from different perspectives including the study of sediment properties and deposition rates (Eadie et al., 1991; Klump et al., 2009; Klump et al., 1997; Manchester-Neesvig et al., 1996), one-dimensional analysis of sediment transport (Hawley & Niester, 1993), transport time scales (Bravo et al., 2019), and satellite-based estimations of surficial sediment transport in lower Green Bay (Hamidi et al., 2017). Despite previous efforts in the development of transport models

for Green Bay (e.g., HydroQual Inc., 1999) and others based on the Princeton Ocean Model (POM) and the Environmental Fluid Dynamics Code (EFDC), the lack of a robust and reliable 3D sediment transport model in the restoration agenda is noticeable.

The purposes of this research were to: a) use the existing database of hydrodynamic, wave, and sediment field data to develop a predictive model of sediment transport in Lake Michigan, with an emphasis in Green Bay; b) use the sediment transport model to contribute to understanding ecological and environmental problems in the bay, and to recommend long-term solutions; and c) analyze summertime patterns of circulation, wave action, current and wave-induced bottom shear stress, thermal structure, and sediment transport in Lake Michigan, with special attention to Green Bay. The sediment transport model is designed to be a compatible component of the NOAA Lake Michigan-Huron Operational Forecast System (LMHOFS) for future water quality and shoreline protection applications for Lake Michigan and other Great Lakes.

This article presents the steps in the development and validation of a physically-based sediment transport model for Green Bay and Lake Michigan and an analysis of summertime hydrodynamic and sediment transport patterns as outlined above. A companion paper under preparation will describe how the model can contribute to understanding the links between sediment and biogeochemical processes in Green Bay. That article will further describe patterns of sediment transport, erosion and deposition, present a sediment budget, and analyze the impacts of the Fox River and Cat Island restoration project on sediment transport.

## 2 Model Components and Formulation

Physically-based sediment transport modeling is essential in Green Bay due to complicated conditions of the system dynamics. Previous efforts intended to understand physical processes and particle dynamics in Green Bay faced obstacles in model development. Major obstacles included the use of Cartesian structured rectangular grids in POM-based models that limits the representation of small-scale shoreline features in Green Bay, and difficulties in modeling thermal structures and stratified flows in the shallow estuarine systems, especially during upwelling or downwelling events. Challenges in the implementation of EFDC-based models were difficult documentation and neglected wind-waves effects. Additionally, those

models are computationally expensive and not very efficient if a high-resolution grid in a large domain such as Lake Michigan is implemented.

To overcome those obstacles, a state-of-the-art modeling approach, the Finite-Volume Community Ocean Model (FVCOM) was used in this research. FVCOM's features such as the use of an unstructured-grid solver and a parallel mode computation option makes it a suitable candidate for the Green Bay sediment transport model. FVCOM is also equipped with several water quality tools that can integrate different physical and biogeochemical processes and enhance the implementation of transport models in restoration applications.

### 2.1 Circulation Model: FVCOM

Developed by Chen et al. (2003), FVCOM is a free-surface, primitive-equation ocean model and is a powerful numerical solution of the conservation of mass, momentum, and energy principals that solves for currents, temperature, salinity, density, and other hydrodynamic variables as follows:

$$\frac{\partial u}{\partial t} + u\frac{\partial u}{\partial x} + v\frac{\partial u}{\partial y} + w\frac{\partial u}{\partial z} - fv = -\frac{1}{\rho_W}\frac{\partial p}{\partial x} + \frac{\partial}{\partial z}\left(K_V\frac{\partial u}{\partial z}\right) + F_u \quad (1)$$

$$\frac{\partial v}{\partial t} + u\frac{\partial v}{\partial x} + v\frac{\partial v}{\partial y} + w\frac{\partial v}{\partial z} + fu = -\frac{1}{\rho_W}\frac{\partial p}{\partial x} + \frac{\partial}{\partial z}\left(K_V\frac{\partial v}{\partial z}\right) + F_v \quad (2)$$

$$\frac{\partial w}{\partial t} + u\frac{\partial w}{\partial x} + v\frac{\partial w}{\partial y} + w\frac{\partial w}{\partial z} = -\frac{1}{\rho_W}\frac{\partial p}{\partial x} + \frac{\partial}{\partial z}\left(K_V\frac{\partial w}{\partial z}\right) + F_w \quad (3)$$

$$\frac{\partial u}{\partial x} + \frac{\partial v}{\partial y} + \frac{\partial w}{\partial z} = 0 \quad (4)$$

$$\frac{\partial TW}{\partial t} + u\frac{\partial TW}{\partial x} + v\frac{\partial TW}{\partial y} + w\frac{\partial TW}{\partial z} = \frac{\partial}{\partial z}\left(K_H\frac{\partial TW}{\partial z}\right) + F_{TW} \quad (5)$$

$$\rho_W = \rho_W(TW, p) \quad (6)$$

where *(u, v, w)* are the components of the current in *(x, y, z)* Cartesian grid space, $\rho_W$ is the water density, *p* is the pressure, *TW* is the water temperature, *f* is the Coriolis coefficient, $K_V$ and $K_H$ are the vertical eddy viscosity and thermal diffusion coefficients, and $F_u$, $F_v$, $F_w$, and $F_{TW}$ represent the momentum and thermal diffusion terms. FVCOM uses a modified MY-Level 2.5

turbulence closure scheme (Mellor & Yamada, 1982) for vertical mixing calculations and Smagorinsky's (1963) eddy scheme for horizontal mixing.

FVCOM has several features that makes it an efficient computational tool for physical modeling of large lakes. FVCOM runs based on unstructured sigma-coordinated (terrain-following) grids, in which the 3D domain is discretized into triangular finite volumes. That feature increases model flexibility in representing irregular geometry of shorelines in Green Bay estuary and preserves fine features of several peninsulas and islands that restrict physical processes in the bay. Additionally, FVCOM is computationally efficient because it runs in parallel and also adopts a split mode numerical scheme, in which it first calculates the water surface elevation and depth-averaged currents in the external mode and then solves for the vertical diffusive transport in a 3D internal mode.

FVCOM has been successfully implemented in various hydrodynamic applications such as coastal modeling (e.g., Chen et al., 2003, 2007; Huang et al., 2008; B. Li et al., 2017; J. Li et al., 2018; Zhang et al., 2018), Great Lakes studies (e.g., Anderson et al., 2010; Anderson & Schwab, 2011; Bai et al., 2013; Mao et al., 2016; Mao & Xia, 2020; Read et al., 2010; Shore, 2009; Xue et al., 2015), and modeling rivers, straits, and channels (e.g., Anderson & Phanikumar, 2011; Anderson & Schwab, 2013; Guerra et al., 2017; Lai et al., 2018). It has also been coupled with water quality and biogeochemical models in various case studies (e.g., Luo et al., 2012; Rowe et al., 2015; Rowe et al., 2017; Safaie et al., 2016; Shen, 2016). In this study, we used FVCOM version 4.1 to develop the physical circulation model of Lake Michigan.

### 2.2 Wave Model: FVCOM-SWAVE

Sediment movement is primarily due to advective-diffusive transport in the water column; however, sediment processes near the bottom are significantly affected by the wave interactions. Therefore, the implementation of wave actions in the sediment model is an important step toward simulations of more realistic current-wave-sediment interactions in the bottom boundary layer. Simulating WAves Nearshore (SWAN) model is adopted by FVCOM (FVCOM-SWAVE) as the wave simulator. SWAN was developed by Booij et al. (1999) and models wave evolution using transport equations to solve for wave action density $N$ as follows:

$$\frac{\partial N}{\partial t}+\frac{\partial c_x N}{\partial x}+\frac{\partial c_y N}{\partial y}+\frac{\partial c_\sigma N}{\partial \sigma}+\frac{\partial c_\theta N}{\partial \theta}=\frac{S_w}{\sigma} \quad (7)$$

where $N$ is the energy density $E$ divided by the relative frequency $\sigma$, $N(\sigma,\theta)= E(\sigma,\theta)/ \sigma$, $(c_x, c_y)$ are the propagation velocities in the $(x, y)$ Cartesian grid coordinates, $\sigma$ and $\theta$ are the intrinsic wave frequency and direction, $c_\sigma$ is the propagation velocity due to variations in depth and currents, $c_\theta$ is the propagation in wave direction, and $S_w$ is acting as a source/sink term to represent the effects of wind-wave generation, energy dissipation due to whitecapping, depth-induced wave breaking, and bottom friction, and nonlinear wave-wave interactions. Specific details of the SWAN model formulation and validation are described in the literature (Booij et al., 2004; Ris et al., 1999). SWAN is a structured-grid wave model and was converted to an unstructured-grid finite-volume model to be consistent with FVCOM (Chen et al., 2013; Qi et al., 2009).

SWAN has become popular in various applications including ocean wave simulations, engineering applications, modeling coastal and estuarine systems, and wave forecasting studies (Chen et al., 2018). SWAN is particularly adjusted for coastal regions with shallow waters, which makes it suitable for modeling sediment transport in Green Bay. Recent applications of the SWAN in studying Lake Michigan wave dynamics has also indicated good performance and applicability of the model for the Green Bay sediment transport studies (Mao et al., 2016; Mao & Xia, 2017).

### 2.3 Sediment Transport Model: FVCOM-SED

We used the FVCOM built-in sediment transport model (FVCOM-SED) in this study to model sediment processes in Green Bay and Lake Michigan. FVCOM-SED was developed based on the Community Model for Coastal Sediment Transport (CMCST) by Warner et al. (2008) and was further modified to account for cohesive and mixed sediment dynamics (Sherwood et al., 2018). CMCST was developed to be coupled with the structured-grid based Regional Ocean Modeling System and was modified to be consistent with FVCOM unstructured-grid solver (Chen et al., 2013).

FVCOM-SED accounts for several sediment mechanisms including suspended and bedload transport, layered bed dynamics, and erosion/deposition actions for an unlimited number of cohesive and non-cohesive sediment classes. Each sediment class is characterized by mean

grain diameter, particle density, settling rates, and bed erosion characteristics. Each bed layer is defined based on the bulk characteristics of sediment classes in that layer and its initial thickness. The FVCOM-SED version 4.1 was only able to initiate the sediment transport model based on the uniform distribution of sediment classes in the entire domain. That seems to be an unrealistic assumption for Lake Michigan sediment stratigraphy. Therefore, we updated the code so that the model can take user-defined non-uniform distribution of sediment classes in the bed layer (Khazaei, 2020; Appendix A).

Bed layer characteristics, in particular thickness, is immediately affected by sediment actions such as erosion and deposition. In order to keep the number of bed layers constant throughout the simulation, an active layer is considered on top of sediment layers. The thickness of this active layer ($z_a$) is calculated in each time step based on the Harris and Wiberg's (2001) formulation as follows:

$$z_a = max\left[k_1(\tau_{sf} - \tau_{ce}),\quad 0\right] + k_2 D_{50} \qquad 8)$$

where $\tau_{sf}$ is the maximum bottom friction shear stress due to combined effects of currents and waves ($N/m^2$), $\tau_{ce}$ is the critical shear stress for erosion ($N/m^2$), $D_{50}$ is the median grain diameter at the sediment-water interface ($m$), and $k_1$ and $k_2$ are empirical constants with values of 0.007 and 6.0, respectively. Sediment transport is limited to the mass available in the active layer in each time step.

The total load is the accumulated suspended load in the water column and bedload. FVCOM-SED calculates the suspended load by accounting for advective and diffusive concentration-based transport in the water column, as follows:

$$\frac{\partial C}{\partial t} + \frac{\partial uC}{\partial x} + \frac{\partial vC}{\partial y} + \frac{\partial wC}{\partial z} = \frac{\partial}{\partial x}\left(A_H \frac{\partial C}{\partial x}\right) + \frac{\partial}{\partial y}\left(A_H \frac{\partial C}{\partial y}\right) + \frac{\partial}{\partial z}\left(A_V \frac{\partial C}{\partial z}\right) + \frac{1}{H_z} C_{Source/sink} \qquad 9)$$

where $C$ is the suspended sediment concentration, $(u, v, w)$ are the three components of currents in the $(x, y, z)$ Cartesian grid space, $A_H$ and $A_V$ are the horizontal and vertical eddy viscosity, and $H_z$ is the thickness of grid cells. $C_{source/sink}$ accounts for additional vertical transport mechanisms due to settling and resuspension:

$$C_{source/sink} = -\frac{\partial \omega C}{\partial S} + E_s \qquad 10)$$

where $\omega$ is the settling velocity positive in the upwards direction (*m/s*) and $E_s$ is the erosion rate (*kg/m²/s*) in the vertical sigma coordinate direction *S*. Ariathurai and Arulanandan (1978) defined erosion rates of cohesive soils as a function of bed erodibility constant, sediment porosity (top layer sediment particles in this case), maximum bottom shear stress, and critical shear stress for erosion. Transport of suspended load is constrained to a zero-flux boundary condition at the surface of the water column and the net balance between erosion and deposition at the bottom.

While the suspended load includes the flux of sediment mass at the sediment-water interface and transport in the water column, the bedload is considered as the horizontal exchange within the top layer of the bed and is estimated based on the Hans Albert Einstein's definition of non-dimensional volumetric sediment flux:

$$q_{bl} = q_{s*} D_{50} \sqrt{(s-1) g D_{50}} \quad (11)$$

where $q_{bl}$ is the horizontal bedload transport rate ($m^2/s$) and $s = \rho_s/\rho_w$ is the specific density of sediments in the water. $q_{s*}$ is the magnitude of the non-dimensional transport rate and could be determined based on the Meyer-Peter and Müller's (1948) scheme.

Mixed-sediment bed processes occur when both cohesive and non-cohesive sediments are present and there is a considerable amount of mud (fine cohesive sediment) in the sediment layer (Mitchener & Torfs, 1996). In these mixed-sediment bed conditions effective critical shear stress of the bottom ($\tau_{ce,eff}$) is calculated based on a weighted combination of critical shear stresses of cohesive and non-cohesive portions of the bed:

$$\tau_{ce,eff} = max[P_c \tau_{cb} + (1 - P_c)\tau_{ce}, \tau_{ce}] \quad (12)$$

where $\tau_{ce}$ is the critical shear stress for each sediment class, $\tau_{cb}$ is the bulk critical shear stress for sediment layer based on Sanford's (2008) approach, and $P_c$ is the dimensionless cohesive behavior parameter. $P_c$ is a function of the mud content in the bed layer with lower values denoting a non-cohesive behavior and vice versa.

FVCOM-SED is fully coupled with the FVCOM ocean model and FVCOM-SWAVE to account for the current-wave-sediment interactions (Chen et al., 2013). More details of the CMCST model, mixed sediment transport mechanisms, and model validation are provided in the

literature (Sherwood et al., 2018; Warner et al., 2008). In section 3.3, we elaborate the characterization of different sediment classes and their properties for the Lake Michigan sediment transport model.

# 3 Model Design

## 3.1 Study Area

While the focus of the current study is Green Bay, to avoid the uncertainty and difficulty of obtaining internal or open-lake boundary conditions at the connection straits with Lake Michigan, a whole-lake model is developed. Green Bay is 190 *km* long in its longest axis and, on average, is about 20 *km* wide. With an average and maximum depths of approximately 20 *m* and 50 *m*, respectively, Green Bay is considered a shallow coastal water body. The maximum depth in Lake Michigan is about 280 *m*.

Chambers Island cross-section divides Green Bay into lower and upper sections. Lower Green Bay is the hotspot of environmental issues, where Fox River discharges runoff from the heavily developed and stressed Fox River watershed into the bay. The watershed is mostly covered by vegetated areas (Khazaei & Wu, 2018), and the cities of Appleton and Green Bay, large industrial sites, and farmlands impact the concentration and quality of particles running into the river (Klump et al., 1997; Velleux et al., 1995). The Fox River alone contributes about two-thirds of the nutrient and particulate tributary loading into Green Bay and almost one-third of the total phosphorus load to Lake Michigan (Harris & Christie, 1987). Figure 1 shows the location of Lake Michigan and Green Bay in the Great Lakes basin and Green Bay AOC.

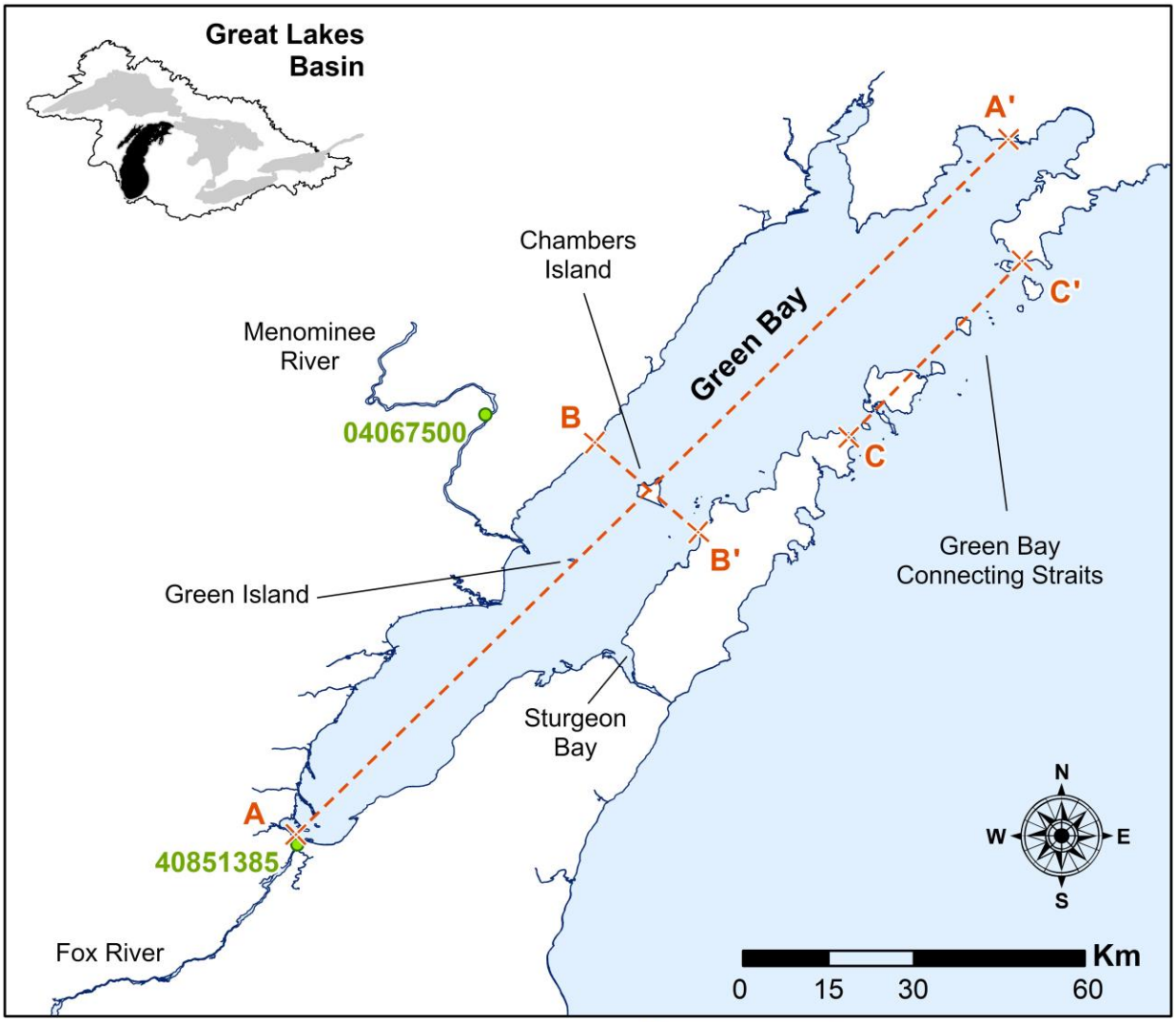


| Station Name | Station ID | latitude | longitude |
|---|---|---|---|
| Southern Green Bay Buoy | 45014 | 44.80 | -87.76 |
| Milwaukee Atwater 20m Buoy | 45013 | 43.10 | -87.85 |
| Northern Michigan Buoy | 45002 | 45.34 | -86.41 |
| Southern Michigan Buoy | 45007 | 42.67 | -87.03 |
| Green Bay West Buoy | GBW | 44.58 | -87.99 |
| Green Bay East Buoy | GBE | 44.55 | -87.96 |
| USGS Fox River Gauge | 40851385 | 44.53 | -88.01 |
| USGS Menominee River Gauge | 04067500 | 45.33 | -87.66 |
| NEW Water Station 13 | NW13 | 44.53 | -88.01 |

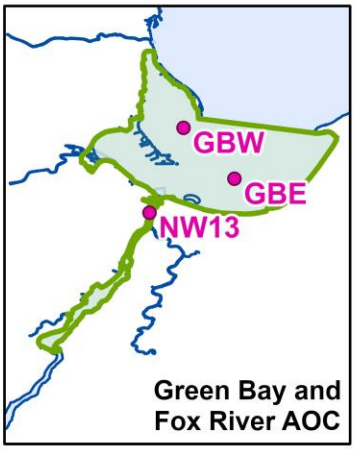


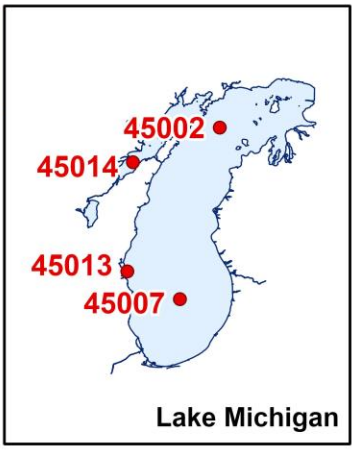


**Figure 1.** Green Bay Location in Lake Michigan and the Great Lakes basin. Lower insets show Lake Michigan and Green Bay Area of Concern (AOC). Buoy stations and USGS gauges used in this study and their abbreviations are also shown in the Figure. Cross-sections A-A', B-B', and C-C' are used to look at transport patterns in different locations across the bay.

### 3.2 Grid and Simulation Specifications

Circulation and transport mechanisms are very sensitive to the morphology of the system. Shallow waters and complex geometry of the Green Bay shorelines require a fine grid that can resolve those detailed features (Figure S1 in the Supporting Information). Long Tail Point and Little Tail Point Islands located on the western shore of lower Green Bay, Green and Chambers Islands in the central bay areas, as well as Plum, Detroit, Washington, Rock, St. Martin, Poverty, Summer, and Little Summer Islands in the exchange zone of the Lake Michigan and Green Bay were incorporated in the grid (see Figure S2 in the Supporting Information). Also, the coastline data was updated to include the Cat Island, a feature that is crucial in modeling the circulation and transport in the Green Bay AOC.

Bathymetry and shoreline data, used to generate the Lake Michigan unstructured grid (Figure S3 in the Supporting Information), are based on NOAA datasets (National Geophysical Data Center, 2015; NOAA, 2017) and were updated in the southern Green Bay to represent recent changes of the bathymetry due to the dredging of navigational channel project.

The Lake Michigan grid in this study includes 52,574 triangular elements/cells, 28,985 nodes, and is vertically discretized to 20 $\sigma$-layers, i.e., layers follow terrain variations. The grid is designed very dense in Green Bay, where element side length varies between 50 *m* to 1500 *m* from the mouth of Fox River to upper Green Bay. Since the focus of our model is to simulate sediment transport in Green Bay, a coarser grid resolution is used for the main body of Lake Michigan for the sake of computational efficiency. Given the suggested summertime baroclinic Rossby radius of 5 *km* in the Great Lakes, it is critical to use a grid size less than 5 *km* within the 8-10 *km* of the coastal areas (Beletsky et al., 1997, 2006b). Therefore, cell side length in the Lake Michigan grid was designed to vary between 1000 *m* in the shorelines to about an average of 5 *km* in the central lake areas. A relatively fine grid is constructed near the connecting straits to be able to accurately account for the exchanges between the lake and the bay.

FVCOM-SWAVE offers various options suitable for the simulation of waves in different physical conditions (Booij et al., 1999; Table 1). In this study, the wave model was adjusted by selecting from those options based on recommendations in the literature (Mao et al., 2016; Ris et al., 1999), and our comparisons of simulated results against the validation buoys in nearshore and deep-water areas of Lake Michigan. In this regard, the third generation of the SWAN wave

model (Booij et al., 1999) with quadruplet wave-wave interactions of Hasselmann et al.'s (1985) was adopted for this study. We also used Komen et al.'s (1984) formulation for wind growth and whitecapping, Hasselmann et al.'s (1973) expressions for bottom friction, and Battjes & Janssen (1978) formulation for depth-induced breaking calculations. We also selected 60 as the number of steps in the relative frequency space.

### 3.3 Sediment Classification and Properties

Sediment transport models require a set of standard parameters for model simulations, which can be obtained through observations, lab experiments, and/or calibration. Those important parameters include particle density ($\rho_s$), mean diameter ($D_{50}$), and porosity ($\varphi$). Prediction of sediment transport is also very sensitive to erosion and deposition characteristics of the particles such as critical shear stress for erosion ($\tau_{ce}$) and settling rates ($\omega$). A previous Lake Michigan sediment transport model has found ~40% deviations in results by changing these parameters (Lee et al., 2005), yet, the model had the most sensitivity to the fraction of fine-grained particles in the sediment mixture. Therefore, it is important in the first place to define the distribution of sediment classes in the bed layer.

We extracted information from several studies to obtain a general understanding and reasonable estimates of sediment characteristics in Green Bay. The next steps included using soil classification methods/standards and consultation with experts to narrow down the ranges defined for each parameter in the literature. Finally, some of these model parameters were adjusted based on model calibration.

There are few studies of Green Bay sediment classes and their distribution. Field observations and analysis of sediment samples (Jones, 2000; Moore et al., 1973; Wisconsin DNR, 2000) have found clay, silt, and sand are the major constituting variables of lower Green Bay. As we move from south, near the mouth of Fox River, to north, near the connecting straits, mud content decreases in the bed layer and the upper Green Bay bed is mostly formed by sand and gravel. We compiled these findings with Lee et al.'s (2007) recommendations for Lake Michigan and estimated bottom sediment stratigraphy as shown in Figure S4 in the Supporting Information. It is important to mention that the composition of the benthic zone in Lake Michigan has significantly changed recently due to the invasion of Quagga and Zebra Mussels (Rowe et al., 2015) and algal growth (Bravo et al., 2019). Those changes are neglected in the

assignment of bottom sediment initial conditions, yet has to be considered in future studies for more realistic simulations of sediment transport (see Figure S5 in the Supporting Information).

We identified six sediment classes for the current model development and determined sediment mean diameter based on the U.S. Department of Agriculture (USDA) soil classification standard (Yolcubal et al., 2004) as shown in Table 1. Density and porosity of different sediment classes were also estimated based on the analysis of sediment samples taken in Green Bay (Manchester-Neesvig et al., 1996; Wisconsin DNR, 2000).

**Table 1.** Sediment properties and erosion/deposition characteristics used in the Lake Michigan sediment transport model.

| **Sediment class** | **1** | **2** | **3** | **4** | **5** | **6** | **Source** |
|---|---|---|---|---|---|---|---|
| **Sediment type** | Clay | Fine Silt | Coarse Silt | Fine Sand | Coarse Sand | Gravel | Moore et al. (1973), Wisconsin DNR (2000), and Lee et al. (2007) |
| $D_{50}$ **(mm)** | 0.001 | 0.008 | 0.05 | 0.1 | 0.5 | 2 | Jones (2000) and Yolcubal et al. (2014) |
| $\rho_s$ **(kg/m$^3$)** | 2300 | 2300 | 2300 | 2450 | 2450 | 2450 | Wisconsin DNR (2000) |
| $\Phi$ **(%)** | 97.5 | 97.5 | 97.5 | 85 | 75 | 60 | Manchester-Neesvig et al. (1996) |
| $\omega$ **(mm/s)** | 0.001 | 0.02 | 1.01 | 4.95 | 57.04 | 175.31 | Garcia (2008) |
| $\tau_{ce}$ **(N/m$^2$)** | 0.008 | 0.029 | 0.09 | 0.18 | 0.25 | 1.10 | Garcia (2008) |
| $E_0$ **(kg/m$^2$/s)** | 0.0005 | 0.0025 | 0.005 | 0.005 | 0.005 | 0.005 | Ariathurai and Arulanandan (1978) |

Previous studies have shown wide ranges of sediment settling/fall velocity in Green Bay. NOAA sediment trap study found settling velocities of about 6-70 *mm/s* in stratified conditions (summertime) and 14-200 *mm/s* during unstratified periods. We used a method proposed by Soulsby (1998) that estimates fall velocity based on sediment mean diameter and density and viscosity of water. This method is suitable for fine-grained sediments, therefore, we used for coarser sediment classes a graphical method explained by García (2008, p. 42), requires the same variables as of Soulsby's method.

While settling velocity governs deposition, bottom erosion and resuspension events are controlled by critical shear stress for erosion which we estimated based on the definition of Shields non-dimensional critical shear stress ($\tau_c^*$). $\tau_c^*$ can be found based on the modified Shields diagram (Parker, 2004) or alternatively for finer particles based on Mantz's (1977) empirical relationship. Critical shear stress for erosion is then a function of $\tau_c^*$, particle density, and mean sediment diameter according to the Shields formulation.

FVCOM-SED requires bed erodibility constant ($E_0$) in order to estimate bottom sediment fluxes. A wide range of values is suggested in the literature for $E_0$. Ariathurai and Arulanandan (1978) conducted several tests on more than 200 natural or lab-synthesized fine and cohesive sediment samples and suggested values between $5\times10^{-4}$ and $5\times10^{-3}$ $kg/m^2/s$. Analysis of those samples has shown that the slope of erosion rate curves increases proportional to critical shear stress for erosion.

### 3.4 River Inputs

Tributary loadings are the major input fluxes into Green Bay. Required river inputs for the circulation, wave, and sediment transport models are discharge, temperature, and total suspended solids (*TSS*) at river mouth that were estimated in this study based on daily USGS observational data.

USGS observations during the 2011-2019 period show average inflowing discharge of 170, 24, 29, and 106 $m^3/s$ and *TSS* concentrations of 24, 0.24, 0.03, and 3 *mg/L* for the Fox, Oconto, Peshtigo, and Menominee Rivers, respectively. Those statistics indicate that the Fox and Menominee Rivers have more influence on circulation and thermal regimes in Green Bay, hence they were included as boundary conditions of the model.

It should be noted that riverine *TSS* loading into the bay is estimated based on empirical relationships developed using USGS observations of discharge and turbidity at the mouth of Fox River (gage ID: 40851385) and cruise measurements of turbidity and *TSS* by the city of Green Bay Sewerage district, now NEW Water, at this location (Khazaei, 2020; Khazaei et al., 2018; NEW Water, 2017).

### 3.5 Field Data

Previous efforts in modeling physical and biogeochemical processes in Green Bay have been challenged by the scarcity of relevant hydrodynamic and water quality observational data. Recent data collection efforts, such as continuous monitoring of turbidity at Green Bay West and East buoys in the southern bay (Miller, 2020), have made development and validation of a sediment transport model for Green Bay possible. As explained above, we used NEW Water turbidity and *TSS* cruise data to convert turbidity observations into *TSS* time series. In addition, four buoy stations in Lake Michigan and Green Bay were used to validate hydrodynamic and wave models, i.e., southern Green Bay, Atwater Beach in Milwaukee nearshore zone, North Michigan, and South Michigan buoys (see Figure 1).

External forcing inputs of the model are based on the interpolation of NOAA National Centers for Environmental Information (NCEI; NOAA, 2018) land-based and buoy stations in the Great Lakes basin. The interpolation scheme is based on a natural neighbor method developed by NOAA Great Lakes Environmental Research Laboratory for application in the Great Lakes forecasting models (Beletsky et al., 2003; Schwab & Beletsky, 1998) and accounts for adjustments of overland to overlake conditions whenever data from land-base stations were used (Beletsky & Schwab, 2001).

### 3.6 Model Skill Criteria

We use Root Mean Squared Error (*RMSE*), Bias Deviation (*BD*), and correlation coefficients (*CC*) to assess model skills of scalar variables (e.g., temperature and *TSS*):

$$RMSE = \frac{1}{N}\left(\sum_{i=1}^{N}(e_i^2)\right)^{1/2} \quad (13)$$

$$BD = \frac{1}{N}\sum_{i=1}^{N}(e_i) \quad (14)$$

$$CC = \frac{\sum_{i=1}^{N}(x_{i,O} - x_{ave,O})(x_{i,P} - x_{ave,P})}{\left[\sum_{i=1}^{N}(x_{i,O} - x_{ave,O})^2\right]^{1/2}\left[\sum_{i=1}^{N}(x_{i,P} - x_{ave,P})^2\right]^{1/2}} \quad (15)$$

where $N$ is the number of observation/prediction points, $e_i$ is the deviation of the predictions from observations (i.e., $e_i = x_{i,O}$-$x_{i,P}$; where $x_{i,O}$ and $x_{i,P}$ are observational and

prediction values at point $i$, respectively), and $x_{ave,o}$ and $x_{ave,P}$ are the mean of observed and predicted data, respectively.

To assess model skills for vector fields (e.g., currents) we use normalized Fourier norm ($F_n$) and average angular difference ($\Delta\theta$):

$$F_n = \frac{\|V_o, V_p\|}{\|V_0, 0\|} = \frac{\left(\frac{1}{N}\sum_{i=1}^{N}|V_{i,o} - V_{i,p}|^2\right)^{1/2}}{\left(\frac{1}{N}\sum_{i=1}^{N}|V_{i,o} - 0|^2\right)^{1/2}} \quad (16)$$

$$\Delta\theta = \frac{1}{\pi N}\sum_{i=1}^{N}\cos^{-1}\left(\frac{V_o . V_p}{|V_o||V_p|}\right) \quad (17)$$

where $V_{i,o}$ and $V_{i,p}$ denote observed and predicted vector fields at point $i$, respectively.

*RMSE* is used to assess model accuracy, i.e., zero indicates perfect model accuracy and as the value increases, model accuracy decreases. *BD* shows model bias and smaller values close to zero denote lower biased performance of the model. *CC* can be used as an indicator of model performance in reproducing the temporal patterns of change in observational data. In this article, *CC* is reported if significant at $p$-value $\leq 0.05$. *Fn* and $\Delta\theta$ assess model accuracy in the prediction of vector fields magnitude and direction, respectively. $F_n$ and $\Delta\theta$ equal to zero indicate a perfect model, values between zero and one are in the acceptable range, and as the value increases, model performance decreases.

## 4 Simulation Details and Model Validation

We ran the model for 2016-2019 years and model simulations were limited to the May-October period of each year to focus on the ice-free period in Lake Michigan and time of active bottom layer sediment dynamics. Model stability requires simulations at a time step of 5 *s*. The circulation model is initiated at rest, i.e., zero currents. 3D temperature fields are interpolated from LMHOFS simulation in Lake Michigan at the initial condition. Also, the model is run using realistic initial water surface elevation in Lake Michigan (NOAA, 2020). The initial bed layer properties are defined as explained in section 3.3 with a bed thickness of 0.5 *m*. We ignored major open boundary conditions around Lake Michigan, e.g., bi-directional flow at the Straits of Mackinac and Chicago River diversion, because they do not have an immediate impact on sediment transport in Green Bay, especially southern areas in the bay.

### 4.1 Validation of Simulated Currents, Waves, and Temperature Fields

Currents are the main driver of transport mechanisms in hydrodynamic simulations. Accurate simulations of sediment transport dynamics rely on accurate simulations of currents near the bottom. Figure 2 compares the observed and predicted daily currents in N-S ($v$ component) and E-W ($u$ component) directions during the May-October of 2016-2019 years. Comparison plots and model skill criteria indicate reasonable agreement between model and buoy observations at two selected locations, given the complex nature of the physical process and the system. Our calculated model skill statistics for currents (or velocity fields) are comparable and in some cases show slight improvements compared with previous Lake Michigan hydrodynamic modeling efforts. For example, *Fn* values of 0.79-1.01 and 0.9-1.05 were reported respectively for barotropic (Schwab, 1983) and POM-based (Beletsky & Schwab, 2001) models of summertime circulation in Lake Michigan built on 5-*km* resolution grids. Rowe et al. (2015) obtained improved performance in modeling summertime hydrodynamics by using interpolated forcing and adopting FVCOM, and reported *Fn* values of 0.83-0.91. Schwab (1983) and Rowe et al. (2015) have respectively reported values of 0.23-0.46 and 0.29-0.31 for $\Delta\theta$ in modeling Lake Michigan currents direction. Wave action complements currents to force sediment movement. Combined current-wave action produces stronger shear stresses at the water-sediment interface and trigger more frequent and/or stronger episodes of resuspension. Hence, an accurate wave model will improve the understanding of sediment processes. Figure 2 shows comparison of the observed and predicted significant wave heights ($W_{Hs}$) and wave directions ($W_{dir}$). $W_{Hs}$ is defined as the average of the highest one-third of the waves, measured between wave trough to crest.

According to the figure and model skill statistics, FVCOM-SWAVE simulations of wave height are in good agreement with observations at three selected buoys. In particular, high correlations between observations and simulations implies that patterns of the wave height variability are reproduced well by the model. However, wave direction predictions are not as accurate as wave heights. Comparison of the model skill statistics with previous wave models of Lake Michigan (Hawley et al., 2004; Mao et al., 2016) also suggests a good (in some cases improved) performance by the FVCOM-SWAVE model and its suitability for applications in modeling sediment transport.

We also validate predictions of temperature fields to assess the performance of the physical model in simulating circulation and transport. Also, temperature governs biogeochemical processes in the lake and is important for Green Bay restorations studies. As shown in Figure 2, temperature is predicted with high accuracy at four selected buoys, except for over-estimation of mid-range bottom temperature at the location of Green Bay buoy (45014). One possible explanation for that is the model's inability to fully capture cold water intrusion from Lake Michigan into the southern bay. Denser cold water from the lake flows near the bottom while warmer water, coming into the bay from rivers, flows on top; forming a two-layered flow condition in Green Bay (Grunert et al., 2018). Yet, high correlations between predicted and observed water temperature at this location, as well as other buoys, shows that the model is capable of producing the patterns of variability in temperature profiles such as upwelling events.

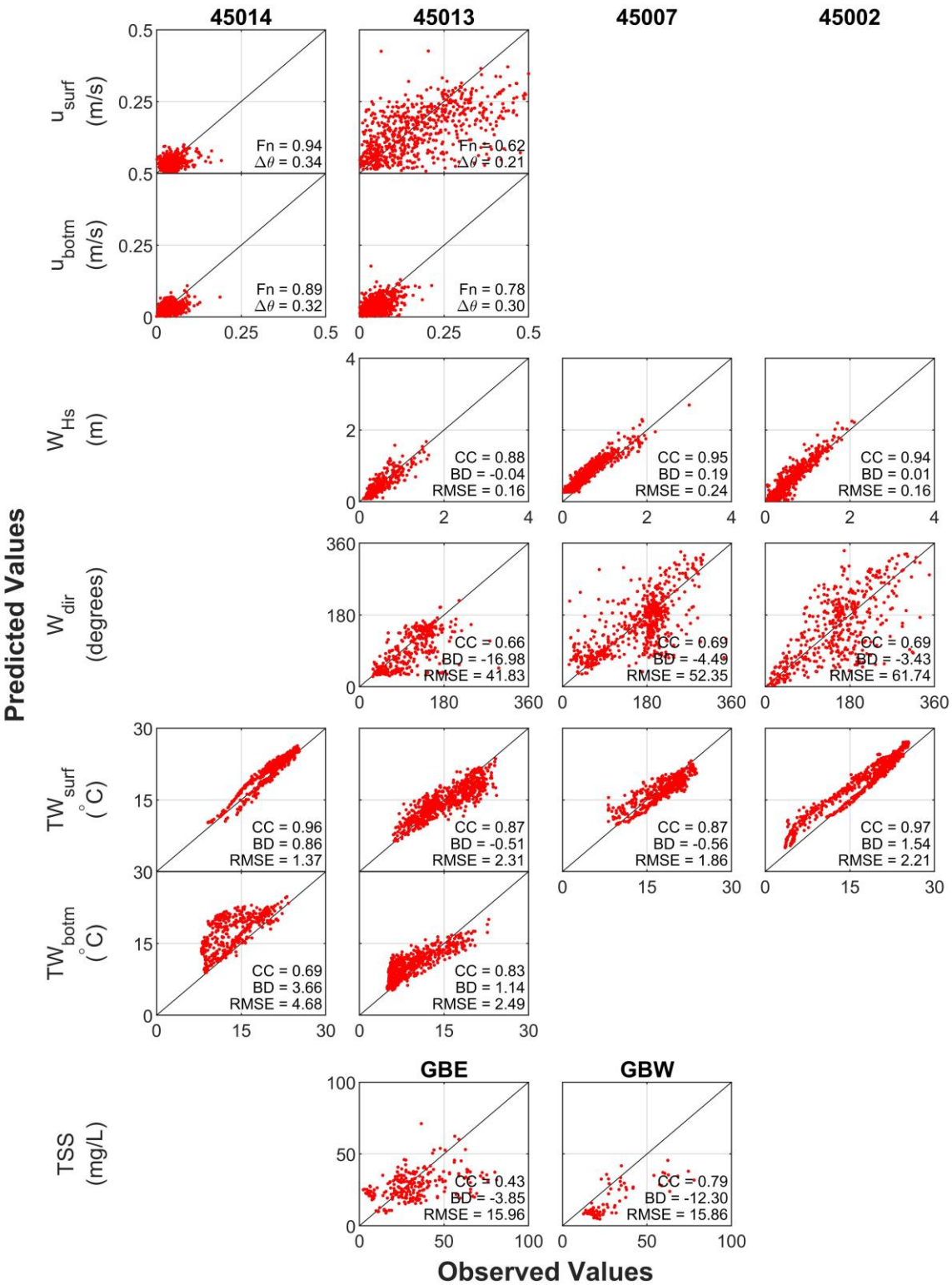


**Figure 2.** Comparison of the daily observed and predicted surface and bottom currents ($u_{surf}$ and $u_{botm}$), significant wave height ($W_{Hs}$) and direction ($W_{dir}$), surface and bottom temperature ($TW_{surf}$ and $TW_{botm}$), and bottom total suspended solids (TSS) at the location of selected validation buoys during 2016-2019 years. Buoy locations are shown in Figure 1. CCs are reported if significant at P-value $\leq 0.05$.

### 4.2 Validation of Simulated Total Suspended Solids

Figure 2 compares predicted daily *TSS* against the observations at GBW and GBE buoys in the Green Bay AOC, where *TSS* observations are available in 2018 and 2019. Turbidity times series obtained at these two locations were converted into *TSS* concentration using *TSS*-turbidity empirical functions for the estimation of river loadings (explained in section 3.4). GBW and GBE buoys are located in very shallow areas of Green Bay (~1 *m* depth) and sensor probes were placed at the mid-depth water column; therefore, observations represent the bottom sediment conditions.

Figure 2 *TSS* implies a fairly good accuracy and overall satisfactory performance of the model, given the physical complexity of the Green Bay system and sediment transport mechanisms. Although the model is biased at GBW buoy, high correlations between observed and predicted *TSS* values at GBW denotes model capability in the simulation of storm events and episodes of resuspensions. Figure S6 of the Supporting Information illustrates examples of resuspension events captured by the model. In some cases, the model significantly underestimated *TSS* observations at both buoys. Those underestimations may be explained by sensor malfunction and/or sudden spikes of *TSS* concentrations due to construction activities near the GBW buoy (e.g., Cat Island project), dredging of Fox River, and navigation channel project.

Figure 3 also compares the surface snapshots of *TSS* concentration based on FVCOM simulations and MODIS imagery for six selected days in 2018. MODIS-based *TSS* maps are estimated based on a procedure explained in Hamidi et al. (2017), using relationships developed between simultaneous surface reflectance and NEW Water *TSS* observations at the location of monitoring stations in lower Green Bay. We used MODIS product *MYD09GA* for the estimation of surface *TSS*. We picked several days during the summer of 2018 by visual inspection, and then used *MYD09GA Surface Reflectance 500m Quality Assurance* and *1km Reflectance Data State QA* layers to filter high-quality and cloud-free data. True-color visualization of raw imagery data is presented in Figure S7 of Supporting Information. Except for small deviations in August that could be explained by inaccurate estimation of *TSS* inputs and/or wind conditions, the model-simulated spatiotemporal patterns of *TSS* in lower Green Bay and decreasing gradient of suspended particles from Green Bay AOC towards Chambers Island match very well with the results of the remote sensing method.

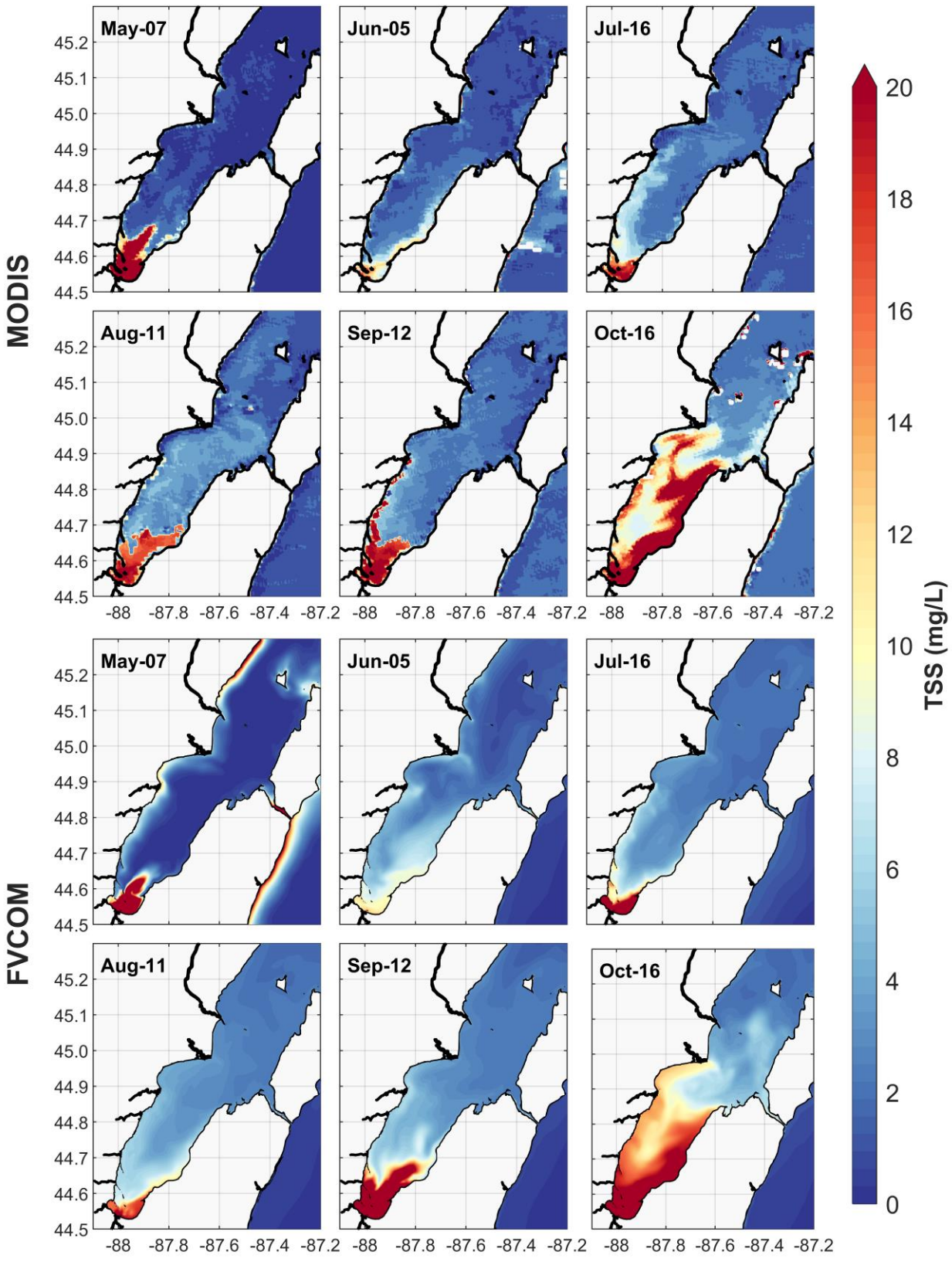


**Figure 3.** Snapshots of the surface total suspended solids (TSS) in Green Bay for six cloud-free selected days in May-October 2018 period based on MODIS imagery (top) and FVCOM simulations (bottom).

# 5 Results and Discussion: Summer Circulation and Transport Regimes in Lake Michigan and Green Bay

The summer circulation and transport regimes are analyzed in sections 5.1 to 5.4 in terms of monthly average fields of wind-induced currents and waves action, bottom shear stress driven by waves and currents, thermal structure, and sediment transport. The results of this study are shown to complement previous modeling studies of Lake Michigan and to provide important additional details on the circulation and transport regimes in Green Bay. Section 5.5 presents and analyzes a climatological study of the summer circulation and transport regimes in Lake Michigan.

## 5.1 Monthly-Averaged Wind-induced Circulation and Wave Action

Circulation and wave actions in Lake Michigan are predominantly wind-driven (Beletsky et al., 2006b), and wind affects the exchange between the Green Bay and Lake Michigan (Waples & Klump, 2002). Figure 4 shows monthly-averaged wind patterns over Lake Michigan, with higher resolution over Green Bay, during the 2016-2019 simulation period. The figure shows stronger wind fields in northern Lake Michigan, as southerly winds accelerate over the approximately 500 *km* lake's longitudinal fetch. Winds are stronger in July-October with prevailing southwesterly and southerly general regimes. Wind patterns over Green Bay are more uniform, yet consistent with winds over Lake Michigan. Eastern winds dominate in May-June, and the wind fields shift to southwesterly and southerly directions in July until October, when winds are the strongest. Analyses of wind fields in the Great Lakes basin, including Lake Michigan, have shown prevailing southwesterly winds during summer, with monthly and seasonal shifts in wind direction/magnitude during 1980-1999 (Waples & Klump, 2002) and Green Bay during 2004-2008 (Hamidi et al., 2015).

In consistency with previous analyses of monthly averaged circulation in Lake Michigan (Beletsky et al., 2006a), Figure 5 shows that cyclonic (counterclockwise) circulation dominates Lake Michigan. Also, currents drive gyres in the lake, and the formation of gyres is more common in the southern basin. Strong currents at the exchange zone affect water, heat, and sediment fluxes between Lake Michigan and Green Bay. In consistency with wind patterns, circulation is weaker in May and currents accelerate starting in June. Bimonthly analysis of currents in the May-October period in Lake Michigan in 1982-1983 and 1994-1995 also suggests

that currents magnitude increase from May to October and currents move counterclockwise and are stronger in the nearshore areas of the southern basin of the lake.

In Green Bay, the currents show more spatial variability than the wind fields, with the widespread formation of gyres, particularly north of Chambers Island and near the exchange zone with Lake Michigan, where strong currents are observed. Currents are generally in the north direction and stronger near the western shore of the bay. Most of these patterns, in particular stronger nearshore currents and frequent formation of gyres in Green Bay during summer, have shown by previous efforts in the simulation of currents in Green Bay for 2004-2008 period using a POM-based circulation model (Hamidi et al., 2015). Those patterns are present along the water column, although currents are much stronger in the surface (Figures S8 and S9 in the Supporting Information).

Current movement and transport in Green Bay are significantly restricted by morphology and lake bottom terrain. Figure 6 shows monthly averaged horizontal current profiles, based on 2016-2019 simulations, along the three cross-sections shown in Figure 1. As illustrated in cross-section A-A' (where red colors show northward currents and blue colors show southward currents along the section), the currents in southern Green Bay (i.e., south of Chambers Island, located at km 85) —which play a main role in the transport of Fox River loads to the northern bay—shift direction in June and move towards the south in the longitudinal cross-section A-A'. The southward current pattern is driven by a combination of wind direction and cold-water intrusion from the lake into the bay as mentioned above. Current profiles north of Chambers Island and south of the exchange zone (between km 85 and km 130) are different from the rest of cross-section. Those patterns can be explained by the presence of gyres in that area, especially away from the shorelines and in the central bay areas where cross-section A-A' cuts through. Figures S8 and S9 in the Supporting information show clearly that the surface currents in Green Bay are predominantly flowing north (especially near the shorelines) and bottom currents flow towards the south, providing more evidence for the summertime stratified flow conditions in the bay.

The current patterns in cross-section B-B' (where red colors show northward currents and blue colors show southward currents perpendicular to the section) show that currents in the western side of Chambers Island are strong and predominantly towards the south. The prevailing

southward and northward currents through the western and eastern sides of Chambers Island, respectively, imply a counterclockwise circulation around the island, as shown in previous studies based on field observations (Hawley & Niester, 1993). Cross-section B-B' shows that, while surface currents are conveying water north, strong currents are moving towards the south near the bottom. Current profiles at cross-section C-C' (where blue colors show currents flowing into the bay and red colors show currents flowing out perpendicular to the section) also provide evidence that lake cold-water intrusion into the bay occurs persistently through deeper sections of the exchange zone profile. Similar to conditions in Chambers Island, currents are regularly swirling around the small islands in this area.

Currents are the dominant driver of circulation and heat transfer in lake systems, yet waves contribute significantly to sediment dynamics, through bottom interactions and resuspension events. According to Figure 7, wave action in Lake Michigan is limited in May-August, gradually increases in September, and escalates in October. In general, the northern basin of Lake Michigan experiences stronger waves, most probably due to dominant southern winds during the modeling period. The wind-dependency of wave actions in Lake Michigan was shown by previous modeling storm and surge peak events (Mao et al., 2016; Mao & Xia, 2017).

In concert with Lake Michigan, waves in the bay are stronger in September and October. Upper Green Bay and the exchange zone experience stronger waves probably due to rapid change in the bottom elevation in that area. As the incoming waves, originated in deep central areas of Lake Michigan, approach shallow waters of Green Bay and small islands at the connecting straits, water depth quickly starts to become less than the wavelength, reducing wave propagation velocity and leading to steepening of the waves and increased wave height.

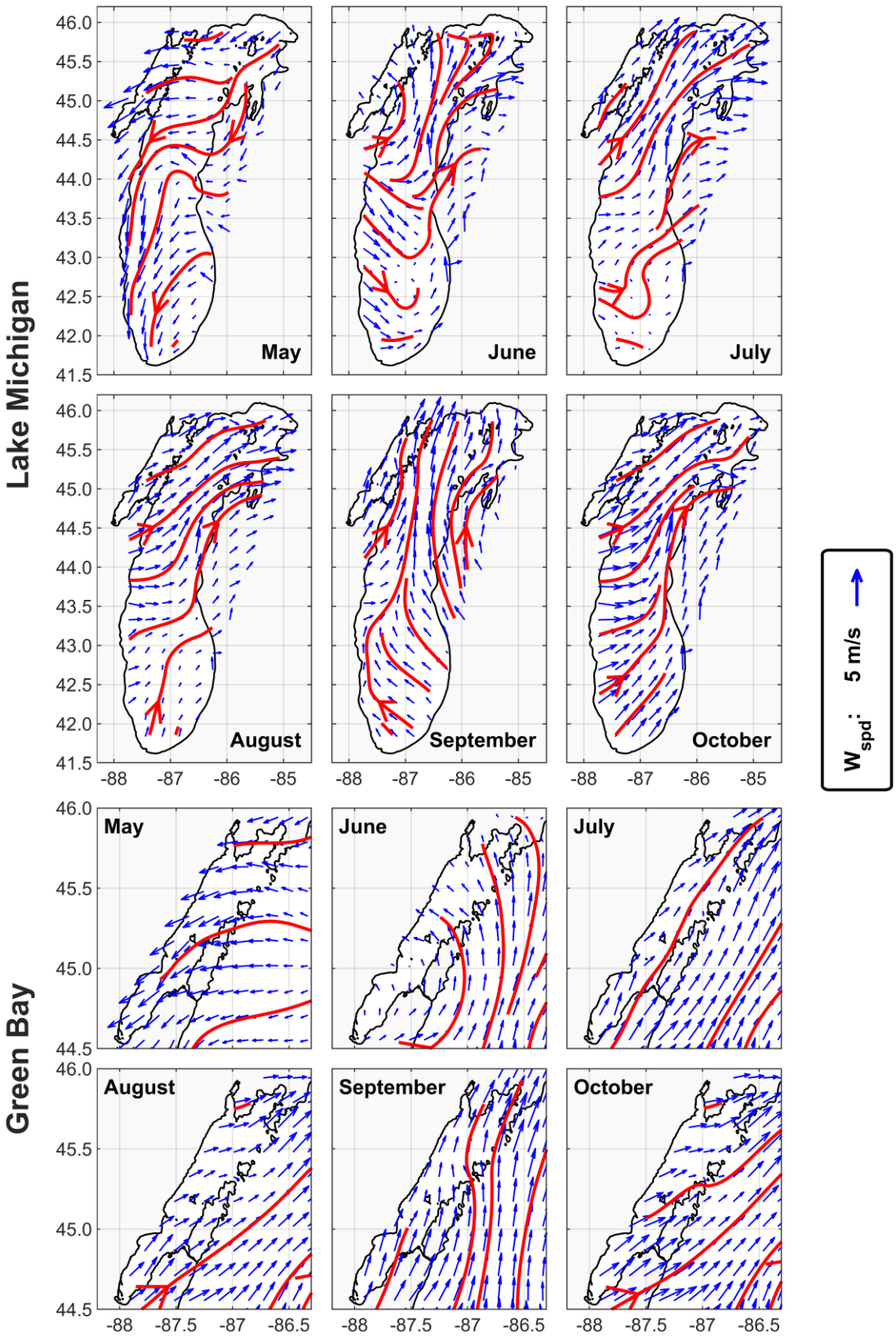


**Figure 4.** Monthly-averaged wind patterns over the surface of Lake Michigan and Green Bay during the period of 2016-2019 years. Bolded red lines indicate dominant wind patterns. $W_{spd}$ denotes wind speed.

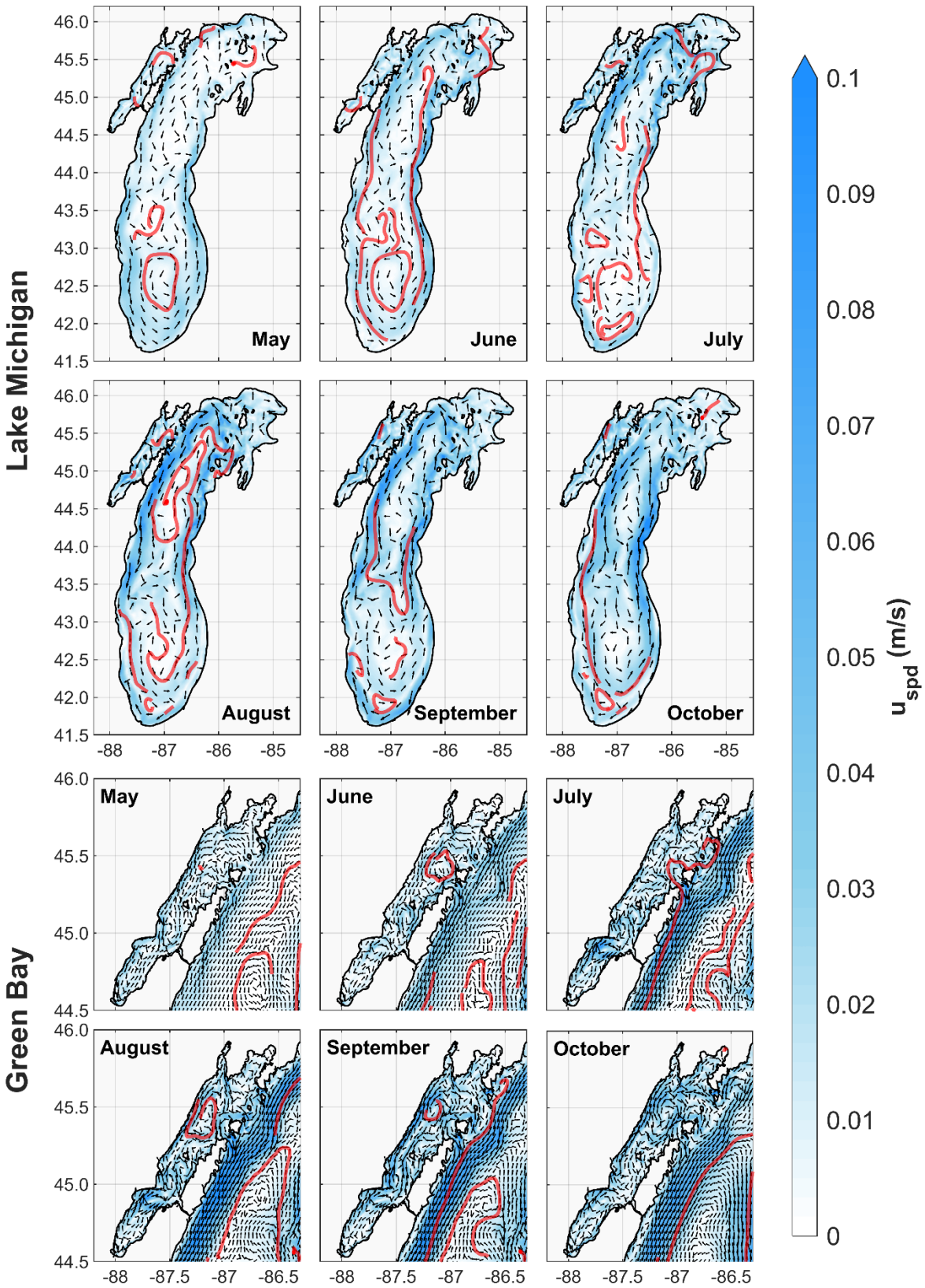


576
577 **Figure 5.** Monthly- and depth-averaged currents in Lake Michigan and Green Bay during the period of 2016-2019
578 years. Bolded red lines indicate dominant circulation patterns. $u_{spd}$ denotes currents magnitude.

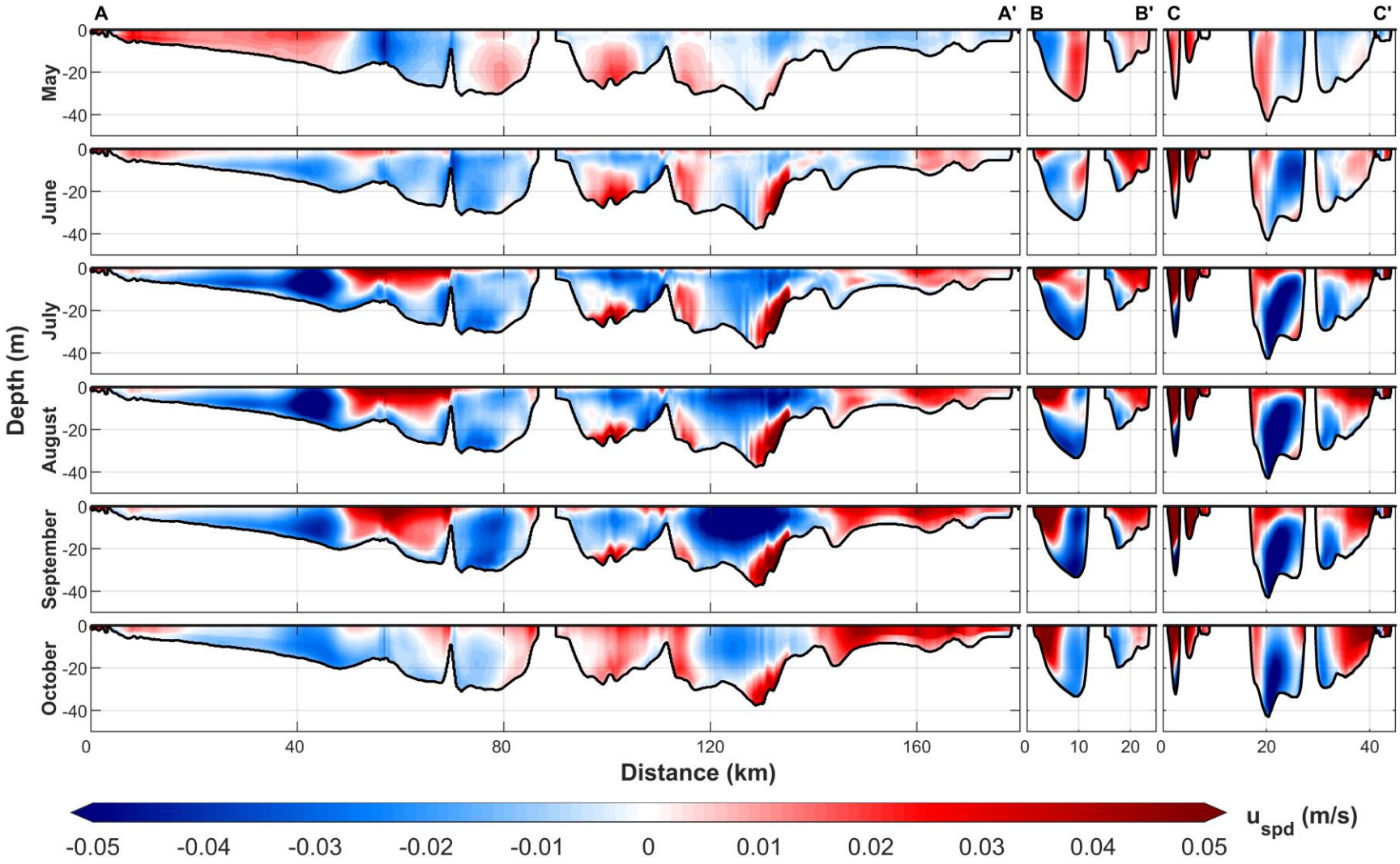


**Figure 6.** Monthly-averaged current profiles along the A-A' (Green Bay longitudinal axis), B-B' (Chambers Island), and C-C' (connecting straits) cross-sections (as shown in Figure 1) during the period of 2016-2019 years. The vertical axis is exaggerated ~700 times. $u_{spd}$ denotes currents magnitude. Colors show current directions along the A-A' cross-section (red/blue indicates northward/southward) and perpendicular to B-B' and C-C' cross-sections (red/blue indicates into/out of cross-sections, respectively).

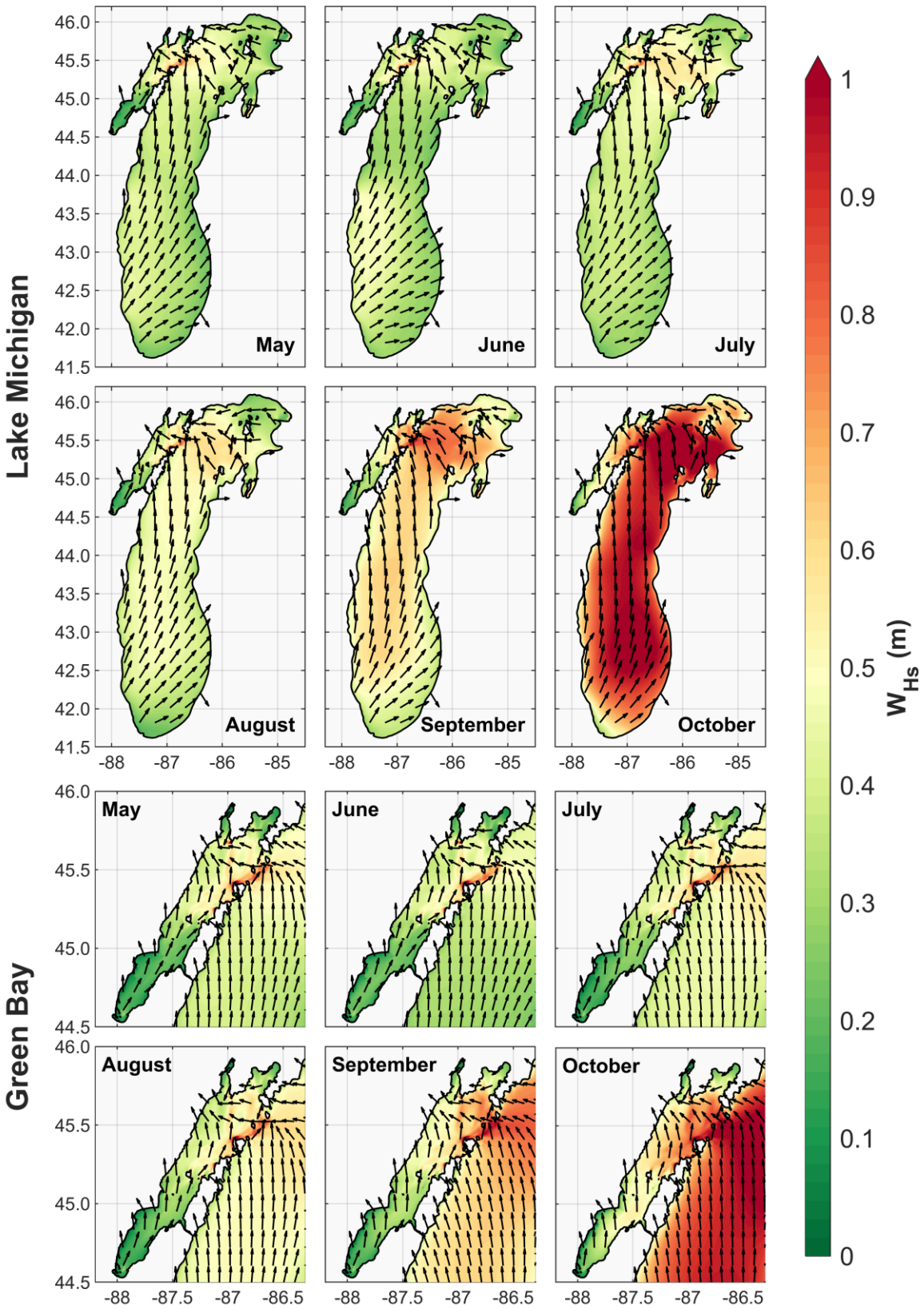


584
585 **Figure 7.** Monthly-averaged significant wave height ($W_{Hs}$) in Lake Michigan and Green Bay during the period of
586 2016-2019 years.

### 5.2 Current-Wave Induced Bottom Shear Stress

Bottom shear stress governs resuspension events and sediment availability in the water column. Figure 8 shows the calculated monthly-averaged bottom shear stress due to the combined effects of current-wave action. While higher shear stress near coastal areas is associated with the stronger nearshore currents, increased wave action in September and October results in augmented shear stress during those months. Western coastal regions, southern and northern shallow areas, and the connecting straits experience higher stress in Green Bay. Also, one would expect strong and frequent resuspension to occur in lower Green Bay in October, produced by the bottom shear stress forcing patterns during that month. Increased shear stress in southwestern Lake Michigan during May is probably associated with a lake-wide cyclonic gyre in the southern basin driven by widespread and strong northerly winds in that area. Southwestern coastal areas of Lake Michigan do not experience such strong wind regimes again until October. Those patterns, in particular high shear stress in the southern and western nearshore areas of Lake Michigan and southern, western, and northern Green Bay, compare well with current and wave bed shear distribution during a March 1998 episode shown by Lee et al. (2007).

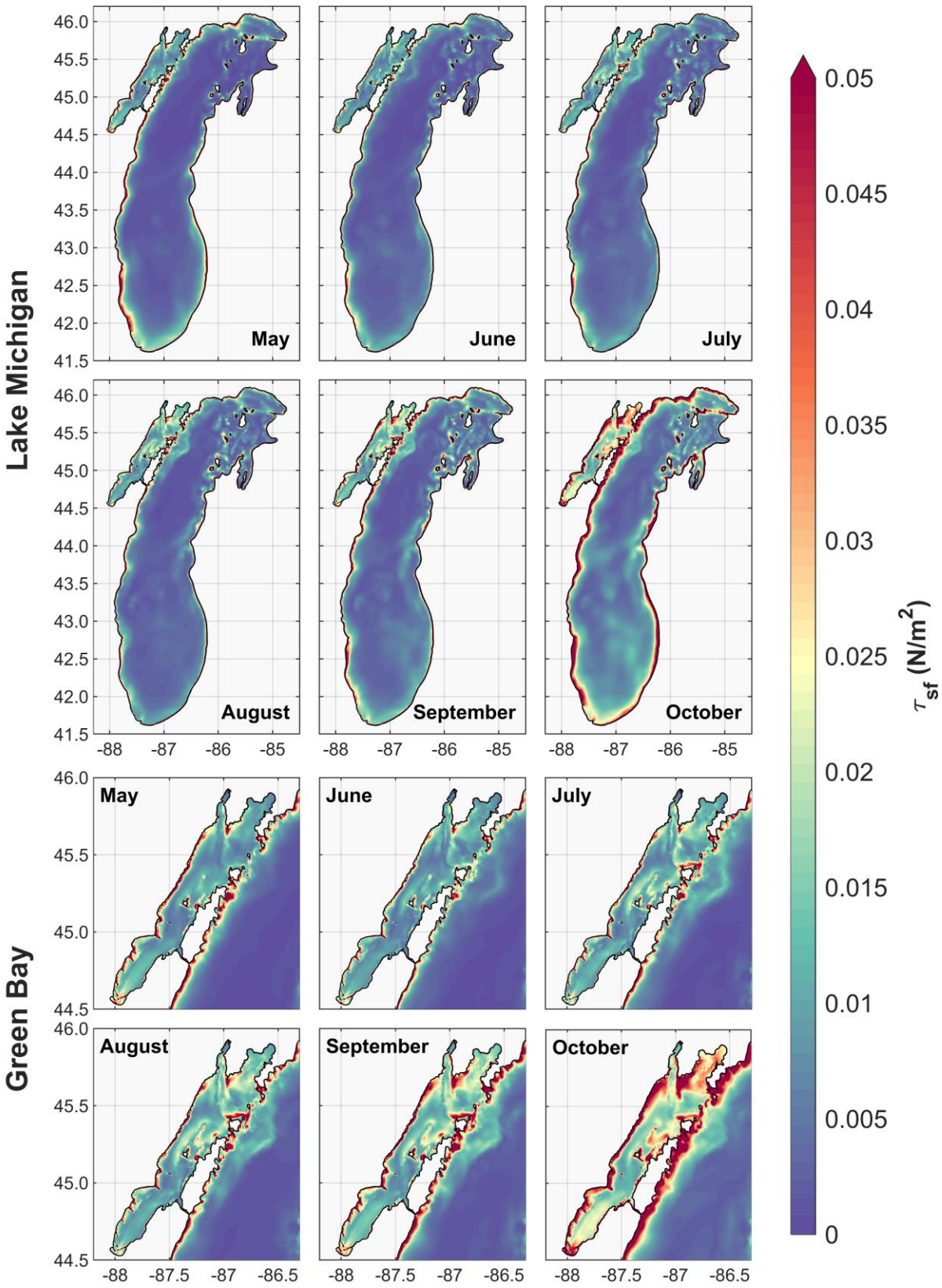


**Figure 8.** Monthly-averaged bottom shear stress ($\tau_{sf}$) due to combined effects of currents and waves in Lake Michigan and Green Bay during the period of 2016-2019 years.

### 5.3 Thermal Structure of the system

Lake Michigan May-October monthly averages surface temperature fields are illustrated in Figure 9, based on 2016-2019 simulations. The southern basin of Lake Michigan is generally warmer than the rest of the lake. Driven by dominant wind direction and coastal upwellings, western nearshore areas of the lake are often slightly colder than the open lake and eastern coastlines. These patterns were also observed by POM-based simulations of thermal structure in Lake Michigan during May-October of 1982-1983 and 1994-1995 (Beletsky & Schwab, 2001). The thermal regime in Green Bay is significantly different than that of Lake Michigan. Warmer temperatures in the bay can be explained by weaker mixing and shallower morphology. July-September are the months with more spatial variability, with higher temperatures in the southern and northern shallow areas, and colder waters near the exchange zone with Lake Michigan, predominantly due to cold water intrusions from the lake.

Stratification is an important aspect of the thermal regime and circulation, and consequently of the ecological functioning of the bay. Figure 10 shows monthly average temperature profiles, based on 2016-2019 simulations, along the three cross-sections shown in Figure 1. The results of this study are consistent with the findings by Hamidi et al. (2015, 2013) and Bravo et al. (2015), showing that stratification in Green Bay starts in June, peaks in July and August, and starts to fade in September, resulting in a duration of about three months. Cross-section A-A' shows that vertical mixing of temperature occurs at faster rates in shallower areas, as expected. The Fox River has a significant influence on the thermal distribution of the southern Green Bay as shown in the first 50 *km* of the cross-section A-A' temperature profiles, closer to the mouth of the Fox River. Cross-section B-B' shows that the temperature gradient is stronger in the western side channel of Chambers Island section compared to the well-mixed, shallower eastern channel. Stratification patterns are preserved at cross-section C-C', where Green Bay meets Lake Michigan, but with a weaker gradient.

One advantage of FVCOM is its ability to capture upwelling events in coastal areas of Lake Michigan. A comparison of simultaneous wind fields, surface currents, and surface temperature fields indicates that northerly and southerly winds promote upwellings on the western and eastern coastal areas, respectively (Figure S10 in the Supporting Information). This

is an important quality when physical models are used to study biogeochemical processes in lake systems.

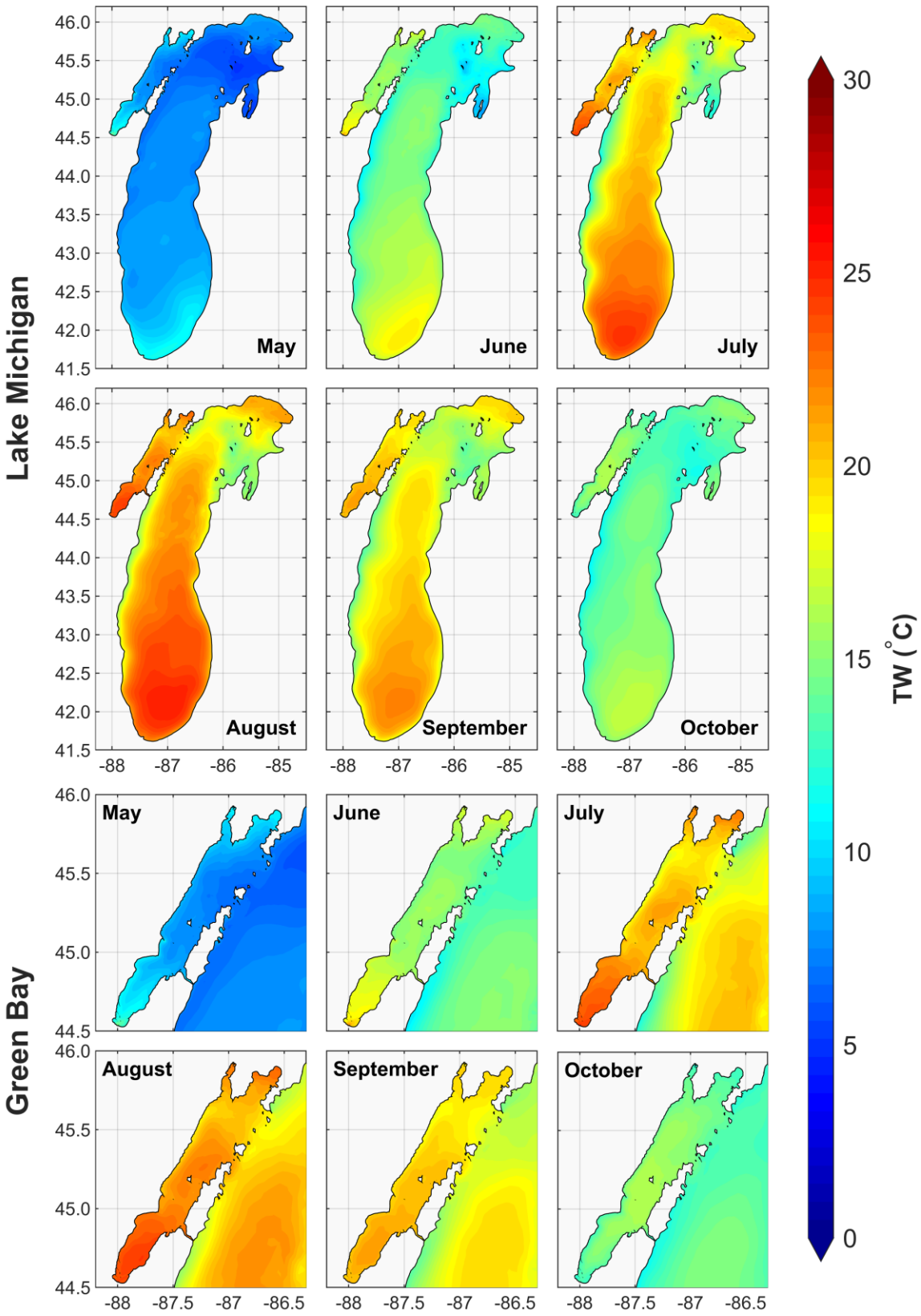


**Figure 9.** Monthly-averaged surface temperature fields (TW) in Lake Michigan and Green Bay during the period of 2016-2019 years.

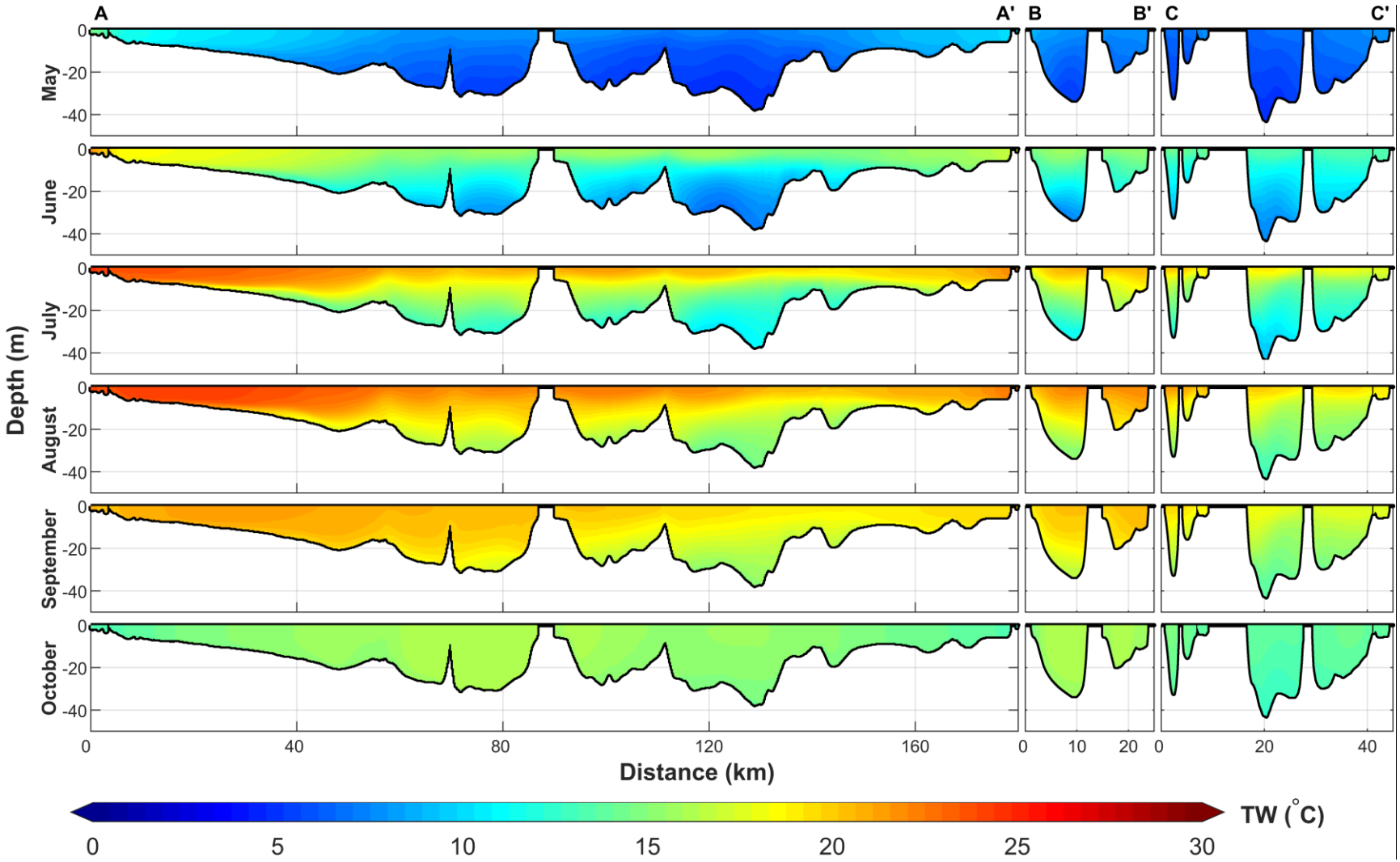


**Figure 10.** Monthly-averaged water temperature (TW) profiles along the A-A' (Green Bay longitudinal axis), B-B' (Chambers Island), and C-C' (connecting straits) cross-sections (as shown in Figure 1) during the period of 2016-2019 years. The vertical axis is exaggerated ~700 times.

644 **5.4 Sediment Transport**

645 Figure 11 shows May-October monthly- and depth-averaged simulated *TSS* concentration
646 in Lake Michigan, with higher resolution in Green Bay, based on 2016-2019 simulations.
647 Consistent with shear stress patterns shown in Figure 8, *TSS* concentration patterns are relatively
648 uniform June through September, with higher concentrations in May and October in the
649 southernmost and northernmost Lake Michigan nearshore areas, as well as southern Green Bay.
650 Periods of resuspension in southwestern Lake Michigan during May are related to wind-driven
651 strong bottom shear stress and the availability of fine-grained sediments in those areas. In almost
652 every month southern Green Bay and southern Lake Michigan experience higher *TSS*
653 concentrations than the rest of the lake. These patterns are similar to those presented by Lee et al.
654 (2007) for March 1998 episodic events, based on physical simulations of sediment transport and
655 satellite imagery-based maps of sediment concentration (Figures 8 and 9 in that article).

656 Sediment transport in Green Bay shows significant differences with the transport patterns
657 in Lake Michigan. The Fox River acts as a point source of *TSS*, and the southern bay shows high
658 *TSS* concentrations every month, while the northern bay is more influenced by the Lake
659 Michigan patterns of transport. In Upper Green Bay the sediment transport is consistent with
660 shear stress patterns and mostly influenced by circulation and waves. The *TSS* spatial distribution
661 in the southern bay seems to be governed by the Fox River persistent and significant *TSS*
662 loading, and by the abundance of fine-grained sediments.

663 An interesting observation in the patterns of sediment circulation in Green Bay is that
664 *TSS* concentration is frequently higher in eastern nearshore areas of lower Green Bay, despite
665 higher current-wave driven shear stresses in the western shorelines. One possible explanation is
666 that the river plume tends to flow along the eastern shore because of the frequent
667 counterclockwise circulation in the southern bay driven by wind direction and the Coriolis effect.
668 In addition, several islands in western Green Bay (shown in Figure S2 in the Supporting
669 Information) cause less and/or weaker resuspensions in that area, therefore, eastern shore
670 contains more sediments, produced mainly by resuspension, than waters near the western shore.

671 The *TSS* concentration profiles along the A-A' longitudinal cross-section of Green Bay,
672 shown in Figure 12, show more sediment dynamics near the mouth of Fox River (point A) and
673 higher *TSS* concentrations in the shallow southern and northern ends of the bay at points A and

A’. The model results show less variability in *TSS* concentration at the Chambers Island (B-B’) and connecting straits (C-C’) cross-sections. Higher sediment concentration west of Chambers Island cross-section (point B) is probably due to stronger currents near the western shoreline. Results also showed higher sediment transport through channels on the north side of the connecting straits (near point C’), probably due to higher shear stresses in that area.

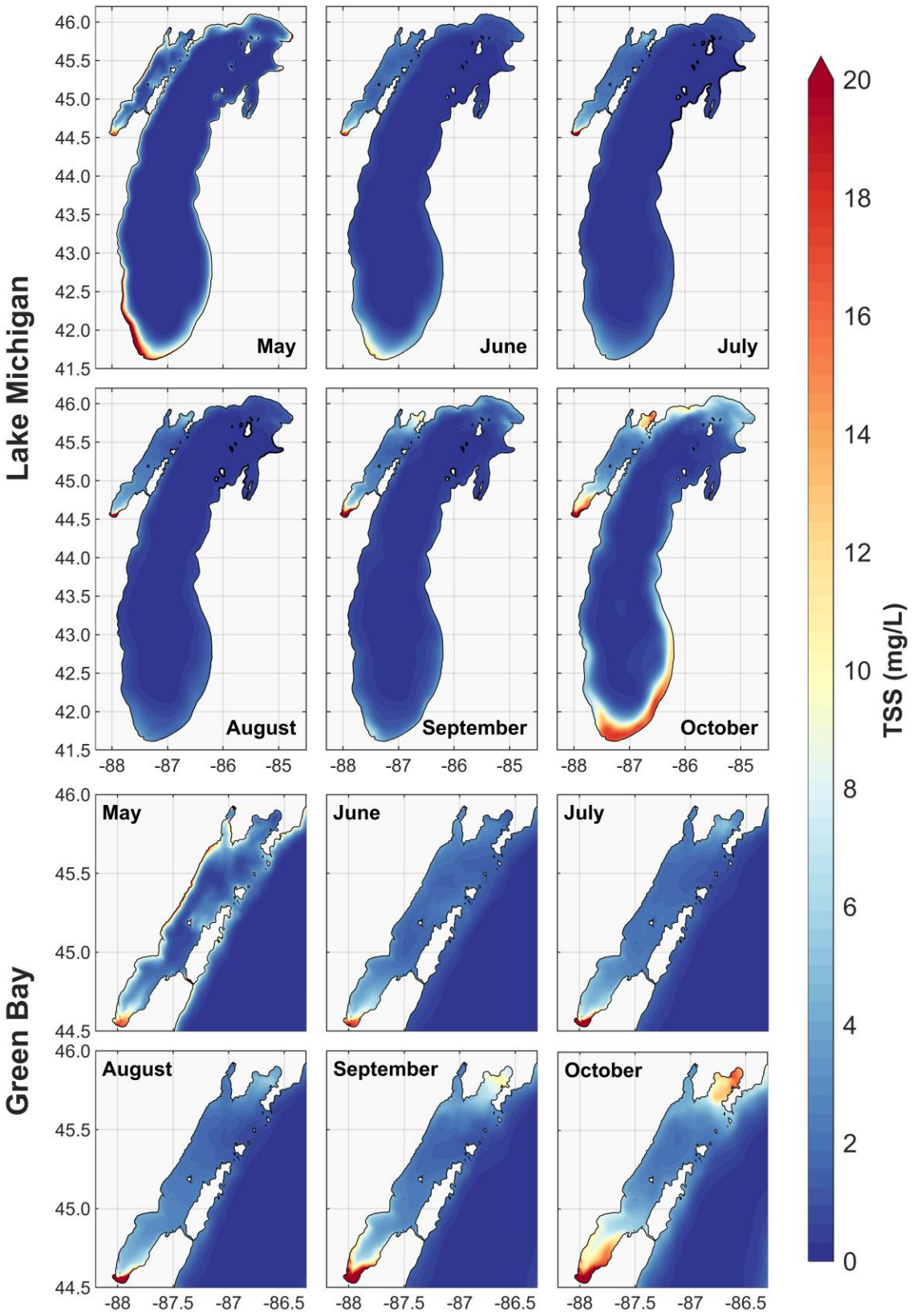


**Figure 11.** Monthly- and depth-averaged total suspended solids (TSS) in Lake Michigan and Green Bay during the period of 2016-2019 years.

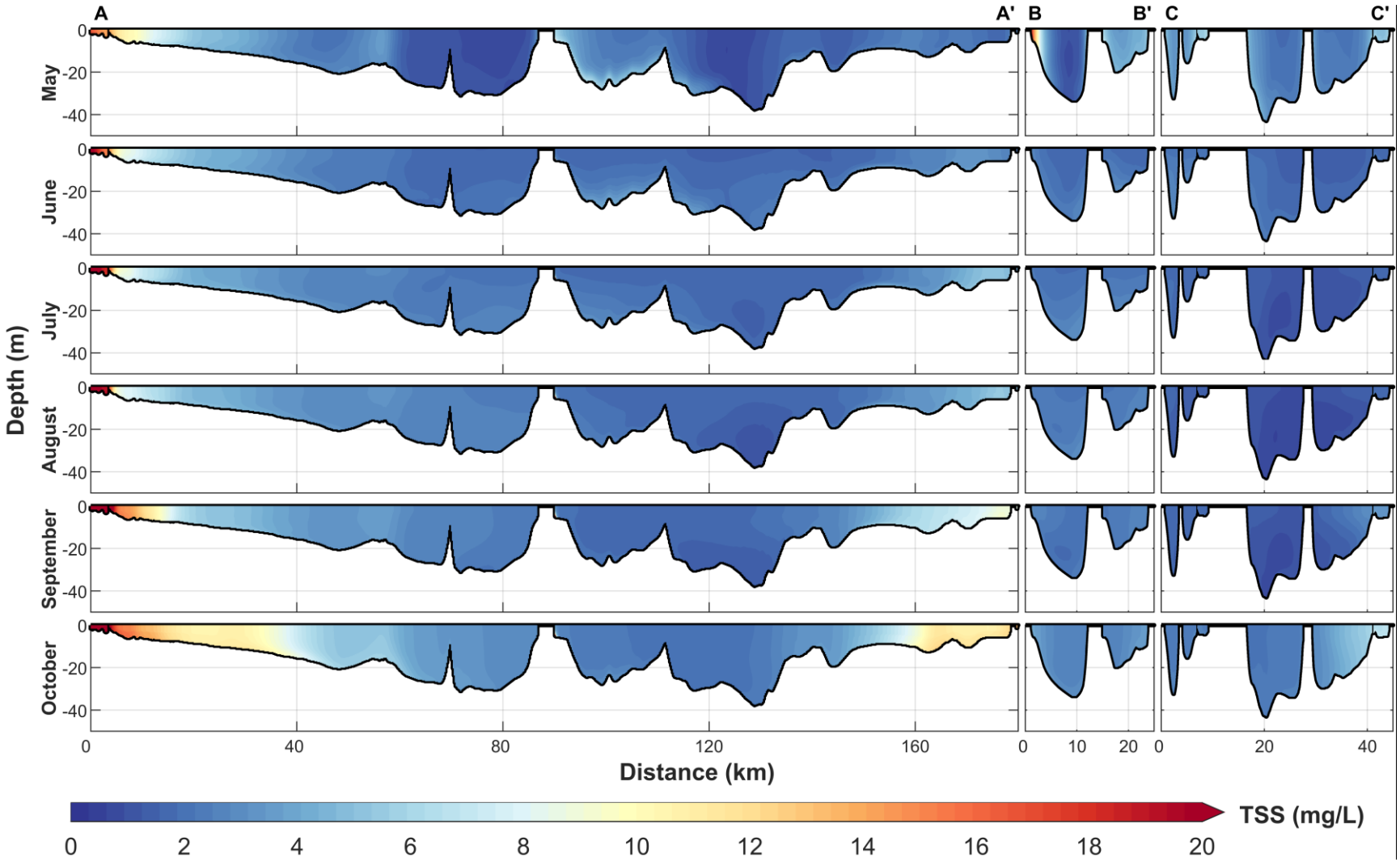


**Figure 12.** Monthly-averaged total suspended solids (TSS) profiles along the A-A' (Green Bay longitudinal axis), B-B' (Chambers Island), and C-C' (connecting straits) cross-sections (as shown in Figure 1) during the period of 2016-2019 years. The vertical axis is exaggerated ~700 times.

### 5.5 Climatological Summer Circulation and Sediment Transport Patterns in Lake Michigan

This section aims to provide maps of summer transport of heat and sediment in Lake Michigan, based simulations using the 2016-2019 meteorological forcing. Figure 13 shows that in general, the prevailing wind direction is southwesterly, and winds are stronger in northern Lake Michigan. The spatial distribution of bottom shear stress shows consistency from year to year, with stronger stresses occurring in the southwestern Lake Michigan, Green Bay, and nearshore areas. The maps of surface temperature show a negative, gradual gradient from south to north and a small decline in surface temperature in the southern basin of the lake from 2016 to 2019. The climatological summer surface water temperature in Green Bay was fairly uniform during the simulation period, except that it was somewhat colder near the exchange zone with Lake Michigan.

The map of *TSS* concentration was fairly steady during the simulation period, but there was a small decrease in *TSS* concentration in southwestern Lake Michigan from 2016 to 2019. That temporal pattern was consistent with decreasing winds over the southern lake surface during that period. Northern Lake Michigan showed neither temporal variability in *TSS* patterns nor dependency on wind fields. Those results imply that sediment dynamics in the southern basin is more sensitive to wind and meteorological variability. That is an important pattern to be considered in coastal conservation and shoreline protection.

The maps of *TSS* concentration showed a different temporal trend in lower Green Bay compared to the whole lake. While *TSS* concentration showed a decreasing temporal trend in southern Lake Michigan, sediment concentration increased in lower Green Bay between 2016 and 2019. The increase is probably due to increased loading rates into the bay and confirms the importance of including the tributary loads, especially from the Fox River in modeling sediment transport and biogeochemical interactions in Green Bay.

The findings of this research confirm the results of previous studies by showing the importance of wind forcing in the circulation and transport in Lake Michigan. Wind forcing is a primary driver of circulation in Lake Michigan and Green Bay and can influence biogeochemical processes by governing the thermal structure of the lake and the fate and transport of sediments. Wind patterns should be given particular attention in restoration studies for Green Bay.

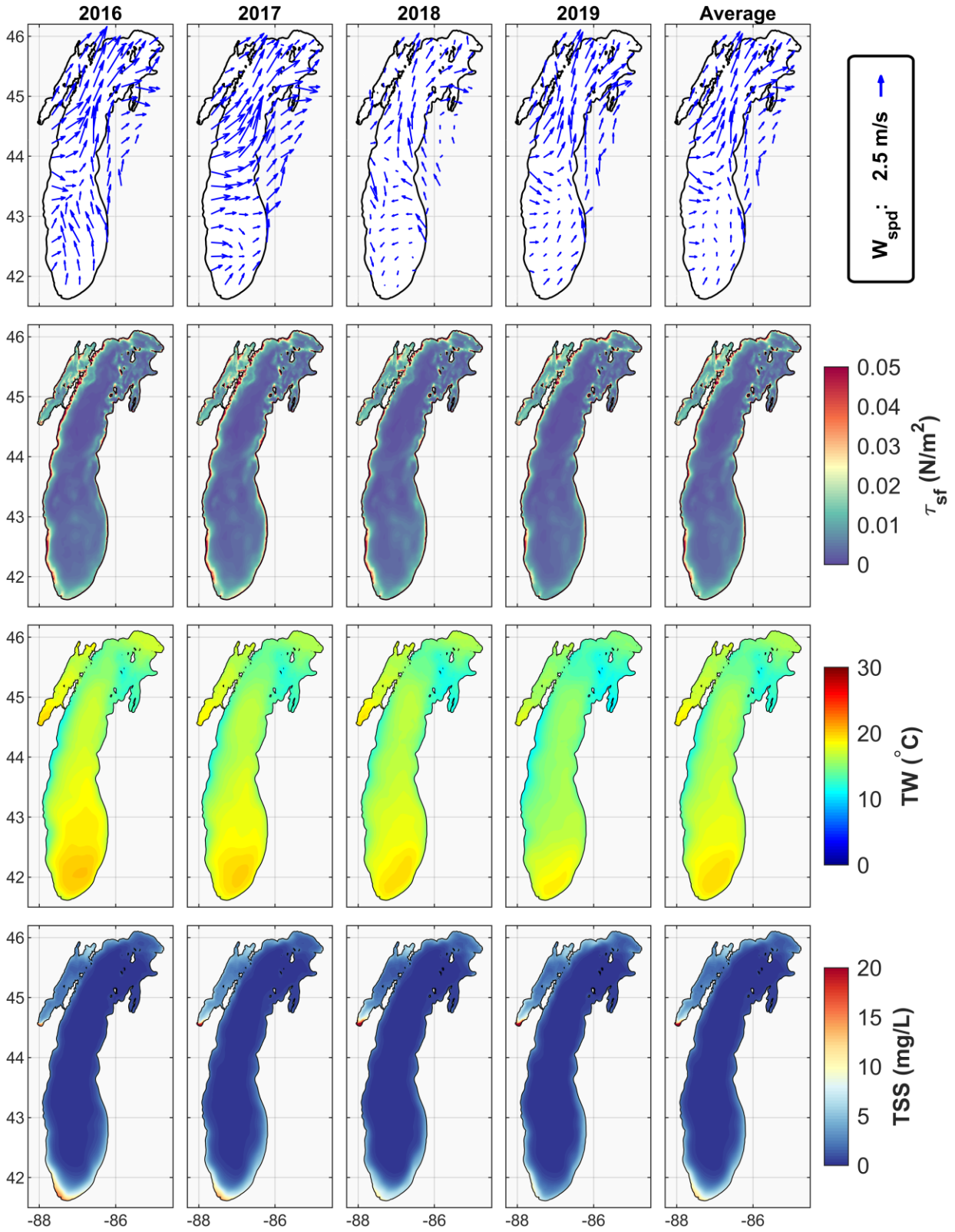


**Figure 13.** Average annual wind fields ($W_{spd}$), current-wave driven bottom shear stress ($\tau_{sf}$), surface temperature fields (TW), and depth-averaged total suspended solids (TSS) in Lake Michigan during the period of 2016-2019 years. The last column shows the average for four simulated years.

## 6 Conclusions

Programs designed to reverse environmental degradation in Green Bay require sound understanding of the links between sediment dynamics and biogeochemical processes. In order to contribute to such understanding, a model was built using the existing database of hydrodynamic, wave, and sediment field data, and simulates within a unique platform the circulation, thermal regime, wind waves, and sediment transport in Lake Michigan, with detailed resolution in Green Bay. A single model of the lake, with detailed resolution in the bay, overcomes conceptual and computational problems that appeared in previously developed nested models.

The physically-based sediment transport model for Lake Michigan and Green Bay was built based on the coupled models FVCOM circulation, FVCOM-SWAVE, and FVCOM-SED to account for sediment interactions based on combined current-wave actions. An important feature of this model is the implementation of a fine resolution grid in Green Bay, updated based on the Cat Island and dredging of navigation channel projects. The Fox and Menominee Rivers are the main tributaries to Green Bay and are included in the model as input boundary conditions and point sources of *TSS* loading to the bay.

The validation of the three models showed overall satisfactory performance, revealed the need for additional field data, and can be used to improve the design of future data collections and monitoring programs. For example, some difficulties in modeling bottom water temperature in Green Bay could be overcome with an updated bathymetry of Green Bay that provides a more accurate model geometry for hydrodynamic simulations and enhances the model capability to capture events of lake water intrusion into the bay. Systematic collection and analysis of bottom samples in Green Bay can improve the performance of the sediment transport model by providing more complete information on the spatial distribution of bottom sediment classes (cohesive or non-cohesive) and sediment characteristics (sizes, settling velocity, critical stress for resuspension, and erosion rates). Observations of sediment concentrations at different locations of the bay, including concentration during resuspension events could help to further improve model development, calibration, and validation. Given the complexity of the system, limited information about sediment distribution and characteristics in Green Bay and Lake Michigan, and uncertainties associated with the implementation of sediment transport physics in a 3D

space, FVCOM-SED showed potential to be a sound platform to investigate sediment dynamics in Green Bay.

The model was used to analyze the summer patterns of circulation, wave action, current- and wave-induced bottom shear stress, thermal structure, and sediment transport in Lake Michigan. The model confirms the findings of previous studies and new insights on all those physical processes in Green Bay. The analysis of summer patterns is presented via monthly averaged maps and climatological summer maps.

Ongoing research will use the model to evaluate sediment dynamics in the bay under different climate conditions and loading scenarios in river/watershed management and flow or total maximum daily load regulation purposes. The model will also be used to evaluate the impact of remedial activities. Plans for future studies include applications of the model as a tool in the design of restoration projects and understanding the links between sediment processes—such as resuspension events and erosion/deposition patterns—and biogeochemical processes in the bay.

## Acknowledgments

This project was funded partially by the University of Wisconsin Sea Grant Omnibus Program Grant 144-AAG3496-UWMKE19A. We appreciate Jeff Houghton for assistance in the fieldwork, Jim Wagner and Jason Bacon for IT support, and Jessie Grow, Dr. Sarah Bartlett, and Dr. Todd Miller for providing field data in Green Bay and Milwaukee Nearshore zone in Lake Michigan.

Lake Michigan bathymetry and shoreline data are obtained from NOAA National Geophysical Data Center (http://maps.ngdc.noaa.gov/viewers/bathymetry/). Input meteorological forcing data is based on NOAA National Centers for Environmental Information (https://www.ncei.noaa.gov/). Buoy observations were also downloaded from NOAA National Data Buoy Center (https://www.ndbc.noaa.gov/), Great Lakes Observing System (https://uwm.edu/glos/), and *lakestat* monitoring program (http://www.lakestat.com/). River inputs are also based on the USGS National Water Information System database (https://waterdata.usgs.gov/nwis). Lake Michigan water level data is downloaded from NOAA Tides and Currents dataset (https://tidesandcurrents.noaa.gov/stations.html?type=Water+Levels).

Turbidity and *TSS* in-situ observations at the mouth of Fox River are provided based on personal communications with Dr. Sarah Bartlett at the NEW Water (http://newwater.us/programs-initiatives/aquatic-monitoring-program/). MODIS imagery products are obtained from the NASA EARTHDATA platform (https://earthdata.nasa.gov/). This is GLERL contribution number XXXX.

## References

Allinger, L. E., & Reavie, E. D. (2013, September 1). The ecological history of Lake Erie as recorded by the phytoplankton community. *Journal of Great Lakes Research*. Elsevier. https://doi.org/10.1016/j.jglr.2013.06.014

Anderson, E. J., & Phanikumar, M. S. (2011). Surface storage dynamics in large rivers: Comparing three-dimensional particle transport, one-dimensional fractional derivative, and multirate transient storage models. *Water Resources Research*, *47*(9). https://doi.org/10.1029/2010WR010228

Anderson, E. J., & Schwab, D. J. (2011). Relationships between wind-driven and hydraulic flow in Lake St. Clair and the St. Clair River Delta. *Journal of Great Lakes Research*, *37*(1), 147–158. https://doi.org/10.1016/J.JGLR.2010.11.007

Anderson, E. J., & Schwab, D. J. (2013). Predicting the oscillating bi-directional exchange flow in the Straits of Mackinac. *Journal of Great Lakes Research*, *39*(4), 663–671. https://doi.org/10.1016/j.jglr.2013.09.001

Anderson, E. J., Schwab, D. J., & Lang, G. A. (2010). Real-Time Hydraulic and Hydrodynamic Model of the St. Clair River, Lake St. Clair, Detroit River System. *Journal of Hydraulic Engineering*, *136*(8), 507–518. https://doi.org/10.1061/(ASCE)HY.1943-7900.0000203

Ariathurai, R., & Arulanandan, K. (1978). Erosion Rates of Cohesive Soils. *J Hydr Div, ASCE*, *101*(5), 635–639.

Bai, X., Wang, J., Schwab, D. J., Yang, Y., Luo, L., Leshkevich, G. A., & Liu, S. (2013). Modeling 1993–2008 climatology of seasonal general circulation and thermal structure in the Great Lakes using FVCOM. *Ocean Modelling*, *65*, 40–63. https://doi.org/10.1016/J.OCEMOD.2013.02.003

808 Battjes, J. A., & Janssen, J. P. F. M. (1978). Energy Loss and Set-Up Due to Breaking of
809 Random Waves. In *Coastal Engineering 1978* (pp. 569–587). New York, NY: American
810 Society of Civil Engineers. https://doi.org/10.1061/9780872621909.034

811 Beletsky, D., & Schwab, D. J. (2001). Modeling circulation and thermal structure in Lake
812 Michigan: Annual cycle and interannual variability. *Journal of Geophysical Research:*
813 *Oceans*, *106*(C9), 19745–19771. https://doi.org/10.1029/2000JC000691

814 Beletsky, D., O'Connor, W. P., Schwab, D. J., Dietrich, D. E., Beletsky, D., O'Connor, W. P., et
815 al. (1997). Numerical Simulation of Internal Kelvin Waves and Coastal Upwelling Fronts*.
816 *Http://Dx.Doi.Org/10.1175/1520-0485(1997)027<1197:NSOIKW>2.0.CO;2*.
817 https://doi.org/10.1175/1520-0485(1997)027<1197:NSOIKW>2.0.CO;2

818 Beletsky, D., Schwab, D. J., Roebber, P. J., McCormick, M. J., Miller, G. S., & Saylor, J. H.
819 (2003). Modeling wind-driven circulation during the March 1998 sediment resuspension
820 event in Lake Michigan. *Journal of Geophysical Research: Oceans*, *108*(C2), n/a-n/a.
821 https://doi.org/10.1029/2001JC001159

822 Beletsky, D., Schwab, D., & McCormick, M. (2006a). Modeling the 1998-2003 summer
823 circulation and thermal structure in Lake Michigan. *Journal of Geophysical Research:*
824 *Oceans*, *111*(10), 1–18. https://doi.org/10.1029/2005JC003222

825 Beletsky, D., Schwab, D., & McCormick, M. (2006b). Modeling the 1998–2003 summer
826 circulation and thermal structure in Lake Michigan. *Journal of Geophysical Research*,
827 *111*(C10), C10010. https://doi.org/10.1029/2005JC003222

828 Booij, N., Ris, R. C., & Holthuijsen, L. H. (1999). A third-generation wave model for coastal
829 regions: 1. Model description and validation. *Journal of Geophysical Research: Oceans*,
830 *104*(C4), 7649–7666. https://doi.org/10.1029/98JC02622

831 Booij, N., Haagsma, I. J. G., Holthuijsen, L. H., Kieftenburg, A. T. M. M., Ris, R. C., van der
832 Westhuysen, A. J., & Zijlema, M. (2004). *SWAN Cycle III version 40.51 Technical*
833 *documentation*. Delft, The Netherlands.

834 Bravo, H. R., Hamidi, S. A., Klump, J. V., & Waples, J. T. (2015). Currents and heat fluxes
835 induce stratification leading to hypoxia in Green Bay, Lake Michigan. *E-Proceedings of the*
836 *36th IAHR World Congress*, (1985), 1–10.

837 Bravo, H. R., Bootsma, H., & Khazaei, B. (2019). Fate of phosphorus from a point source in the
838 Lake Michigan nearshore zone. *Journal of Great Lakes Research*, *45*(6), 1182–1196.
839 https://doi.org/10.1016/j.jglr.2019.09.007

840 Bravo, H. R., Hamidi, S. A., Anderson, E. J., Klump, J. V., & Khazaei, B. (2019). Timescales of
841 Transport Through Lower Green Bay. *Journal of Great Lakes Research*, (In Press.).
842 https://doi.org/https://doi.org/10.1016/j.jglr.2020.06.010

843 Chen, C., Liu, H., & Beardsley, R. C. (2003). An unstructured grid, finite-volume, three-
844 dimensional, primitive equations ocean model: Application to coastal ocean and estuaries.
845 *Journal of Atmospheric and Oceanic Technology*, *20*(1), 159–186.
846 https://doi.org/10.1175/1520-0426(2003)020<0159:AUGFVT>2.0.CO;2

847 Chen, C., Huang, H., Beardsley, R. C., Liu, H., Xu, Q., & Cowles, G. (2007). A finite volume
848 numerical approach for coastal ocean circulation studies: Comparisons with finite difference
849 models. *Journal of Geophysical Research*, *112*(C3), C03018.
850 https://doi.org/10.1029/2006JC003485

851 Chen, C., Beardsley, R. C., Cowles, G., Qi, J., Lai, Z., Gao, G., et al. (2013). *An Unstructured
852 Grid , Finite-Volume Community Ocean Model FVCOM User Manual*. Retrieved from
853 http://fvcom.smast.umassd.edu/

854 Chen, T., Zhang, Q., Wu, Y., Ji, C., Yang, J., & Liu, G. (2018). Development of a wave-current
855 model through coupling of FVCOM and SWAN. *Ocean Engineering*, *164*, 443–454.
856 https://doi.org/10.1016/J.OCEANENG.2018.06.062

857 Clites, A. H., Smith, J. P., Hunter, T. S., & Gronewold, A. D. (2014). Visualizing relationships
858 between hydrology, climate, and water level fluctuations on Earth's largest system of lakes.
859 *Journal of Great Lakes Research*, *40*(3), 807–811.
860 https://doi.org/10.1016/J.JGLR.2014.05.014

861 Destouni, G., Asokan, S. M., & Jarsjö, J. (2010). Inland hydro-climatic interaction: Effects of
862 human water use on regional climate. *Geophysical Research Letters*, *37*(18), n/a-n/a.
863 https://doi.org/10.1029/2010GL044153

864 Eadie, B. J., Bell, G. L., & Hawley, N. (1991). *Sediment Trap Study in the Green Bay Mass
865 Balance Program: Mass and Organic Carbon Fluxes, Resuspension, and Particle Settling*

*Velocities*. NOAA Technical Memorandum ERL GLERL-75. Great Lakes Environmental Research Laboratory Ann Arbor, Michigan July 1991.

García, M. H. (2008). Sediment Transport and Morphodynamics. In M. H. García (Ed.), *Sedimentation Engineering: Processes, Measurements, Modeling, and Practice* (pp. 21–163). Reston, VA: American Society of Civil Engineers. https://doi.org/10.1061/9780784408148.ch02

Grunert, B. K., Brunner, S. L., Hamidi, S. A., Bravo, H. R., & Klump, J. V. (2018). Quantifying the influence of cold water intrusions in a shallow, coastal system across contrasting years: Green Bay, Lake Michigan. *Journal of Great Lakes Research*, *44*(5), 851–863. https://doi.org/10.1016/J.JGLR.2018.07.009

Guerra, M., Cienfuegos, R., Thomson, J., & Suarez, L. (2017). Tidal energy resource characterization in Chacao Channel, Chile. *International Journal of Marine Energy*, *20*, 1–16. https://doi.org/10.1016/J.IJOME.2017.11.002

Hamidi, Sajad Ahamd, Bravo, H. R., & Klump, J. V. (2013). Evidence of Multiple Physical Drivers on the Circulation and Thermal Regime in the Green Bay of Lake Michigan. In *World Environmental and Water Resources Congress 2013* (pp. 1719–1726). Reston, VA: American Society of Civil Engineers. https://doi.org/10.1061/9780784412947.169

Hamidi, Sajad Ahmad, Bravo, H. R., Val Klump, J., & Waples, J. T. (2015). The role of circulation and heat fluxes in the formation of stratification leading to hypoxia in Green Bay, Lake Michigan. *Journal of Great Lakes Research*, *41*(4), 1024–1036. https://doi.org/10.1016/j.jglr.2015.08.007

Hamidi, Sajad Ahmad, Hosseiny, H., Ekhtari, N., & Khazaei, B. (2017). Using MODIS remote sensing data for mapping the spatio-temporal variability of water quality and river turbid plume. *Journal of Coastal Conservation*, *21*(6), 939–950. https://doi.org/10.1007/s11852-017-0564-y

Harris, C. K., & Wiberg, P. L. (2001). A two-dimensional, time-dependent model of suspended sediment transport and bed reworking for continental shelves. *Computers & Geosciences*, *27*(6), 675–690. https://doi.org/10.1016/S0098-3004(00)00122-9

Harris, H. J., Wenger, R. B., Sager, P. E., & Val Klump, J. (2018). The Green Bay saga:

Environmental change, scientific investigation, and watershed management. *Journal of Great Lakes Research*, *44*(5), 829–836. https://doi.org/10.1016/J.JGLR.2018.08.001

Harris, V. A., & Christie, J. (1987). *The lower Green Bay Remedial Action Plan: nutrient and eutrophication management. Technical Advisory Committee report*. Publication No. WR-167-87. Wisconsin Department of Natural Resources. Madison, WI.

Hasselmann, K., Barnett, T. P., Bouws, E., Carlson, H. K., Cartwright, D. E., Enke, K., et al. (1973). Measurements of wind-wave growth and swell decay during the Joint North Sea Wave Project (JONSWAP).

Hasselmann, S., Hasselmann, K., Allender, J. H., & Barnett, T. P. (1985). Computations and Parameterizations of the Nonlinear Energy Transfer in a Gravity-Wave Specturm. Part II: Parameterizations of the Nonlinear Energy Transfer for Application in Wave Models. *Journal of Physical Oceanography*, *15*(11), 1378–1391. https://doi.org/10.1175/1520-0485(1985)015<1378:CAPOTN>2.0.CO;2

Hawley, N., & Niester, J. (1993). Measurement of Horizontal Sediment Transport in Green Bay, May-October, 1989. *Journal of Great Lakes Research*, *19*(2), 368–378. https://doi.org/10.1016/S0380-1330(93)71225-3

Hawley, N., Lesht, B. M., & Schwab, D. J. (2004). A comparison of observed and modeled surface waves in southern Lake Michigan and the implications for models of sediment resuspension. *Journal of Geophysical Research*, *109*(C10), C10S03. https://doi.org/10.1029/2002JC001592

Hecky, R. E., Bootsma, H. A., & Kingdon, M. L. (2003). Impact of land use on sediment and nutrient yields to Lake Malawi/Nyasa (Africa). *Journal of Great Lakes Research*, *29*(SUPPL. 2), 139–158. https://doi.org/10.1016/S0380-1330(03)70544-9

Huang, H., Chen, C., Cowles, G. W., Winant, C. D., Beardsley, R. C., Hedstrom, K. S., & Haidvogel, D. B. (2008). FVCOM validation experiments: Comparisons with ROMS for three idealized barotropic test problems. *Journal of Geophysical Research*, *113*(C7), C07042. https://doi.org/10.1029/2007JC004557

HydroQual Inc. (1999). *Hydrodynamics, Sediment Transport, and Sorbent Dynamics in Green Bay*. Report to Wisconsin Department of Natural Resources, Madison, Wisconsin.

924 Jones, C. A. (2000). *An Accurate Model of Sediment Transport*. University of California, Santa
925 Barbara.

926 Khazaei, B. (2020). *Development of a Hydrodynamic and Sediment Transport Model for Green*
927 *Bay, Lake Michigan*. University of Wisconsin-Milwaukee.

928 Khazaei, B., & Wu, C. (2018). Estimation of Vegetation Coverage Based on Seasonal
929 Variabilities in MODIS-Based Vegetation Indices. In *World Environmental and Water*
930 *Resources Congress 2018* (pp. 11–20). Reston, VA: American Society of Civil Engineers.
931 https://doi.org/10.1061/9780784481400.002

932 Khazaei, B., Hamidi, S. A., & Nabizadeh, A. (2018). An Empirical Approach to Estimate Total
933 Suspended Sediment using Observational Data in Fox River and Southern Green Bay, WI.
934 In *World Environmental and Water Resources Congress*. Minneapolis, MN, USA.

935 Khazaei, B., Anderson, E. J., Klump, J. V., & Bravo, H. R. (2019). Development of an Fvcom-
936 Based 3-D Sediment Transport Model for Green Bay, Lake Michigan. In *E-proceedings of*
937 *the 38th IAHR World Congress, Panama City, Panama, September 1-6* (pp. 68–82).
938 Panama City, Panama: IAHR. https://doi.org/10.3850/38WC092019-1680

939 Klump, J. V., Brunner, S. L., Grunert, B. K., Kaster, J. L., Weckerly, K., Houghton, E. M., et al.
940 (2018). Evidence of persistent, recurring summertime hypoxia in Green Bay, Lake
941 Michigan. *Journal of Great Lakes Research*, *44*(5), 841–850.
942 https://doi.org/10.1016/J.JGLR.2018.07.012

943 Klump, J. Val, Fitzgerald, S. A., & Waplesa, J. T. (2009). Benthic biogeochemical cycling,
944 nutrient stoichiometry, and carbon and nitrogen mass balances in a eutrophic freshwater
945 bay. *Limnology and Oceanography*, *54*(3), 692–712.
946 https://doi.org/10.4319/lo.2009.54.3.0692

947 Klump, J. Val, Bratton, J., Fermanich, K., Forsythe, P., Harris, H. J., Howe, R. W., & Kaster, J.
948 L. (2018). Green Bay, Lake Michigan: A proving ground for Great Lakes restoration.
949 *Journal of Great Lakes Research*, *44*(5), 825–828.
950 https://doi.org/10.1016/J.JGLR.2018.08.002

951 Klump, J.V. V, Edgington, D. N. N., Sager, P. E. E., & Robertson, D. M. M. (1997).
952 Sedimentary phosphorus cycling and a phosphorus mass balance for the Green Bay (Lake

953 Michigan) ecosystem. *Canadian Journal of Fisheries and Aquatic Sciences*, *54*(1), 10–26.
954 Retrieved from http://www.nrcresearchpress.com/doi/10.1139/f96-247

955 Komen, G. J., Hasselmann, K., & Hasselmann, K. (1984). On the Existence of a Fully
956 Developed Wind-Sea Spectrum. *Journal of Physical Oceanography*, *14*(8), 1271–1285.
957 https://doi.org/10.1175/1520-0485(1984)014<1271:OTEOAF>2.0.CO;2

958 Lai, W., Pan, J., & Devlin, A. T. (2018). Impact of tides and winds on estuarine circulation in the
959 Pearl River Estuary. *Continental Shelf Research*, *168*, 68–82.
960 https://doi.org/10.1016/J.CSR.2018.09.004

961 Lee, C., Schwab, D. J., & Hawley, N. (2005). Sensitivity analysis of sediment resuspension
962 parameters in coastal area of southern Lake Michigan. *Journal of Geophysical Research C:*
963 *Oceans*, *110*(3), 1–16. https://doi.org/10.1029/2004JC002326

964 Lee, C., Schwab, D. J., Beletsky, D., Stroud, J., & Lesht, B. (2007). Numerical modeling of
965 mixed sediment resuspension, transport, and deposition during the March 1998 episodic
966 events in southern Lake Michigan. *Journal of Geophysical Research: Oceans*, *112*(2), 1–17.
967 https://doi.org/10.1029/2005JC003419

968 Li, B., Tanaka, K. R., Chen, Y., Brady, D. C., & Thomas, A. C. (2017). Assessing the quality of
969 bottom water temperatures from the Finite-Volume Community Ocean Model (FVCOM) in
970 the Northwest Atlantic Shelf region. *Journal of Marine Systems*, *173*, 21–30.
971 https://doi.org/10.1016/J.JMARSYS.2017.04.001

972 Li, J., Pan, S., Chen, Y., Fan, Y.-M., & Pan, Y. (2018). Numerical estimation of extreme waves
973 and surges over the northwest Pacific Ocean. *Ocean Engineering*, *153*, 225–241.
974 https://doi.org/10.1016/J.OCEANENG.2018.01.076

975 Luo, L., Wang, J., Schwab, D. J., Vanderploeg, H., Leshkevich, G., Bai, X., et al. (2012).
976 Simulating the 1998 spring bloom in Lake Michigan using a coupled physical-biological
977 model. *J. Geophys. Res*, *117*, 10011. https://doi.org/10.1029/2012JC008216

978 Manchester-Neesvig, J. B., Andren, A. W., & Edgington, D. N. (1996). Patterns of Mass
979 Sedimentation and of Deposition of Sediment Contaminated by PCBs in Green Bay.
980 *Journal of Great Lakes Research*, *22*(2), 444–462. https://doi.org/10.1016/S0380-
981 1330(96)70969-3

Mantz, P. A. (1977). Incipient transport of fine grains and flakes by fluids-extended Shields diagram. *Journal of the Hydraulics Division*, *103*(HY6).

Mao, M., & Xia, M. (2017). Dynamics of wave–current–surge interactions in Lake Michigan: A model comparison. *Ocean Modelling*, *110*, 1–20. https://doi.org/10.1016/J.OCEMOD.2016.12.007

Mao, M., & Xia, M. (2020). Monthly and episodic dynamics of summer circulation in Lake Michigan. *Journal of Geophysical Research: Oceans*, *125*(6). https://doi.org/10.1029/2019jc015932

Mao, M., van der Westhuysen, A. J., Xia, M., Schwab, D. J., & Chawla, A. (2016). Modeling wind waves from deep to shallow waters in Lake Michigan using unstructured SWAN. *Journal of Geophysical Research: Oceans*, *121*(6), 3836–3865. https://doi.org/10.1002/2015JC011340

Marx, S. K., Rashid, S., & Stromsoe, N. (2016, June 1). Global-scale patterns in anthropogenic Pb contamination reconstructed from natural archives. *Environmental Pollution*. Elsevier Ltd. https://doi.org/10.1016/j.envpol.2016.02.006

Mellor, G. L., & Yamada, T. (1982). Development of a turbulence closure model for geophysical fluid problems. *Reviews of Geophysics*, *20*(4), 851. https://doi.org/10.1029/RG020i004p00851

Meyer-Peter, E., & Müller, R. (1948). Formulas for Bed-Load transport. *IAHSR 2nd Meeting, Stockholm, Appendix 2*. Retrieved from https://repository.tudelft.nl/islandora/object/uuid%3A4fda9b61-be28-4703-ab06-43cdc2a21bd7

Miller, T. R. (2020). Lakestat. Retrieved November 12, 2019, from http://www.lakestat.com/

Mitchener, H., & Torfs, H. (1996). Erosion of mud/sand mixtures. *Coastal Engineering*, *29*(1–2), 1–25. https://doi.org/10.1016/S0378-3839(96)00002-6

Moore, J. R., Meyer, R. P., & Morgan, C. L. (1973). *Investigation of the Sediments and Potential Manganese Nodule Resources of Green Bay, Wisconsin*. University of Wisconsin, Sea Grant College Program. Technical Report-WIS. WISCU-T-73-001.

National Geophysical Data Center. (2015). Bathymetric Data Viewer. Retrieved January 1, 2017, from http://maps.ngdc.noaa.gov/viewers/bathymetry/

NEW Water. (2017). Aquatic Monitoring Program › NEW Water. Retrieved October 1, 2018, from http://newwater.us/programs-initiatives/aquatic-monitoring-program/

NOAA. (2017). Bathymetry of Lake Michigan. Retrieved January 1, 2017, from https://ngdc.noaa.gov/mgg/greatlakes/michigan.html

NOAA. (2018). National Centers for Environmental Information (NCEI). Retrieved November 1, 2018, from https://gis.ncdc.noaa.gov/maps/ncei/cdo/hourly

NOAA. (2020). Station Selection - NOAA Tides & Currents. Retrieved January 5, 2020, from https://tidesandcurrents.noaa.gov/stations.html?type=Water+Levels

Parker, G. (2004). *1D Morphodynamics of Rivers and Turbidity Currents*. Saint Anthony Falls Lab., Univ. of Minn., Minneapolis. [Available at http://hydrolab.illinois.edu/people/parkerg/morphodynamics_e-book.htm].

Qi, J., Chen, C., Beardsley, R. C., Perrie, W., Cowles, G. W., & Lai, Z. (2009). An unstructured-grid finite-volume surface wave model (FVCOM-SWAVE): Implementation, validations and applications. *Ocean Modelling*, *28*(1–3), 153–166. https://doi.org/10.1016/J.OCEMOD.2009.01.007

Read, J., Klump, V., Johengen, T., Schwab, D., Paige, K., Eddy, S., et al. (2010). Working in Freshwater: The Great Lakes Observing System Contributions to Regional and National Observations, Data Infrastructure, and Decision Support. *Marine Technology Society Journal*, *44*(6), 84–98. https://doi.org/10.4031/MTSJ.44.6.12

Ris, R. C., Holthuijsen, L. H., & Booij, N. (1999). A third-generation wave model for coastal regions: 2. Verification. *Journal of Geophysical Research: Oceans*, *104*(C4), 7667–7681. https://doi.org/10.1029/1998JC900123

Rowe, M.D., Anderson, E. J., Wang, J., & Vanderploeg, H. A. (2015). Modeling the effect of invasive quagga mussels on the spring phytoplankton bloom in Lake Michigan. *Journal of Great Lakes Research*, *41*, 49–65. https://doi.org/10.1016/J.JGLR.2014.12.018

Rowe, Mark D., Obenour, D. R., Nalepa, T. F., Vanderploeg, H. A., Yousef, F., & Kerfoot, W.

C. (2015). Mapping the spatial distribution of the biomass and filter-feeding effect of invasive dreissenid mussels on the winter-spring phytoplankton bloom in Lake Michigan. *Freshwater Biology*, *60*(11), 2270–2285. https://doi.org/10.1111/fwb.12653

Rowe, Mark D., Anderson, E. J., Vanderploeg, H. A., Pothoven, S. A., Elgin, A. K., Wang, J., & Yousef, F. (2017). Influence of invasive quagga mussels, phosphorus loads, and climate on spatial and temporal patterns of productivity in Lake Michigan: A biophysical modeling study. *Limnology and Oceanography*, *62*(6), 2629–2649. https://doi.org/10.1002/lno.10595

Safaie, A., Wendzel, A., Ge, Z., Nevers, M. B., Whitman, R. L., Corsi, S. R., & Phanikumar, M. S. (2016). Comparative Evaluation of Statistical and Mechanistic Models of *Escherichia coli* at Beaches in Southern Lake Michigan. *Environmental Science & Technology*, *50*(5), 2442–2449. https://doi.org/10.1021/acs.est.5b05378

Sanford, L. P. (2008). Modeling a dynamically varying mixed sediment bed with erosion, deposition, bioturbation, consolidation, and armoring. *Computers and Geosciences*, *34*(10), 1263–1283. https://doi.org/10.1016/j.cageo.2008.02.011

Schwab, D.J., & Beletsky, D. (1998). *Lake Michigan Mass Balance Study: Hydrodynamic Modeling Project. ERL GLERL-108*. NOAA GLERL, Ann Arbor, MI.

Schwab, David J. (1983). Numerical Simulation of Low-Frequency Current Fluctuations in Lake Michigan. *Journal of Physical Oceanography*, *13*(12), 2213–2224. https://doi.org/10.1175/1520-0485(1983)013<2213:NSOLFC>2.0.CO;2

Shen, C. (2016). *Modeling of dreissenid mussel impacts on Lake Michigan*. *ProQuest Dissertations and Theses*. University of Wisconsin-Milwaukee. Retrieved from https://search.proquest.com/docview/1844987331?accountid=6180%0Ahttp://dw2zn6fm9z.search.serialssolution.com?ctx_ver=Z39.88-2004&ctx_enc=info:ofi/enc:UTF-8&rfr_id=info:sid/ProQuest+Dissertations+%26+Theses+Global&rft_val_fmt=info:ofi/fmt:kev:mtx:dissertat

Sherwood, C. R., Aretxabaleta, A. L., Harris, C. K., Paul Rinehimer, J., Verney, R., & Ferré, B. (2018). Cohesive and mixed sediment in the Regional Ocean Modeling System (ROMS v3.6) implemented in the Coupled Ocean-Atmosphere-Wave-Sediment Transport Modeling System (COAWST r1234). *Geoscientific Model Development*, *11*(5), 1849–1871.

https://doi.org/10.5194/gmd-11-1849-2018

Shibuo, Y., Jarsjö, J., & Destouni, G. (2007). Hydrological responses to climate change and irrigation in the Aral Sea drainage basin. *Geophysical Research Letters*, *34*(21), L21406. https://doi.org/10.1029/2007GL031465

Shore, J. A. (2009). Modelling the circulation and exchange of Kingston Basin and Lake Ontario with FVCOM. *Ocean Modelling*, *30*(2–3), 106–114. https://doi.org/10.1016/J.OCEMOD.2009.06.007

Smagorinsky, J. (1963). General circulation experiments with the primitive equations, I. The basic experiment. *Monthly Weather Review*, *91*(3), 99–164. https://doi.org/10.1175/1520-0493(1963)091<0099:GCEWTP>2.3.CO;2

Soulsby, R. L. (1998). Dynamics of marine sands.

Velleux, M., Endicott, D., Steuer, J., Jaeger, S., & Patterson, D. (1995). Long-Term Simulation of PCB Export from the Fox River to Green Bay. *Journal of Great Lakes Research*, *21*(3), 359–372. https://doi.org/10.1016/S0380-1330(95)71047-4

Waples, J. T., & Klump, J. V. (2002). Biophysical effects of a decadal shift in summer wind direction over the Laurentian Great Lakes. *Geophysical Research Letters*, *29*(8), 43-1-43–4. https://doi.org/10.1029/2001GL014564

Warner, J. C., Sherwood, C. R., Signell, R. P., Harris, C. K., & Arango, H. G. (2008). Development of a three-dimensional, regional, coupled wave, current, and sediment-transport model. *Computers & Geosciences*, *34*(10), 1284–1306. https://doi.org/10.1016/J.CAGEO.2008.02.012

Wisconsin DNR. (2000). *Model Evaluation Workgroup Technical Memorandum 2f: Estimation of Sediment Bed Properties for Green Bay*.

Xue, P., Schwab, D. J., & Hu, S. (2015). An investigation of the thermal response to meteorological forcing in a hydrodynamic model of Lake Superior. Retrieved from https://www.semanticscholar.org/paper/An-investigation-of-the-thermal-response-to-forcing-Xue-Schwab/40eca7b276ebcad8589f9df017dbd724b1ffc00d

Yolcubal, I., Brusseau, M. L., Artiola, J. F., Wierenga, P., & Wilson, L. G. (2004).

ENVIRONMENTAL PHYSICAL PROPERTIES AND PROCESSES. *Environmental Monitoring and Characterization*, 207–239. https://doi.org/10.1016/B978-012064477-3/50014-X

Zhang, J., Xiong, M., Yin, C., & Gan, S. (2018). Inner shelf response to storm track variations over the east LeiZhou Peninsula, China. *International Journal of Applied Earth Observation and Geoinformation*, *71*, 56–69. https://doi.org/10.1016/J.JAG.2018.03.011

**Figure 1.**





| Station Name | Station ID | latitude | longitude |
|---|---|---|---|
| Southern Green Bay Buoy | 45014 | 44.80 | -87.76 |
| Milwaukee Atwater 20m Buoy | 45013 | 43.10 | -87.85 |
| Northern Michigan Buoy | 45002 | 45.34 | -86.41 |
| Southern Michigan Buoy | 45007 | 42.67 | -87.03 |
| Green Bay West Buoy | GBW | 44.58 | -87.99 |
| Green Bay East Buoy | GBE | 44.55 | -87.96 |
| USGS Fox River Gauge | 40851385 | 44.53 | -88.01 |
| USGS Menominee River Gauge | 04067500 | 45.33 | -87.66 |
| NEW Water Station 13 | NW13 | 44.53 | -88.01 |

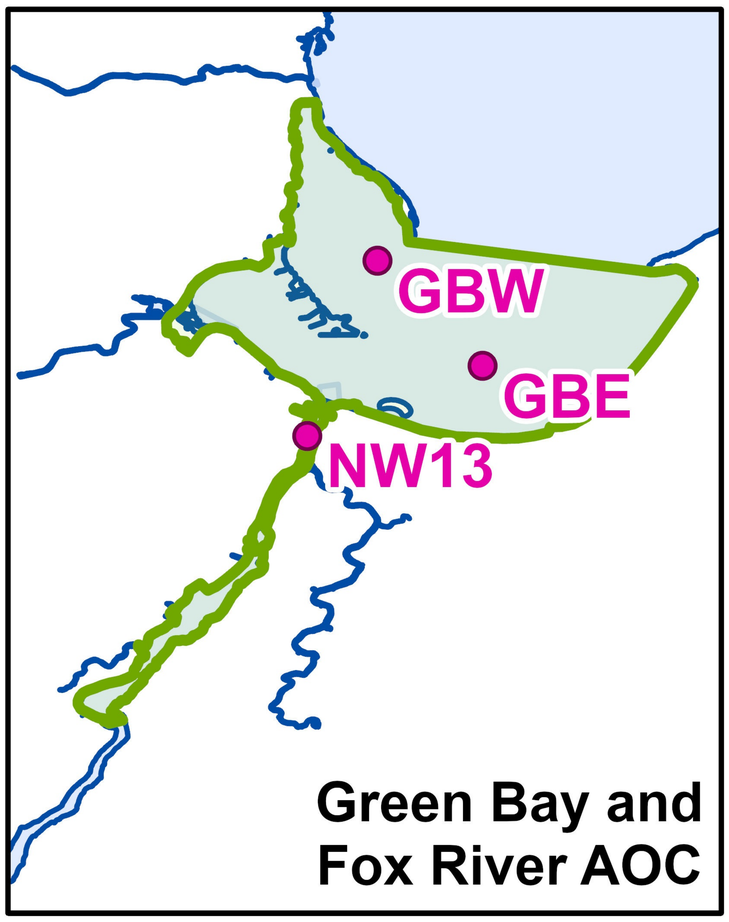


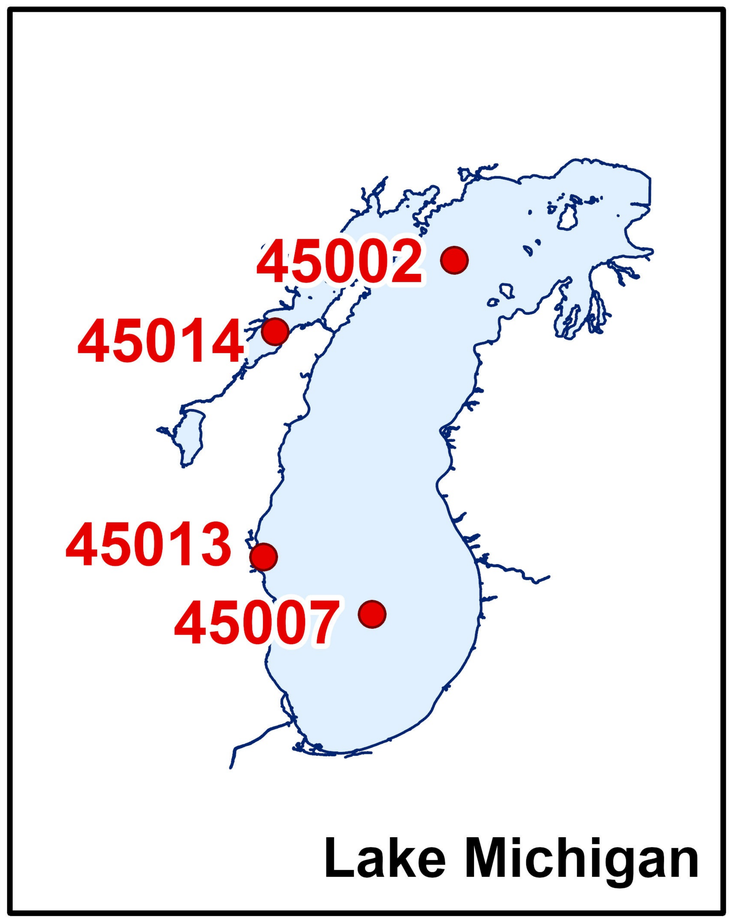

**Figure 2.**

45014

45013

45007

45002

$u_{surf}$ (m/s)

$u_{botm}$ (m/s)

Fn = 0.94
$\Delta\theta$ = 0.34

Fn = 0.62
$\Delta\theta$ = 0.21

Fn = 0.89
$\Delta\theta$ = 0.32

Fn = 0.78
$\Delta\theta$ = 0.30

$W_{Hs}$ (m)

CC = 0.88
BD = -0.04
RMSE = 0.16

CC = 0.95
BD = 0.19
RMSE = 0.24

CC = 0.94
BD = 0.01
RMSE = 0.16

$W_{dir}$ (degrees)

CC = 0.66
BD = -16.98
RMSE = 41.83

CC = 0.69
BD = -4.49
RMSE = 52.35

CC = 0.69
BD = -3.43
RMSE = 61.74

$TW_{surf}$ (°C)

CC = 0.96
BD = 0.86
RMSE = 1.37

CC = 0.87
BD = -0.51
RMSE = 2.31

CC = 0.87
BD = -0.56
RMSE = 1.86

CC = 0.97
BD = 1.54
RMSE = 2.21

$TW_{botm}$ (°C)

CC = 0.69
BD = 3.66
RMSE = 4.68

CC = 0.83
BD = 1.14
RMSE = 2.49

GBE

GBW

TSS (mg/L)

CC = 0.43
BD = -3.85
RMSE = 15.96

CC = 0.79
BD = -12.30
RMSE = 15.86

**Predicted Values**

**Observed Values**

**Figure 3.**

MODIS

May-07 | Jun-05 | Jul-16

Aug-11 | Sep-12 | Oct-16

FVCOM

May-07 | Jun-05 | Jul-16

Aug-11 | Sep-12 | Oct-16

45.2
45.1
45.0
44.9
44.8
44.7
44.6
44.5

-88 -87.8 -87.6 -87.4 -87.2

TSS (mg/L)

20
18
16
14
12
10
8
6
4
2
0

**Figure 4.**

Lake Michigan

May
June
July
August
September
October

Green Bay

May
June
July
August
September
October

$W_{spd}$: 5 m/s

**Figure 5.**

Lake Michigan

Green Bay

May

June

July

August

September

October

46.0
45.5
45.0
44.5
44.0
43.5
43.0
42.5
42.0
41.5

-88
-87.5
-87
-86.5
-86
-85

0.1
0.09
0.08
0.07
0.06
0.05
0.04
0.03
0.02
0.01
0

$u_{spd}$ (m/s)

**Figure 6.**

A
A'
B
B'
C
C'
May
June
July
August
September
October
Depth (m)
0
-20
-40
0
40
80
120
160
0
10
20
0
20
40
Distance (km)
-0.05
-0.04
-0.03
-0.02
-0.01
0
0.01
0.02
0.03
0.04
0.05
$u_{spd}$ (m/s)

**Figure 7.**

Lake Michigan

Green Bay

May

June

July

August

September

October

46.0
45.5
45.0
44.5
44.0
43.5
43.0
42.5
42.0
41.5

-88
-87.5
-87
-86.5
-86
-85

1
0.9
0.8
0.7
0.6
0.5
0.4
0.3
0.2
0.1
0

$W_{Hs}$ (m)

**Figure 8.**

Lake Michigan

Green Bay

May

June

July

August

September

October

46.0
45.5
45.0
44.5
44.0
43.5
43.0
42.5
42.0
41.5

-88
-87.5
-87
-86.5
-86
-85

0.05
0.045
0.04
0.035
0.03
0.025
0.02
0.015
0.01
0.005
0

$\tau_{sf}$ (N/m$^2$)

**Figure 9.**

Lake Michigan

May
June
July
August
September
October

Green Bay

May
June
July
August
September
October

46.0
45.5
45.0
44.5
44.0
43.5
43.0
42.5
42.0
41.5

-88
-87.5
-87
-86.5
-86
-85

TW (°C)
30
25
20
15
10
5
0

**Figure 10.**

A
A'
B
B'
C
C'
May
June
July
August
September
October
Depth (m)
0
-20
-40
0
40
80
120
160
0
10
20
0
20
40
Distance (km)
TW (˚C)
0
5
10
15
20
25
30

**Figure 11.**

Lake Michigan

Green Bay

May

June

July

August

September

October

46.0
45.5
45.0
44.5
44.0
43.5
43.0
42.5
42.0
41.5

-88
-87.5
-87
-86.5
-86
-85

TSS (mg/L)

20
18
16
14
12
10
8
6
4
2
0

**Figure 12.**

A
A'
B
B'
C
C'
May
June
July
August
September
October
0
-20
-40
Depth (m)
0
40
80
120
160
0
10
20
0
20
40
Distance (km)
TSS (mg/L)
0
2
4
6
8
10
12
14
16
18
20

**Figure 13.**

2016 2017 2018 2019 Average

46 45 44 43 42

$W_{spd}$: 2.5 m/s

$\tau_{sf}$ (N/m$^2$) 0.05 0.04 0.03 0.02 0.01 0

TW ($^\circ$C) 30 20 10 0

TSS (mg/L) 20 15 10 5 0

-88 -86

**Figure S1.**

Lake Michigan Bathymetry (m)

280.0
245.0
210.0
175.0
140.0
105.0
70.0
35.0
0.0

Green Bay Bathymetry (m)

50.0
40.0
30.0
20.0
10.0
0.0

**Figure S2.**

Little Summer Island
Fairport
St. Martin Island
Summer Island
Poverty Island
Washington Island
Plum Island
Rock Island
Detroit Island
Northport
N
W
E
S
0
10
20
Km
Little Suamico River
Little Tail Point
Suamico River
Long Tail Point
Cat Island
Duck Creek
Bay Beach Island
Fox River
East River
N
W
E
S
0
4
8
Km

**Figure S3.**

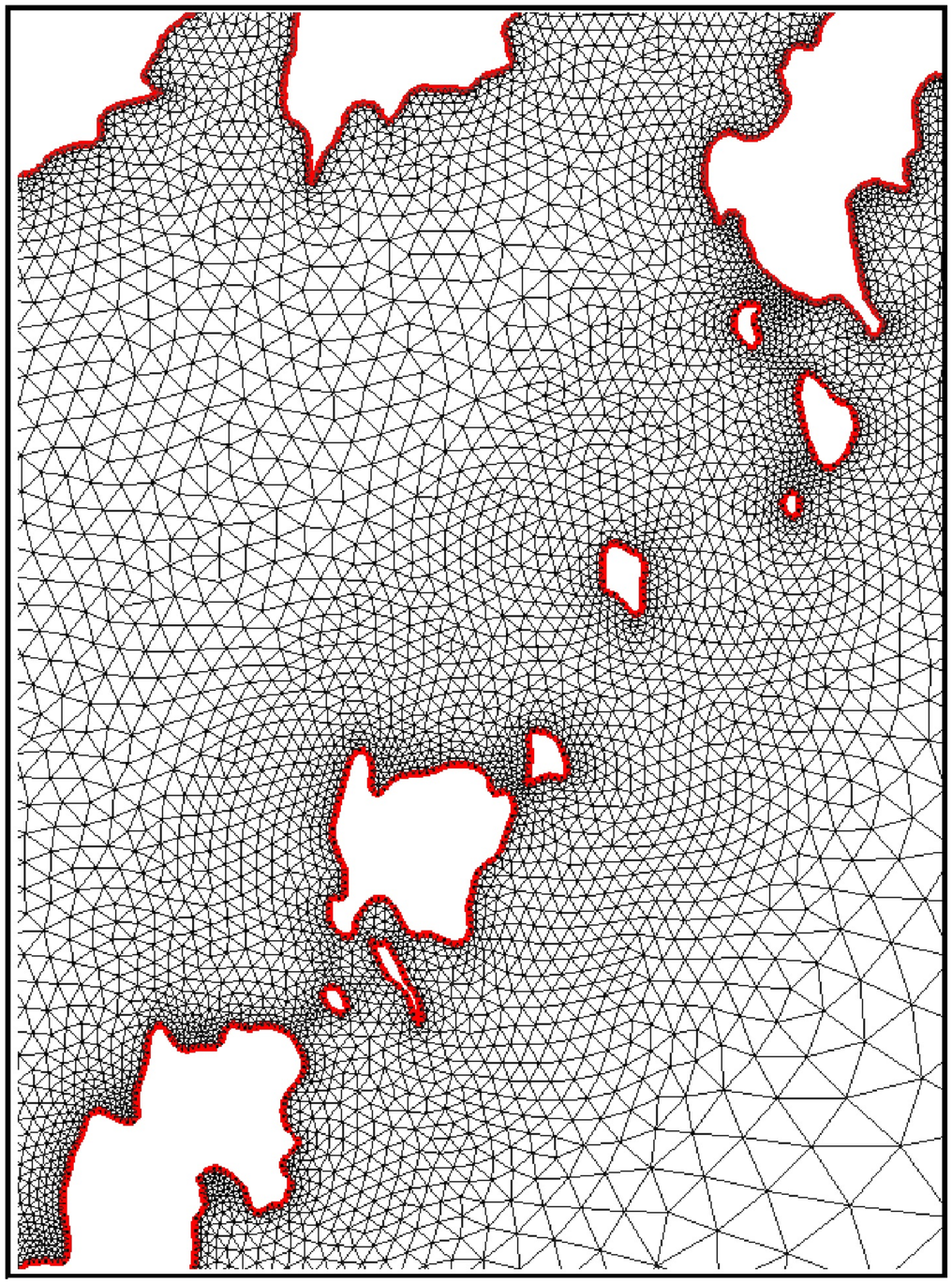

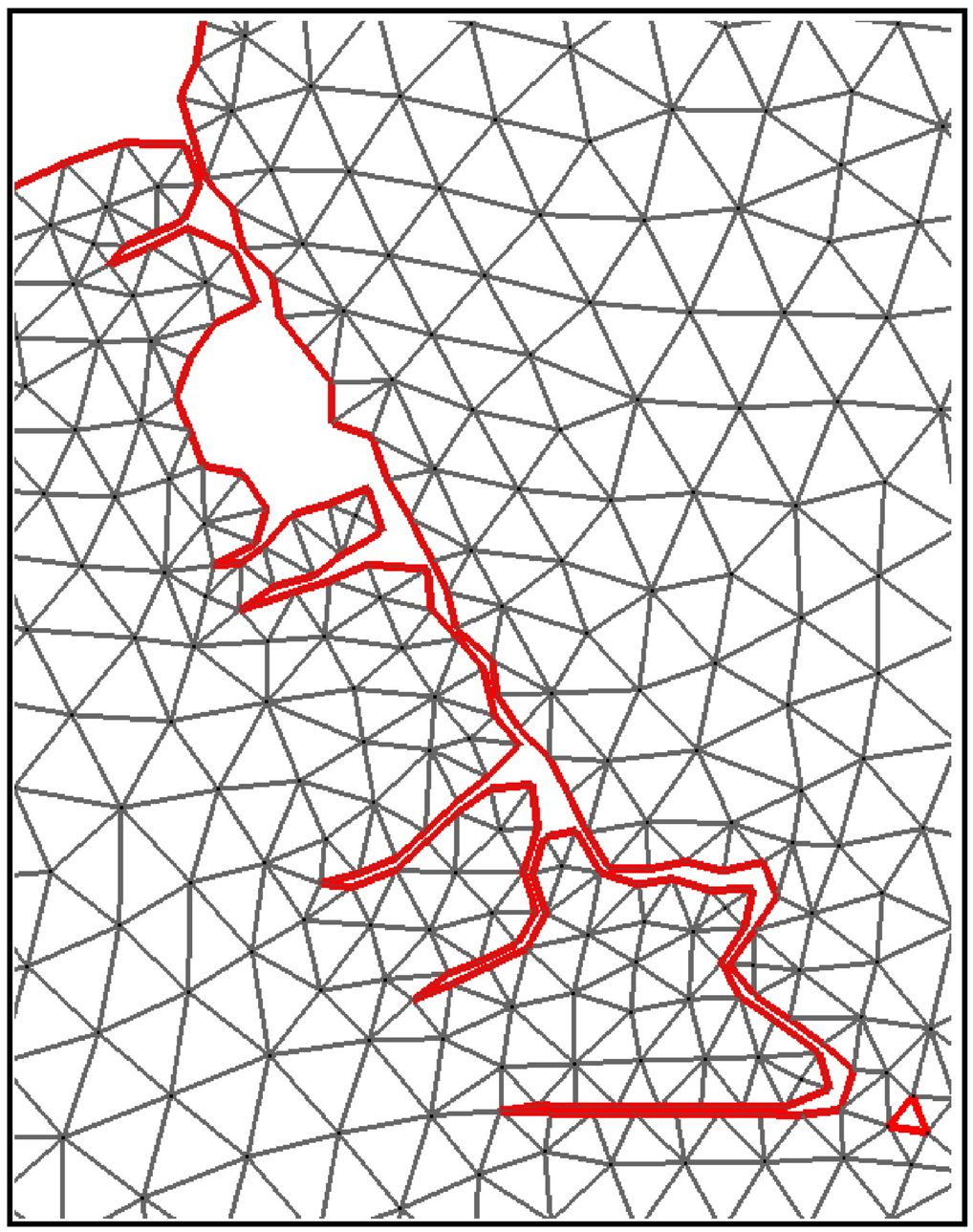

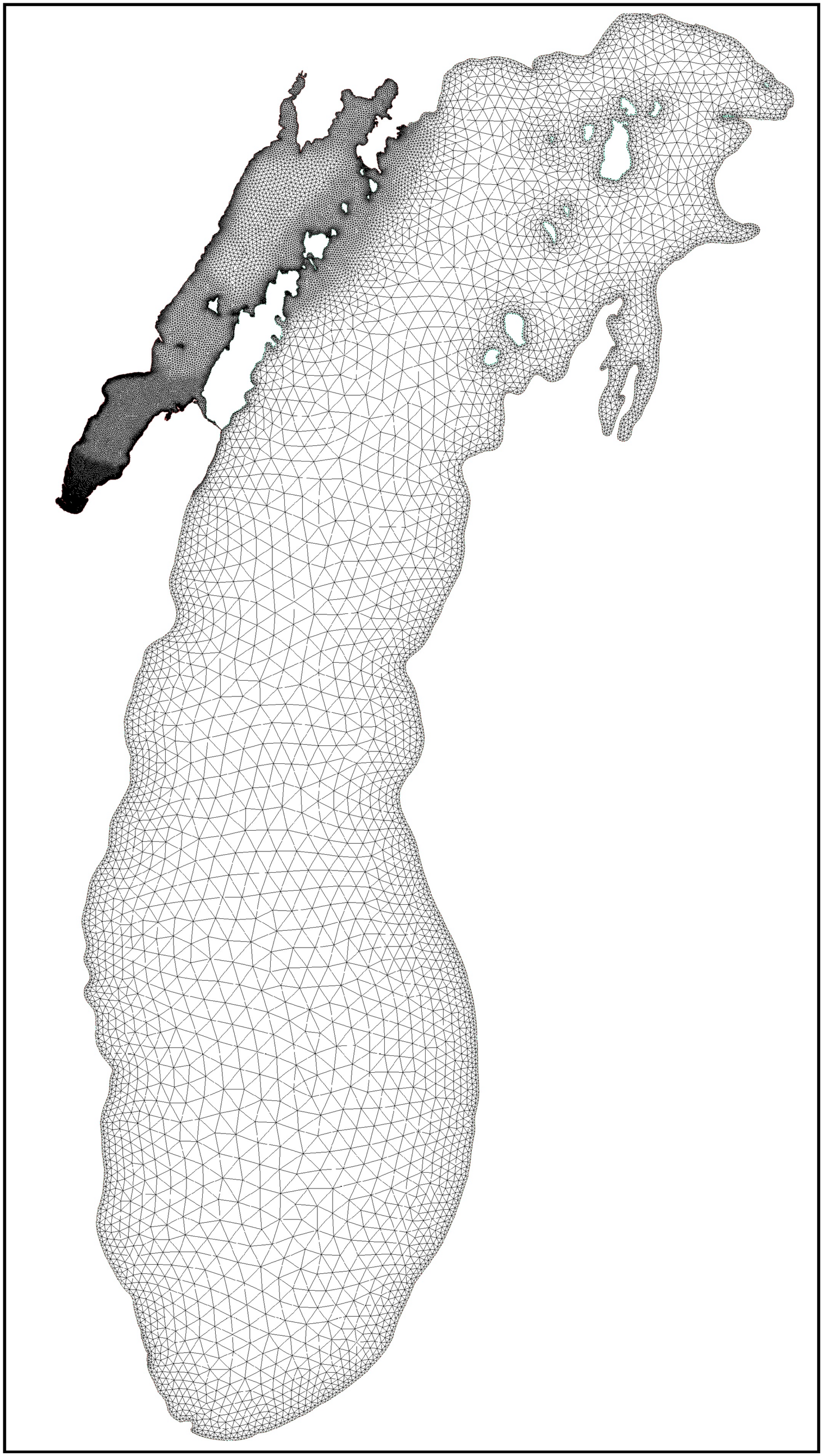

**Figure S4.**

46
45.5
45
44.5
44
43.5
43
42.5
42
41.5
-88
-87
-86
-85

**Fine-grained Sediments**

**Coarse Sediments**

**Percentage**

0
20
40
60
80
100

**Figure S5.**


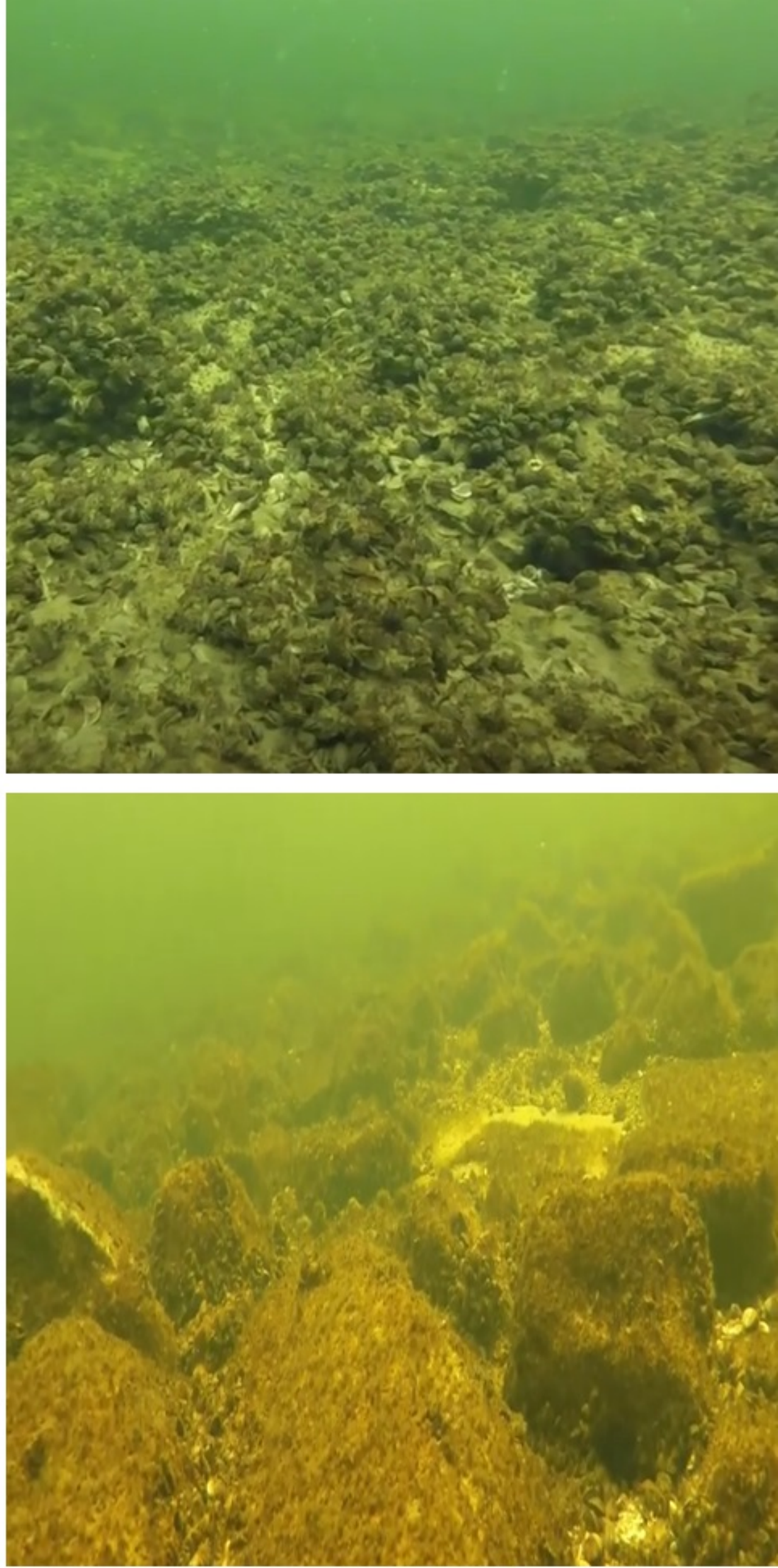

**Figure S6.**

GBE Station

$W_{spd}$= 2 m/s; SE direction

TSS (mg/L)

0 10 20 30 40 50 60 70 80

Jun 17 Jun 20 Jun 23 Jun 26 Jun 29

2018

GBE Station

$W_{spd}$= 2 m/s; SE direction

0 10 20 30 40 50 60 70 80

Aug 27 Aug 28 Aug 29 Aug 30 Aug 31

2018

GBW Station

$W_{spd}$= 2 m/s; SE direction

TSS (mg/L)

0 10 20 30 40 50 60 70 80

Jul 18 Jul 20 Jul 22 Jul 24 Jul 26

2018

GBW Station

$W_{spd}$= 2 m/s; SE direction

0 10 20 30 40 50 60 70 80

Sep 09 Sep 10 Sep 11 Sep 12

2018

Observed Predicted

**Figure S7.**

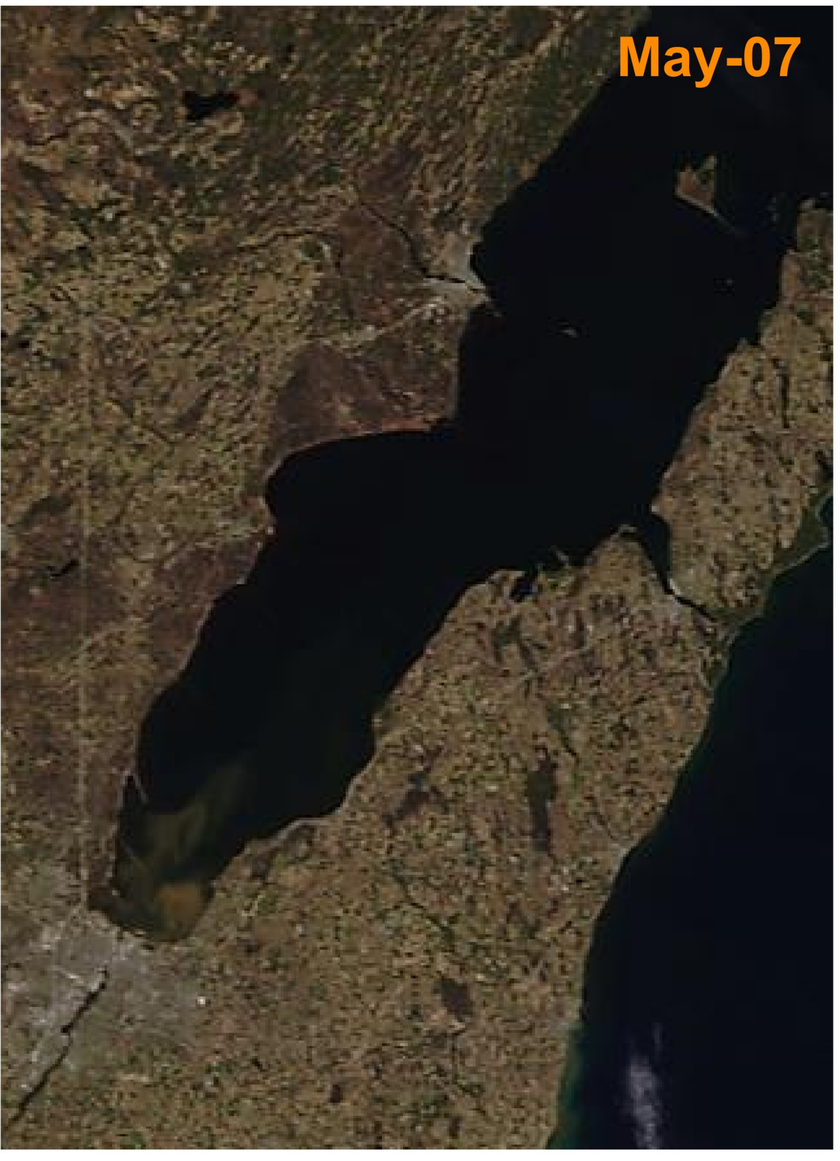
May-07


Jun-05

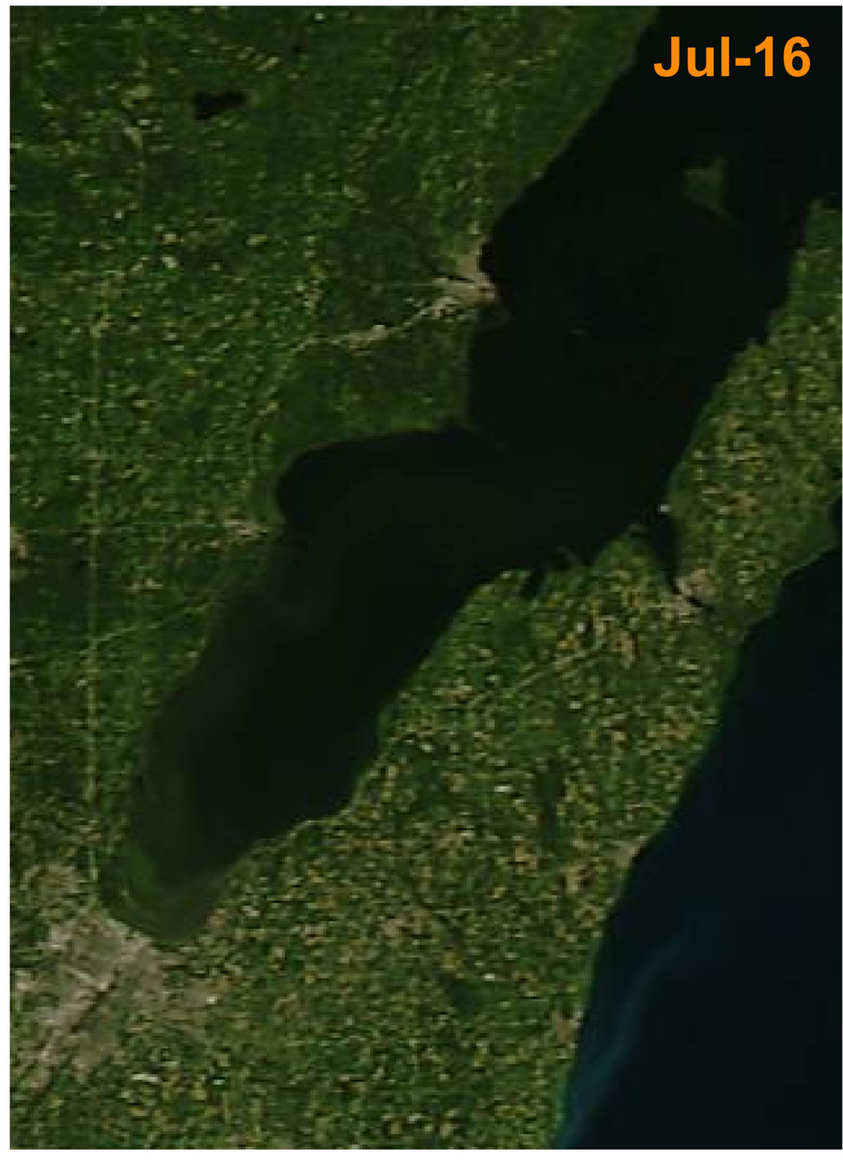
Jul-16


AUG-11

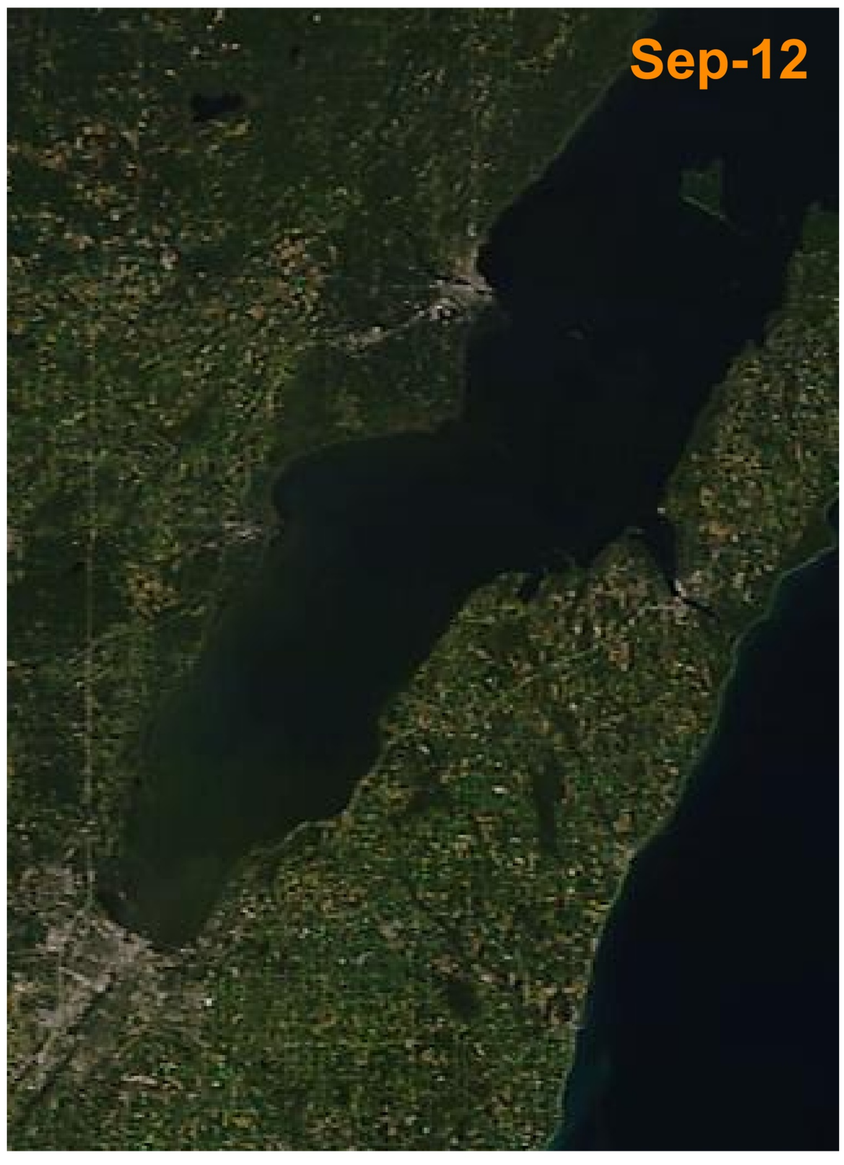
Sep-12


Oct-16

**Figure S8.**

Lake Michigan

Green Bay

May

June

July

August

September

October

46.0
45.5
45.0
44.5
44.0
43.5
43.0
42.5
42.0
41.5

-88
-87
-86
-85

-87.5
-87
-86.5

0.1
0.09
0.08
0.07
0.06
0.05
0.04
0.03
0.02
0.01
0

$u_{spd}$ (m/s)

**Figure S9.**

Lake Michigan

Green Bay

May

June

July

August

September

October

46.0
45.5
45.0
44.5
44.0
43.5
43.0
42.5
42.0
41.5

-88
-87.5
-87
-86.5
-86
-85

0.1
0.09
0.08
0.07
0.06
0.05
0.04
0.03
0.02
0.01
0

$u_{spd}$ (m/s)

**Figure S10.**

Date: Jul 13, 2016

Date: Aug 05, 2016

Date: Sep 02, 2016

Wind Fields

5 m/s

Surface Currents

0.25 m/s

Surface Temperature

T (°C)

30

20

10

0

46

45

44

43

42

-88

-87

-86

-85

*Journal of Geophysical Research—Oceans*

Supporting Information for

# Development of a Physically-based Sediment Transport Model for Green Bay, Lake Michigan

Bahram Khazaei[1,4], Hector R. Bravo[1], Eric J. Anderson[2], and Jeffrey V. Klump[3]

1- Department of Civil and Environmental Engineering, University of Wisconsin-Milwaukee

2- Great Lakes Environmental Research Laboratory, National Oceanic and Atmospheric Administration

3- School of Freshwater Sciences, University of Wisconsin-Milwaukee

4- Current position: Research Application Laboratory, National Center for Atmospheric Research

## Contents of this file



## Additional Supporting Information (Files uploaded separately)



## Introduction

Figures included in this Supporting Information provide more details of the study area and support the performance of the hydrodynamic and sediment transport models. Animated movies are also included in the Additional Supporting Information to provide more details of thermal structure and sediment transport patterns in Green Bay.

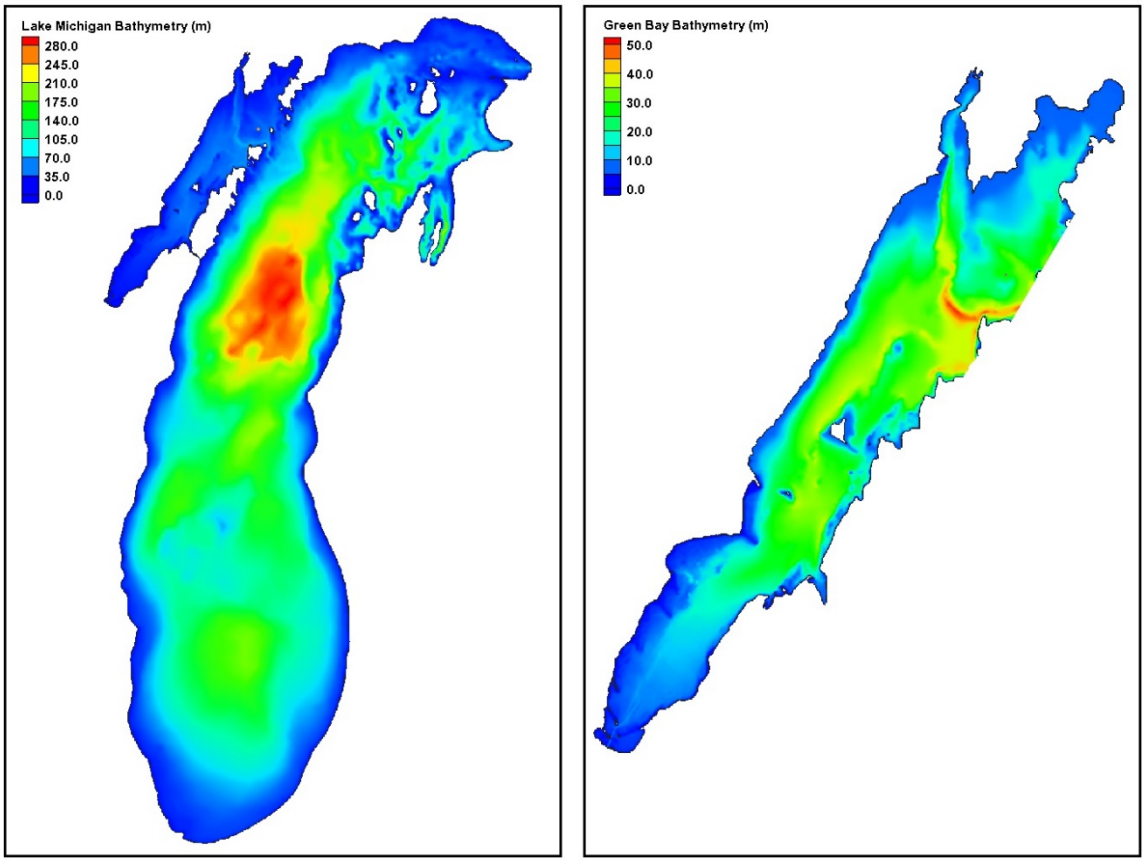


**Figure S1.** Bathymetry of Lake Michigan (left) and Green Bay (right).

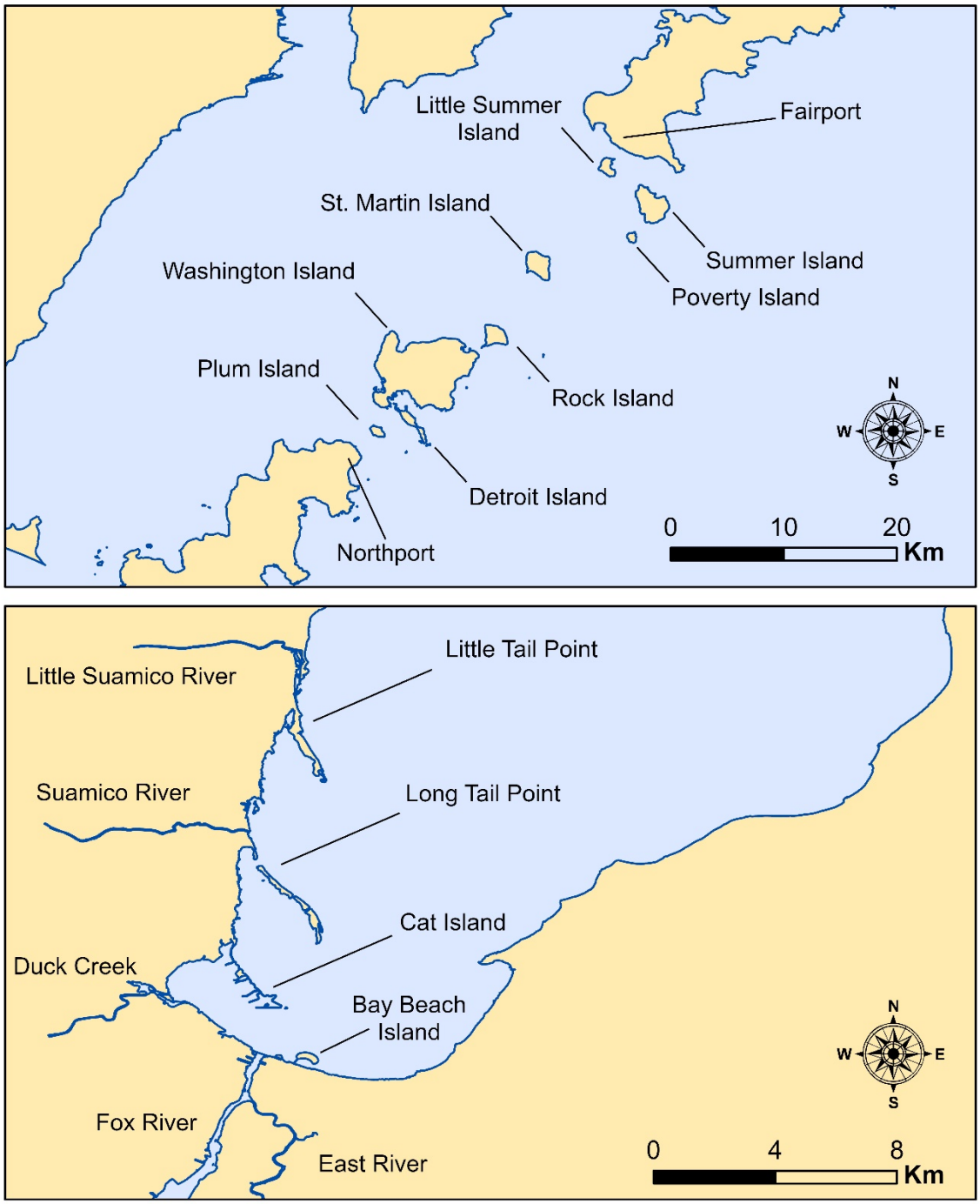


**Figure S2.** Islands at the area of exchange between Lake Michigan and Green Bay (top) and Lower Green Bay islands (bottom). The latter provide shoreline protection in the western coastal areas where currents and waves are more frequent and stronger in the lower bay.

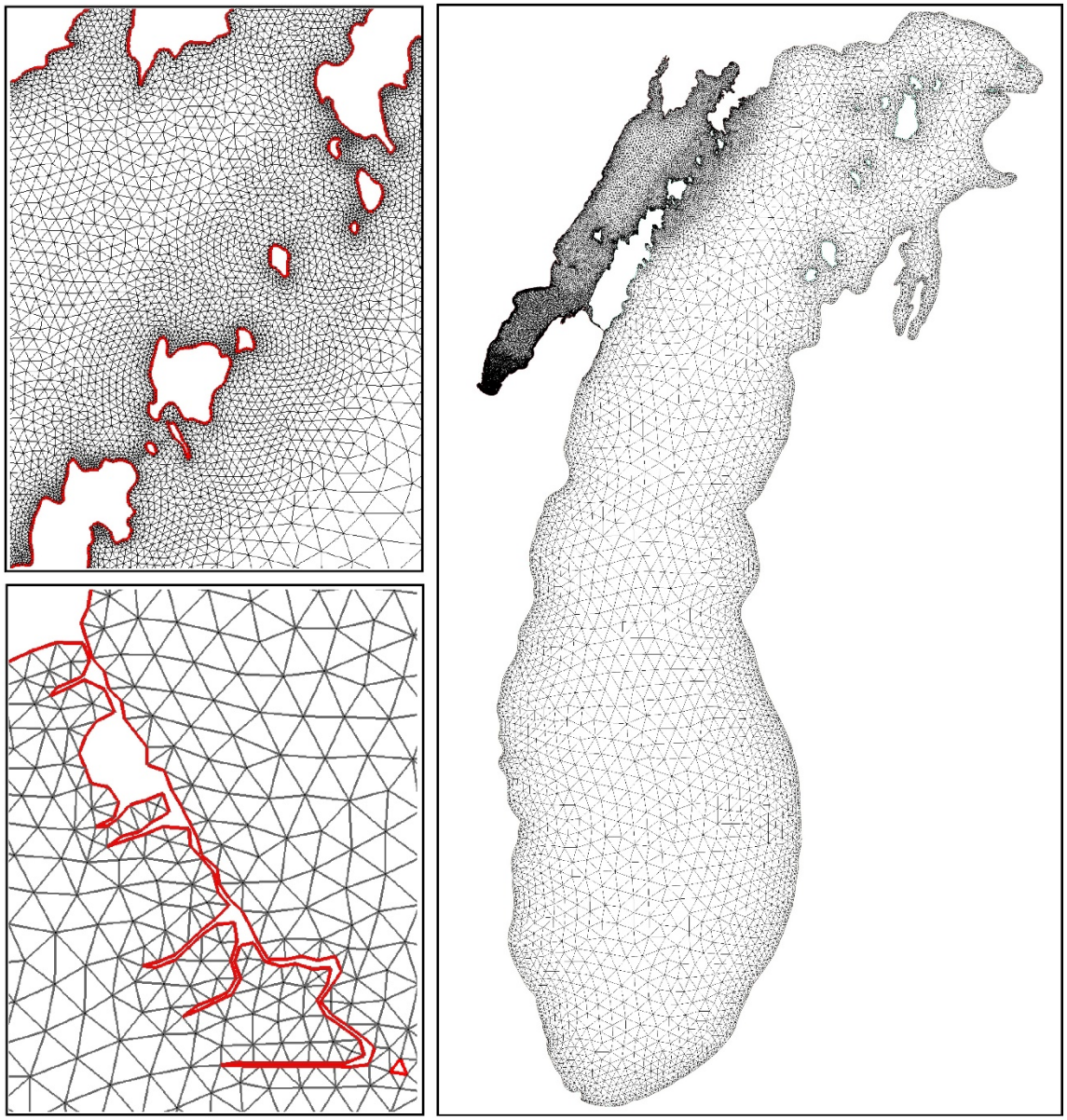

**Figure S3.** Lake Michigan grid resolution (right), details in Lake Michigan-Green Bay exchange area (top left), and Cat Island (bottom left).

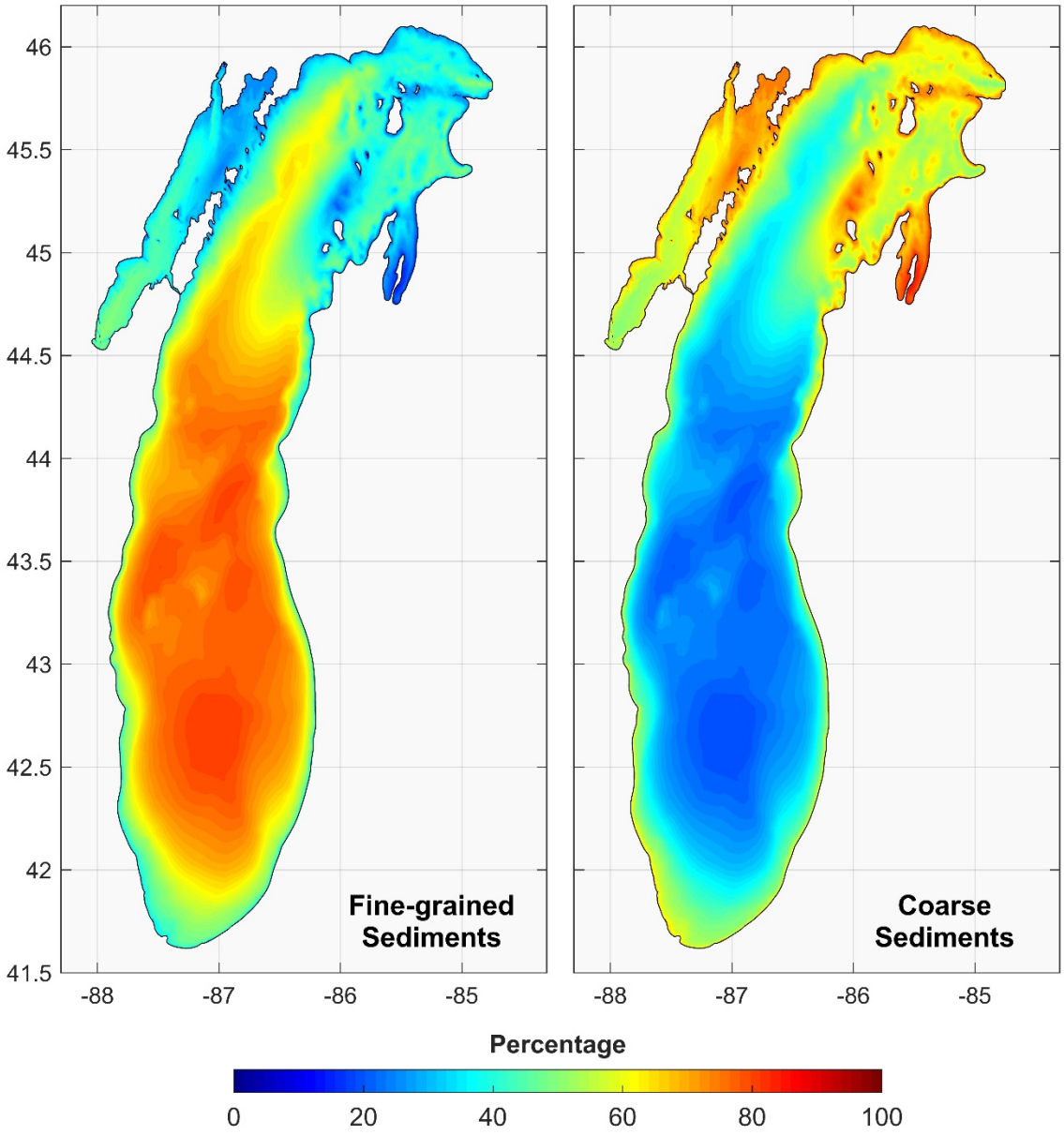


**Figure S4.** Distribution of fine-grained and coarse sediment classes in Lake Michigan used to initialize the sediment transport model. We defined Clay, Fine Silt, Coarse Silt, and Fine Sand as fine sediments and Coarse Sand, and Gravel as coarse sediments.

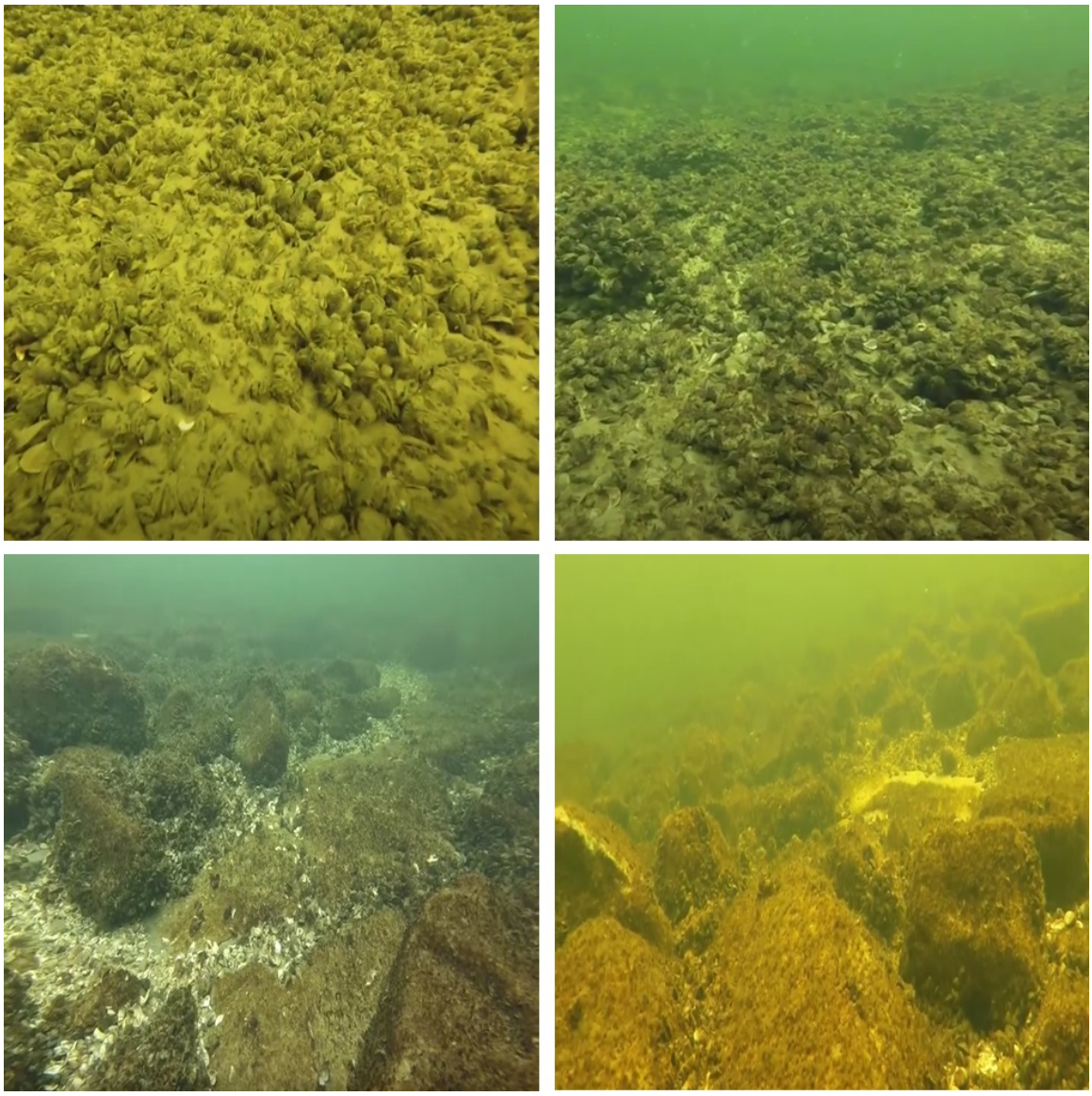

**Figure S5.** Recent observations of the Green Bay bed conditions in lower Green Bay near the inlet of Sturgeon Bay. These photos are selected as examples to show the population of mussels over the sediment layer, which may affect summertime sediment transport significantly. Photos are the courtesy of Jeff Hugoton (https://www.youtube.com/user/TheRotax1/videos).

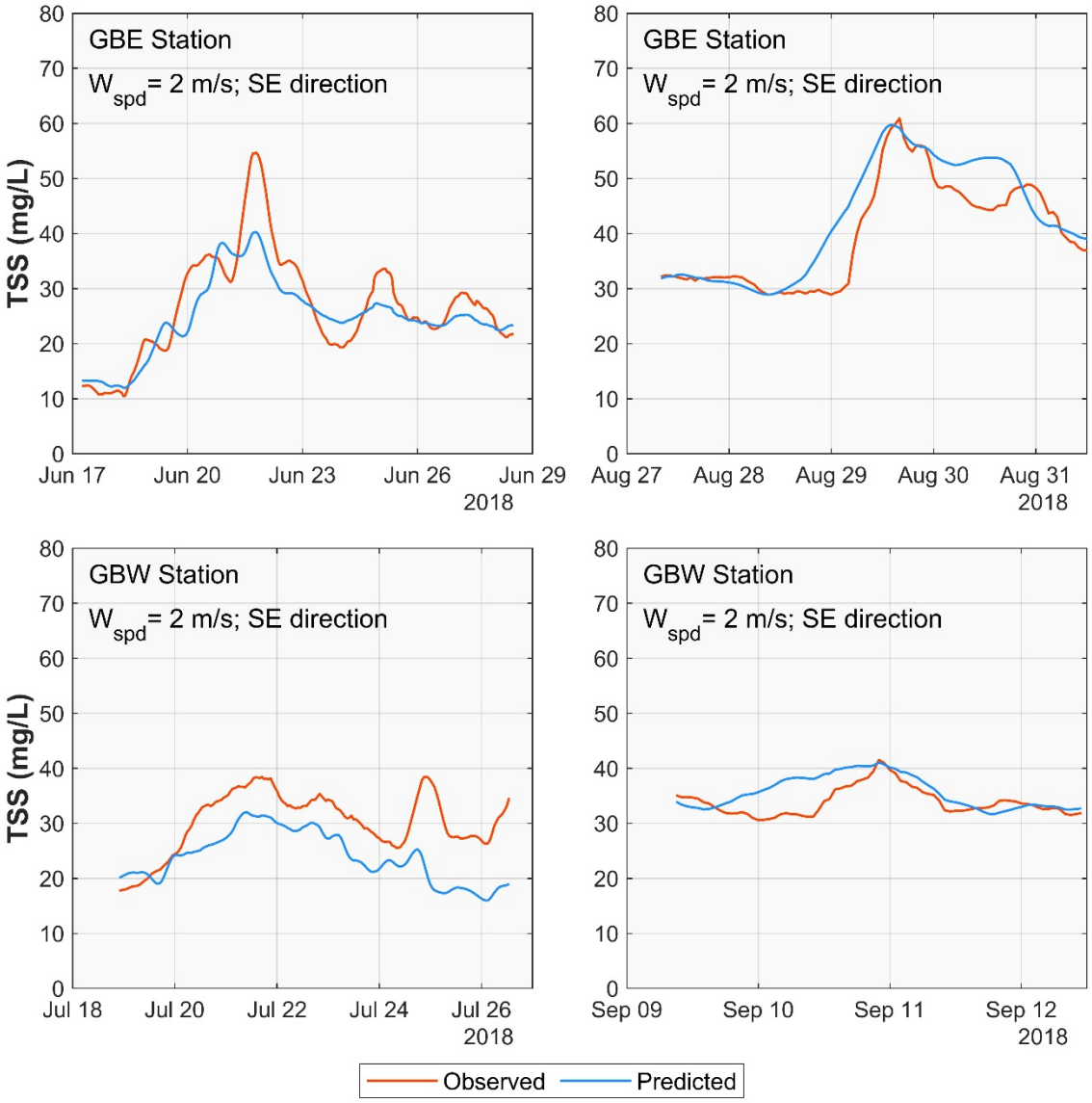


**Figure S6.** Examples of resuspension episodes in the lower Green Bay and comparison of the observed vs predicted total suspended solids (TSS).

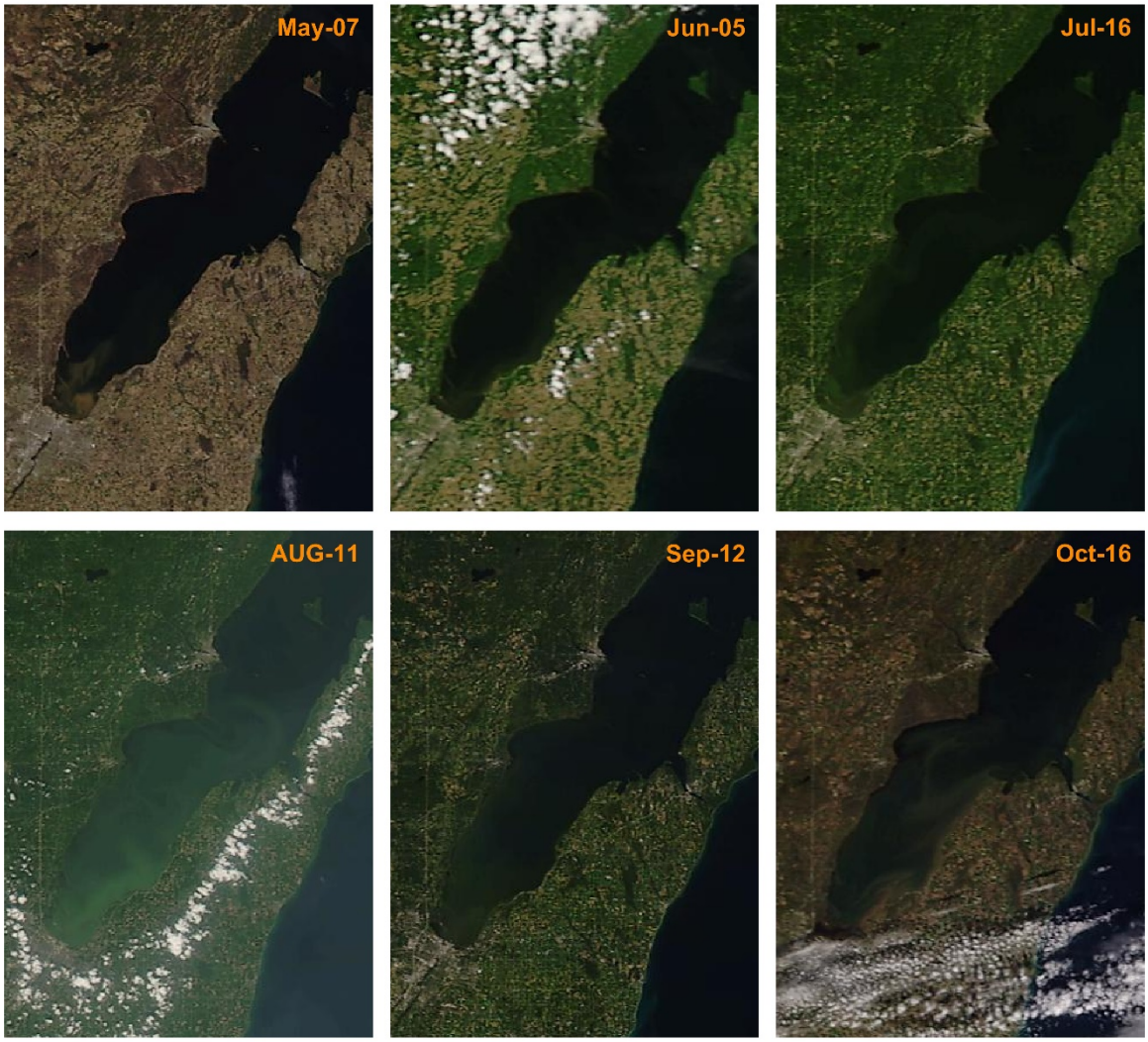


**Figure S7.** True-color visualization of MODIS imagery data used for mapping surface TSS concentration in the lower Green Bay for six selected days in summer 2018. Data was obtained from MODIS Today (http://ge.ssec.wisc.edu/modis-today/).

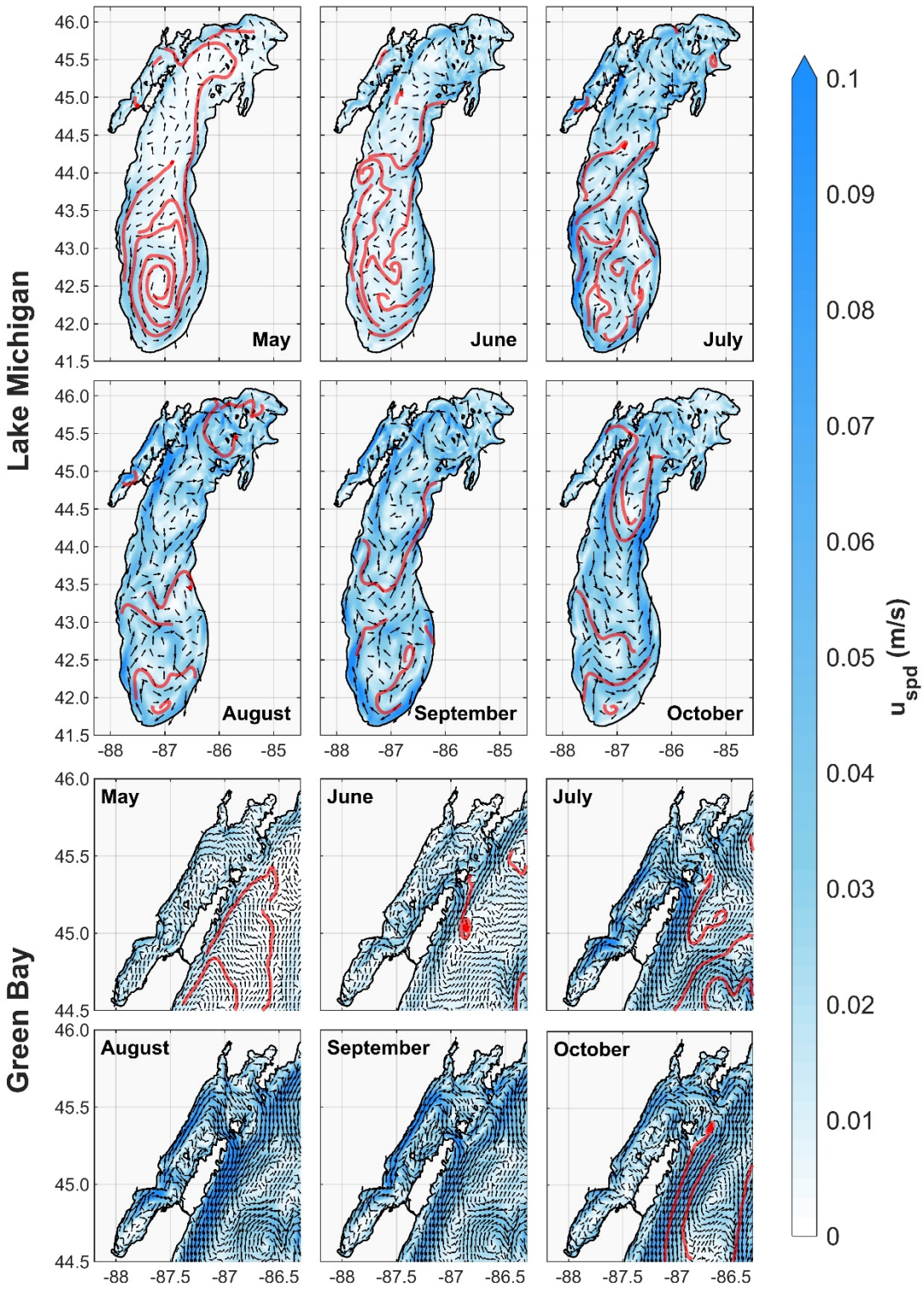


**Figure S8.** Monthly-averaged surface currents in Lake Michigan and Green Bay during the 2016-2019 period. Bolded red lines indicate dominant circulation patterns. $U_{spd}$ denotes currents magnitude.

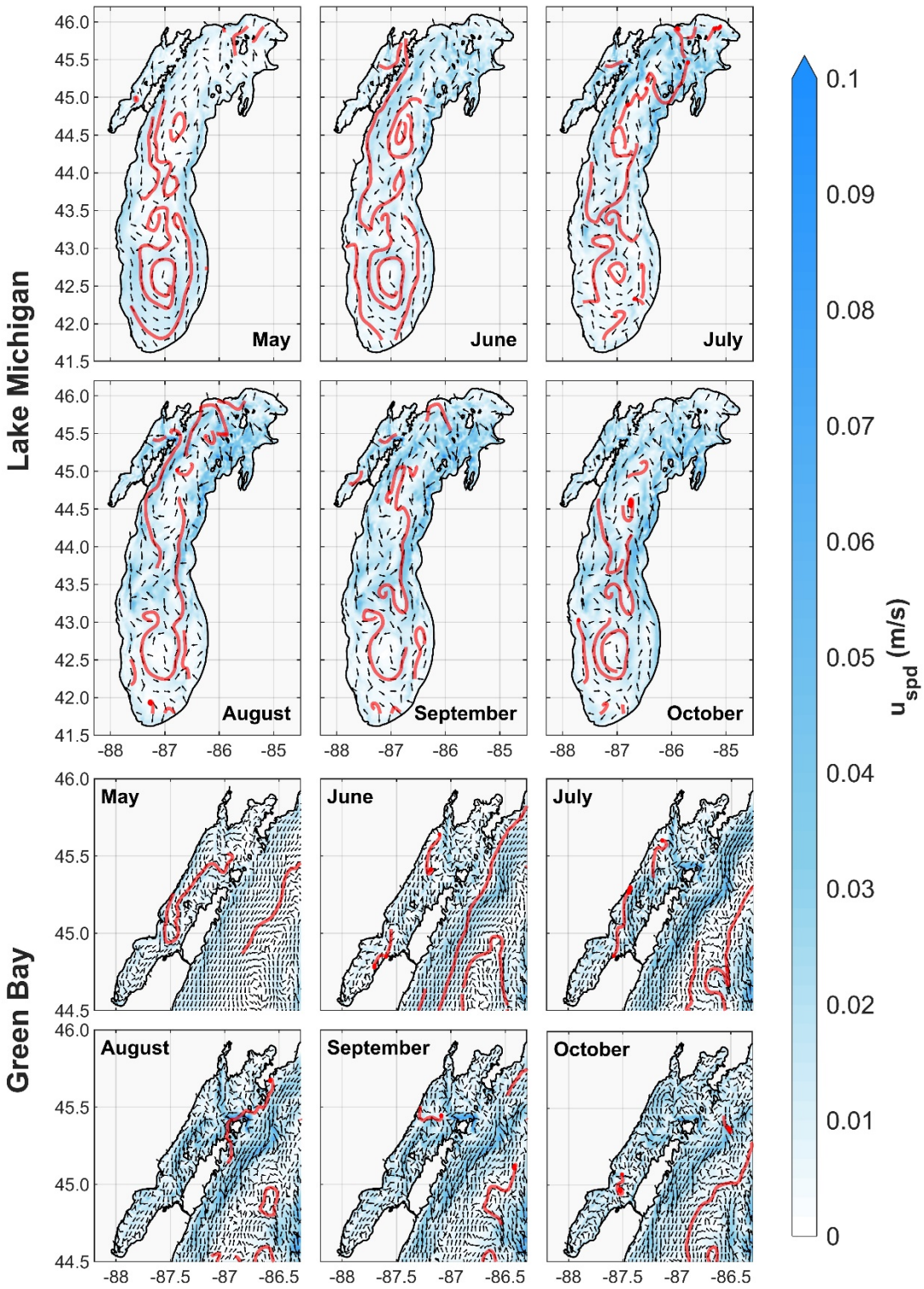


**Figure S9.** Monthly-averaged bottom currents in Lake Michigan and Green Bay during the 2016-2019 period. Bolded red lines indicate dominant circulation patterns. $U_{spd}$ denotes currents magnitude.

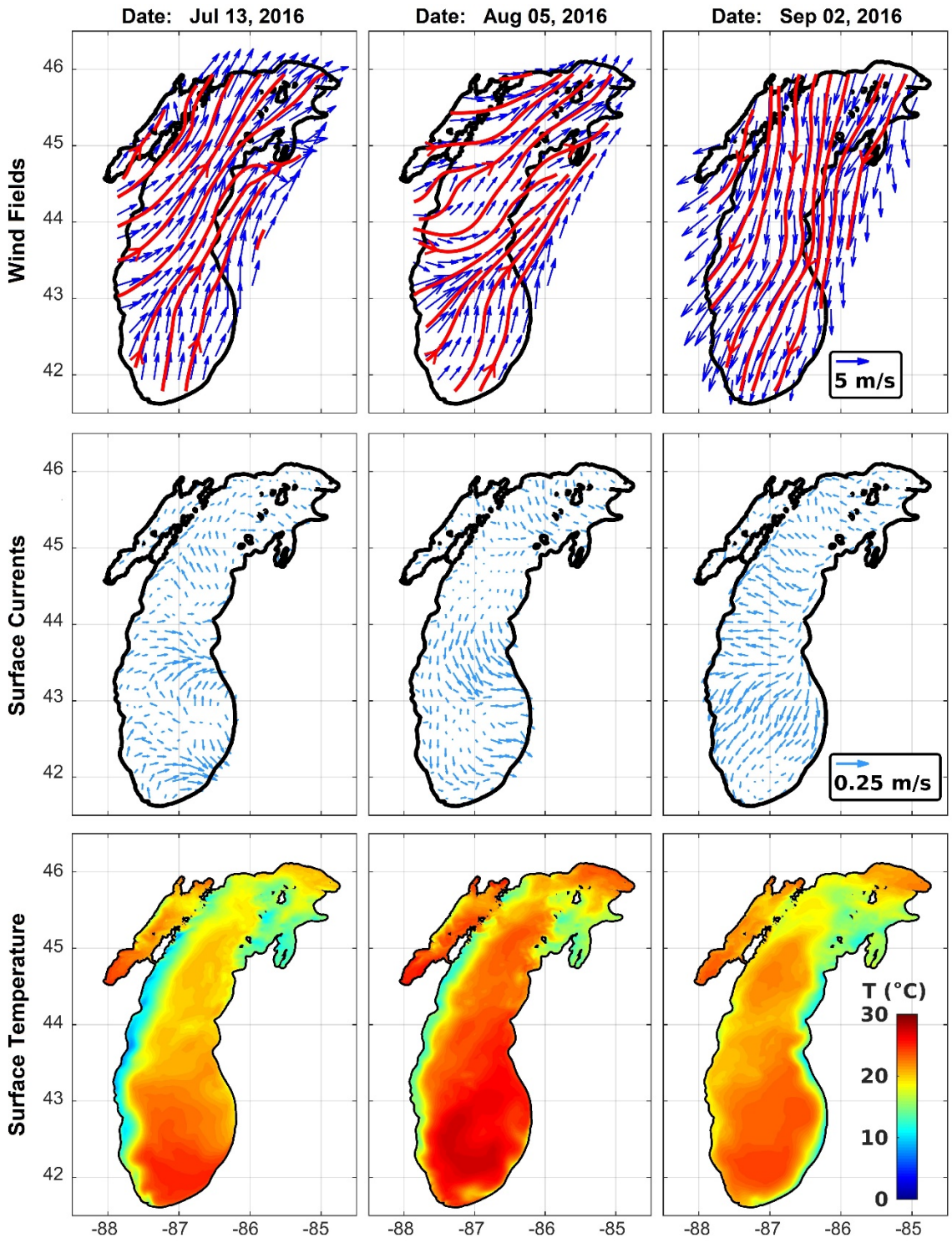


Figure S10. Examples of the upwelling events in Lake Michigan in July, August, and September of 2016 (bottom row) with their corresponding surface currents (middle row) and wind fields (top row). The figure clearly shows that N-S winds drive currents offshore and generate upwellings in Lake Michigan nearshore areas.

**Movie S1.** Animated daily-averaged snapshots of water temperature (TW) profile along the A-A′ (Green Bay longitudinal axis) cross-section (as shown in Figure 1) during the period of May-October 2018. The vertical axis is exaggerated ~700 times.

**Movie S2.** Animated daily-averaged snapshots of total suspended solids (TSS) profile along the A-A′ (Green Bay longitudinal axis) cross-section (as shown in Figure 1) during the period of May-October 2018. The vertical axis is exaggerated ~700 times.

**Movie S3.** Animated daily- and depth-averaged snapshots of total suspended solids (TSS) in Green Bay during the period of May-October 2018. Right-bottom inset provides high-resolution details of TSS transport in the Green Bay AOC and near the mouth of Fox River.